

University of New Hampshire

## University of New Hampshire Scholars' Repository

---

Doctoral Dissertations

Student Scholarship

---

Fall 2008

### Sources and sinks of selected trace gases in the tropospheric boundary layer of the eastern United States

Marguerite L. White

*University of New Hampshire, Durham*

Follow this and additional works at: <https://scholars.unh.edu/dissertation>

---

#### Recommended Citation

White, Marguerite L., "Sources and sinks of selected trace gases in the tropospheric boundary layer of the eastern United States" (2008). *Doctoral Dissertations*. 454.

<https://scholars.unh.edu/dissertation/454>

This Dissertation is brought to you for free and open access by the Student Scholarship at University of New Hampshire Scholars' Repository. It has been accepted for inclusion in Doctoral Dissertations by an authorized administrator of University of New Hampshire Scholars' Repository. For more information, please contact [Scholarly.Communication@unh.edu](mailto:Scholarly.Communication@unh.edu).

SOURCES AND SINKS OF SELECTED TRACE GASES IN THE TROPOSPHERIC  
BOUNDARY LAYER OF THE EASTERN UNITED STATES

BY

Marguerite L. White

Bachelor of Arts in Chemistry, Connecticut College, 1993

Master of Science in Secondary Education, Indiana University, 1997

Master of Science in Geochemical Systems, University of New Hampshire, 2003

DISSERTATION

Submitted to the University of New Hampshire

in Partial Fulfillment of

the Requirements for the Degree of

Doctor of Philosophy

In

Earth and Environmental Science

September 2008

UMI Number: 3333531

Copyright 2008 by  
White, Marguerite L.

All rights reserved.

### INFORMATION TO USERS

The quality of this reproduction is dependent upon the quality of the copy submitted. Broken or indistinct print, colored or poor quality illustrations and photographs, print bleed-through, substandard margins, and improper alignment can adversely affect reproduction.

In the unlikely event that the author did not send a complete manuscript and there are missing pages, these will be noted. Also, if unauthorized copyright material had to be removed, a note will indicate the deletion.

**UMI**<sup>®</sup>

---

UMI Microform 3333531

Copyright 2008 by ProQuest LLC.

All rights reserved. This microform edition is protected against  
unauthorized copying under Title 17, United States Code.

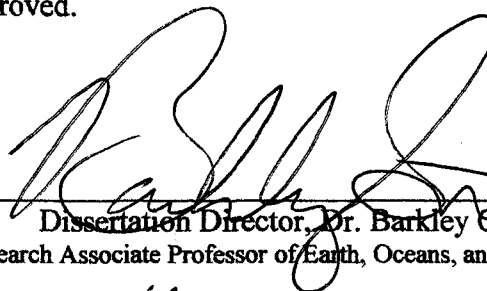
ProQuest LLC  
789 E. Eisenhower Parkway  
PO Box 1346  
Ann Arbor, MI 48106-1346

All Rights Reserved

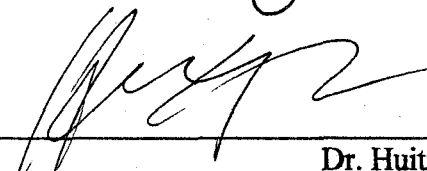
2008

Marguerite L. White

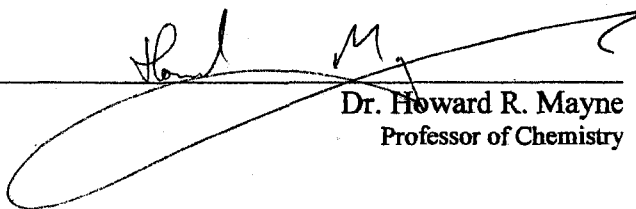
This dissertation has been examined and approved.



Dissertation Director, Dr. Barkley E. Sive  
Research Associate Professor of Earth, Oceans, and Space



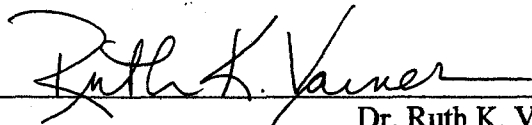
Dr. Huiting Mao  
Research Associate Professor of Earth, Oceans, and Space



Dr. Howard R. Mayne  
Professor of Chemistry



Dr. Robert W. Talbot  
Research Professor of Earth Sciences and Earth, Oceans, and Space



Dr. Ruth K. Varner  
Research Assistant Professor of Earth, Oceans, and Space and  
Affiliate Assistant Professor of Earth Sciences

July 14, 2008

Date

## ACKNOWLEDGEMENTS

I would like to thank my advisor, Dr. Barkley Sive, and my Ph.D. committee, Dr. Huiting Mao, Dr. Ruth Varner, Dr. Robert Talbot, and Dr. Howard Mayne, for all the help, constructive criticism, and valuable time they gave in guiding me through this process. I am grateful for their belief in my abilities and the work presented here. Financial support for the research was provided through the Office of Oceanic and Atmospheric Research at NOAA, the National Science Foundation, and the EPA STAR program. I would also like to thank the National Science Foundation Graduate Research Fellowship program, the UNH AIRMAP program, and the UNH TESSE program for providing financial support for me during my years as a graduate student. I would especially like to acknowledge the VOC research group, whose countless hours in the field and lab made this dissertation possible: Rachel Russo, Yong Zhou, Karl Haase, Jesse Ambrose, Leanna Conway, and Elizabeth Frinak. Thank you as well to the many others who contributed to this research and provided assistance and advice including Oliver Wingenter, Pieter Beckman, Sean Wadsworth, Su Youn Kim, Tzu-Ling Lai, Pallavi Mittal, Kathryn Allain, Tess Finnigan-Allan, and Adam Csakai. Finally, I would like to thank my parents, Jack and Mary White, and my husband, Mike Jeanneau, for always being there for me and never losing faith that I would indeed complete this dissertation.

## TABLE OF CONTENTS

ACKNOWLEDGEMENTS	iv
LIST OF TABLES	viii
LIST OF FIGURES	ix
ABSTRACT	xi

CHAPTER	PAGE
1. INTRODUCTION	1
2. VOLATILE ORGANIC COMPOUNDS IN NORTHERN NEW ENGLAND MARINE AND CONTINENTAL ENVIRONMENTS DURING THE ICARTT 2004 CAMPAIGN	
2.1 Introduction	4
2.2 Site Descriptions and VOC Measurements	6
2.3 Results and Discussion	10
2.3.1 Comparison of VOC Reactivity at Thompson Farm and Appledore Island	10
2.3.2 NMHC Flux Estimates at Thompson Farm	19
2.3.3 The Influence of LPG Leakage Sources	22
2.3.4 The Influence of Gasoline Evaporation Sources	29
2.4 Conclusions	34
3. ARE BIOGENIC EMISSIONS A SIGNIFICANT SOURCE OF ATMOSPHERIC TOLUENE IN THE RURAL NORTHEAST?	35
3.1 Introduction	35
3.2 Methods	38

3.2.1 Thompson Farm Ambient VOC Measurements	38
3.2.2 Thompson Farm Vegetative Flux Measurements	40
3.2.3 Duke Forest Vegetative Flux Measurements	41
3.3 Warm Season Toluene Enhancements at Thompson Farm	42
3.4 Evidence for Various Toluene Source Influences at Thompson Farm	46
3.5 Estimates of Source Contributions to Summer Toluene Enhancements	53
3.5.1 Fuel Evaporation	53
3.5.2 Biogenic	54
3.6 Conclusions	56
4. CARBONYL SULFIDE EXCHANGE IN A TEMPERATE LOBLOLLY PINE FOREST GROWN UNDER AMBIENT AND ELEVATED CO <sub>2</sub>	58
4.1 Introduction	58
4.2 Methods	61
4.2.1 Site Description	61
4.2.2 Canopy Measurements, September 2004	62
4.2.3 Vertical Profile Measurements, September 2004 and June 2005	63
4.2.4 Vegetation Flux Measurements, June 2005	64
4.2.5 Soil Flux Measurements, June and September 2005	66
4.2.6 Estimates of Net Ecosystem Flux, September 2004 and June 2005	68
4.2.6.1 Gradient Flux Calculations	68
4.2.6.2 Nighttime Flux Calculation	71
4.3 Results and Discussion	72
4.3.1 Canopy Measurements, September 2004	72

4.3.2 Vertical Profiles, September 2004 and June 2005	76
4.3.3 Vegetation Flux Measurements, June 2005	78
4.3.3.1 Post Catalyst COS Levels	81
4.3.3.2 Stomatal Conductance and Photosynthetic Capacity	84
4.3.4 Soil Flux Measurements, June and September 2005	89
4.3.5 Estimates of Net Ecosystem Flux, September 2004 and June 2005	93
4.3.5.1 Gradient Flux Estimates	94
4.3.5.2 Nighttime Flux Estimates	97
4.4 Conclusions	102
REFERENCES	103

## LIST OF TABLES

Table 2.1:	Mean mixing ratios of compounds measured at Thompson Farm and Appledore Island during the ICARTT campaign	9
Table 2.2:	Mean reactivities for major classes of compounds measured at Thompson Farm Appledore Island during the ICARTT campaign	11
Table 2.3:	Positive net nighttime fluxes and estimated loss and emission rates for NMHCs at Thompson Farm during the ICARTT campaign	22
Table 2.4:	Mean nighttime mixing ratios and rate constants for select NMHCs at Thompson Farm during the ICARTT campaign	22
Table 2.5:	Net nighttime fluxes for select NMHCs during the regional diurnal study, 18 to 19 August 2003	26
Table 2.6:	Representative hydrocarbon ratios at Thompson Farm and Appledore Island during the ICARTT campaign	31
Table 3.1:	Seasonal means for toluene and benzene mixing ratios and the toluene/benzene ratio from Thompson Farm daily can measurements, 2004-2007	44
Table 3.2:	Vegetative toluene net flux rates	50
Table 3.3:	Estimates of warm season toluene source contributions at Thompson Farm	54
Table 4.1:	Mean COS and CO <sub>2</sub> deposition velocities for loblolly pine and sweet gum trees at the Duke Forest FACE site	83
Table 4.2:	Mean COS fluxes, deposition velocities, temperatures and soil moisture content from soil static enclosure measurements at the Duke Forest FACE site	90
Table 4.3:	Comparison of mean net ecosystem COS flux estimates from gradient flux and nighttime flux calculations for Duke Forest FACE site	94
Table 4.4:	Comparison of net ecosystem, vegetation and soil COS flux estimates for the Duke Forest FACE site in September 2004 and June 2005	100

## LIST OF FIGURES

Figure 2.1: Measurement site locations during the ICARTT campaign and the 2003 regional diurnal study	7
Figure 2.2: The reactivities of the major classes of compound measured at Thompson Farm and Appledore Island during the ICARTT campaign	12
Figure 2.3: The reactivities of OVOCs, alkenes, and alkanes measured at Thompson Farm and Appledore Island during the ICARTT campaign	15
Figure 2.4: Representative 2-day backward trajectories from 13 to 19 July 2004	16
Figure 2.5: The reactivities of alkanes, aromatics, biogenics, and OVOCs at Thompson Farm and Appledore Island from 13 to 19 July 2004	17
Figure 2.6: Hourly mixing ratios of ethane and propane at Thompson Farm during the ICARTT campaign	24
Figure 2.7: Results from the 2003 regional diurnal study	25
Figure 2.8: Time series of propane/benzene and $\Sigma$ pentane/benzene at Thompson Farm and Appledore Island from 13 to 19 July 2004	28
Figure 2.9: 24 hour backward trajectories during peak $\Sigma$ pentane/benzene at Thompson Farm and Appledore Island	32
Figure 3.1: Time series of benzene and toluene mixing ratios from daily can measurements at Thompson Farm, 2004-2007	43
Figure 3.2: Time series of $C_2H_2/CO$ and toluene/benzene ratios from daily can measurements at Thompson Farm, 2004-2007	45
Figure 3.3: Time series of i-pentane and toluene mixing ratios from daily can measurements at Thompson Farm, 2004-2007	47
Figure 3.4: Toluene vs. i-pentane mixing ratios at Thompson Farm during summer 2004, 2005, and 2006	48
Figure 3.5: Alfalfa enclosure measurements of toluene production before and after harvesting, 25 September 2007	49
Figure 3.6: Toluene and $\alpha$ -pinene flux from loblolly pine, June 2005	51

Figure 4.1: Dynamic branch enclosure schematic	65
Figure 4.2: Comparison of R1 and R2 ambient COS and ethane mixing ratios at the Duke Forest FACE site, September 2004	73
Figure 4.3: Time series of COS, CO <sub>2</sub> and meteorological measurements in at the Duke Forest FACE site, September 2004	74
Figure 4.4: Hourly mean COS mixing ratios during non-hurricane periods in R1 and R2 at the Duke Forest FACE site, September 2004	75
Figure 4.5: Vertical profiles of COS at the Duke Forest FACE site, September 2004	77
Figure 4.6: Time series of loblolly pine branch enclosure measurements, June 2005	79
Figure 4.7: Time series of sweet gum branch enclosure measurements, June 2005	80
Figure 4.8: Relationships between vegetation net COS flux and PC COS levels from branch enclosure measurements, June 2005	82
Figure 4.9: Relationships between vegetation COS and CO <sub>2</sub> deposition velocities from branch enclosure measurements, June 2005	85
Figure 4.10: Soil net COS fluxes at the Duke Forest FACE site, June and September 2005	90
Figure 4.11: Relationships between soil net COS flux and environmental variables at Duke Forest FACE site	92
Figure 4.12: Comparison of COS and ethane net ecosystem flux estimates at Duke Forest FACE site from gradient flux calculations, September 2004	96

## ABSTRACT

### SOURCES AND SINKS OF SELECT TRACE GASES IN THE TROPOSPHERIC BOUNDARY LAYER OF THE EASTERN UNITED STATES

By

Marguerite L. White

University of New Hampshire, September, 2008

This dissertation describes three major research projects with the common goal of characterizing sources and sinks of trace gases of strong relevance to regional air quality and global climate issues.

In the first study, volatile organic compound (VOC) measurements collected at a marine and continental site in northern New England were compared and examined for evidence of regional VOC sources. Biogenic VOCs, including isoprene, monoterpenes, and oxygenated VOCs, were significant components of the total reactivity at both locations. However, very different VOC distributions were observed for each site. The impact of local anthropogenic hydrocarbon sources such as liquefied petroleum gas (LPG) leakage was also evident at both sites. During the campaign, a propane flux of  $9 (\pm 2) \times 10^9$  molecules  $\text{cm}^{-2} \text{s}^{-1}$  was calculated for the continental site.

In the second study, three hydrocarbon sources were investigated for their potential contributions to the summertime atmospheric toluene enhancements observed at a rural location in southern New Hampshire. These sources included: 1) warm season fuel evaporation emissions, 2) local industrial emissions, and 3) local vegetative emissions. The estimated contribution of fuel evaporation emissions (16-30 pptv  $\text{d}^{-1}$ )

could not fully account for observed summertime toluene enhancements (20-50 pptv d<sup>-1</sup>). Vegetation enclosure measurements suggested biogenic toluene emissions (5 and 12 pptv d<sup>-1</sup> for alfalfa and pine trees) made significant contributions to summertime enhancements. Industrial toluene emissions, estimated at 7 pptv d<sup>-1</sup>, most likely occurred year round rather than seasonally.

Finally, controls over carbonyl sulfide (COS) uptake in a temperate loblolly pine forest grown under ambient and elevated CO<sub>2</sub> were examined in the third study. Vegetative consumption dominated net ecosystem COS uptake (10 to 40 pmol m<sup>-2</sup> s<sup>-1</sup>) under both CO<sub>2</sub> regimes. Environmental controls over vegetation stomatal conductance and photosynthetic capacity were the major factors influencing COS uptake rates. The loblolly pines exhibited substantial COS consumption overnight (50% of daytime rates) that was independent of CO<sub>2</sub> assimilation. This suggests current estimates of the global vegetative COS sink, which assume that COS and CO<sub>2</sub> are consumed simultaneously, may need to be reevaluated.

## CHAPTER 1

### INTRODUCTION

The chemical composition of the earth's atmosphere is intimately linked to the biological, geological, and anthropogenic activities that occur at the surface of the earth. Living organisms, volcanoes, industrial activities, biomass burning, fossil fuel combustion, and solvent and fuel evaporation all emit trace gases that can play important roles in atmospheric chemistry and the biogeochemical cycles of carbon, nitrogen, oxygen, and sulfur [Brasseur *et al.*, 1999]. The cycling of these trace gases through the atmosphere can have large impacts on global climate and regional air quality and have been linked to tropospheric ozone formation [Wang *et al.*, 1998], secondary aerosol production and growth [Bowman *et al.*, 1995; Schauer *et al.*, 2002], stratospheric ozone depletion [Kurylo *et al.*, 1999; Notholt *et al.*, 2003], and climate change [Brasseur *et al.*, 1999; Charlson *et al.*, 1990; Robertson *et al.*, 2000]. For these reasons, it is critical to understand the individual sources and sinks to the atmosphere which can impact the chemistry and regional distribution of these trace gases.

This dissertation describes three major research projects focused on characterizing the sources and sinks of select trace gases in the troposphere. Chapter 2 compares volatile organic compounds (VOCs) measured during the 2004 International Consortium for Atmospheric Research on Transport and Transformation (ICARTT) field campaign at Thompson Farm, a continental site in the New Hampshire seacoast region, and Appledore Island, a marine site 10 km off the Maine coast. Chapter 3 examines the contributions of

three hydrocarbon sources to the warm season toluene enhancements observed at Thompson Farm during 2004 – 2006. Finally, Chapter 4 presents an analysis of vegetation, soil, and ecosystem carbonyl sulfide (COS) exchange in a temperate loblolly pine forest grown under ambient and elevated CO<sub>2</sub>.

While the specific compounds, sources, sinks, and site locations differ between each project, all three parts are unified under the common goal of characterizing processes that affect the tropospheric distribution of trace gases with strong relevance to regional air quality and global climate issues. VOCs, including the wide variety of non-methane hydrocarbons (NMHCs) and oxygenated VOCs (OVOCs) presented in Chapter 2 and 3, can have a significant effect on tropospheric air quality. Their oxidation in the presence of nitrogen oxides (NO<sub>x</sub>) leads to the photochemical formation of tropospheric ozone (O<sub>3</sub>), a secondary pollutant and respiratory irritant [Wang *et al.*, 1998]. VOC oxidation products can also partition into particulate matter, becoming a significant component of fine aerosol mass [Schauer *et al.*, 2002]. Furthermore, COS, discussed in Chapter 4, is the major atmospheric reservoir of sulfur available for transport to the stratosphere [Watts, 2000]. In the stratosphere, its photolysis and oxidation contribute to the formation of the stratospheric sulfate aerosol layer which influences the earth's radiation balance by reflecting incoming solar radiation and provides a surface for heterogeneous ozone depletion reactions [Chin and Davis, 1995; Turco *et al.*, 1980].

Bearing these implications in mind, specific objectives for this research were:

- 1) To compare VOC mixing ratios at a marine and a continental site in close proximity in coastal northern New England with particular attention given to evidence of local NMHC emissions,

- 2) To calculate the nighttime net flux of propane at a rural continental site in coastal New Hampshire and estimate regional propane emissions from liquefied petroleum gasoline (LPG) leakage,
- 3) To estimate contributions from gasoline evaporation, biogenic production, and industrial emissions to summertime enhancements of atmospheric toluene observed at a rural continental site in coastal New Hampshire,
- 4) To quantify plant, soil and ecosystem COS exchange rates in a temperate North Carolina forest grown under ambient and elevated CO<sub>2</sub>, and
- 5) To determine the significant environmental factors affecting net COS exchange under ambient and elevated CO<sub>2</sub> conditions.

## CHAPTER 2

### VOLATILE ORGANIC COMPOUNDS IN NORTHERN NEW ENGLAND MARINE AND CONTINENTAL ENVIRONMENTS DURING THE ICARTT 2004 CAMPAIGN

#### **2.1 Introduction**

Volatile organic compounds (VOCs), including methane (CH<sub>4</sub>), nonmethane hydrocarbons (NMHCs) and oxygenated volatile organic compounds (OVOCs), have a significant impact on regional air quality as their oxidation in the presence of nitrogen oxides (NO<sub>x</sub>) leads to tropospheric ozone (O<sub>3</sub>) formation. VOC oxidation products can also partition into particulate matter becoming a significant component of fine aerosol mass [Schauer *et al.*, 2002]. The long range transport of VOCs and NO<sub>x</sub> can affect air quality in locations far downwind from source regions. For example, frequent summertime pollution episodes in New England when O<sub>3</sub> levels exceeded the U.S. Environmental Protection Agency National Ambient Air Quality Standards have been linked to transport of photochemically aged air masses from urban areas located to the south and southwest of the region [Fischer *et al.*, 2004; Griffin *et al.*, 2004; Mao and Talbot, 2004b; Ray *et al.*, 1996]. On a larger scale, polluted air masses transported across North America have been sampled over eastern Canada [Millet *et al.*, 2006], the north Atlantic [Daum *et al.*, 1996; Lewis *et al.*, 2007], and Europe [Stohl and Trickl, 1999].

The atmospheric sources of VOCs include a variety of anthropogenic emissions such as fossil fuel combustion, biomass burning, and evaporation of solvents and fuels as well as natural emissions from vegetation, soil, and the ocean [Guenther *et al.*, 1995].

The major atmospheric sink for most VOC species is oxidation by hydroxyl radical (OH) [Thompson, 1992], which dominates during the mid-latitude summer. Under certain conditions, reaction of VOCs with O<sub>3</sub> [Goldstein *et al.*, 2004], NO<sub>3</sub> [Brown *et al.*, 2004; Geyer and Platt, 2002], and atomic Cl [Finlayson-Pitts, 1993; Wingenter *et al.*, 1999] can also be a significant oxidation pathway. Recognizing that the photochemical processes for a particular compound measured in the atmosphere are dependent on both the oxidant and its concentration, the potential contributions of different VOCs to photochemistry can generally be characterized by reactivity with OH as follows:

$$\text{Reactivity} = [X] \cdot k_{\text{OH},X} \quad (1)$$

where [X] is the concentration of the VOC in molecules cm<sup>-3</sup> and k<sub>OH</sub> is the literature rate constant for each hydrocarbon with OH at 298K in cm<sup>3</sup> molecules<sup>-1</sup> sec<sup>-1</sup> [Atkinson, 1994; 1997; Atkinson *et al.*, 2004]. The reactivity is a measure of the initial rate of peroxy radical production, which is often the rate limiting reaction in the process of O<sub>3</sub> formation. Whether or not O<sub>3</sub> is produced from a particular hydrocarbon depends on a variety of factors including NO<sub>x</sub> concentrations, the presence of other VOCs, and the oxidation mechanism [Carter, 1994].

This chapter presents VOC measurements at two locations, a continental and a marine site in close proximity in Northern New England, during the summer of 2004 as part of the International Consortium for Atmospheric Research on Transport and Transformation (ICARTT) campaign [Fehsenfeld *et al.*, 2006]. In this analysis, individual VOC contributions to potential OH reactivity were quantified and used to identify the most significant compounds affecting the local photochemistry at each site. Local nighttime fluxes of monoterpenes and propane were also estimated for the

continental site. Finally, the influence of regional anthropogenic NMHC sources such as liquefied petroleum gas (LPG) leakage and gasoline evaporation were examined for each location.

## **2.2 Site Descriptions and VOC Measurements**

The measurements presented here were conducted at two of the University of New Hampshire's AIRMAP Observing Network sites: an inland site at Thompson Farm (TF, 43.11 °N, 70.95 °W, 24 m) and a coastal marine location on Appledore Island (AI, 42.97 °N, 70.62 °W, 5 m) (Figure 2.1).

Situated 25 km from the Gulf of Maine and 5 km northeast of Great Bay in rural Durham, NH, the Thompson Farm observing station is established on an active corn farm surrounded by mixed forest and corn fields. VOC measurements, including C<sub>2</sub>-C<sub>10</sub> NMHCs, C<sub>1</sub>-C<sub>2</sub> halocarbons and C<sub>1</sub>-C<sub>5</sub> alkyl nitrates, were made at this site using an automated gas chromatograph (GC) system equipped with two flame ionization detectors (FIDs) and two electron capture detectors (ECDs) [Sive *et al.*, 2005; Zhou *et al.*, 2005, 2008]. Air was continuously drawn from a PFA-Teflon lined manifold at the top of a 12 m tower and sub-samples were analyzed every 40 minutes. Measurements included in this study were made from 12 July to 13 August 2004.

Appledore Island, on which the second AIRMAP station is located, is one of the Isles of Shoals located 10 km off the coast of New Hampshire and Maine (Figure 2.1). Air samples were drawn from the top of a ~20 m tall World War II-era coastal surveillance tower and collected in canisters on an hourly basis from 2 July to 13 August 2004. Samples were returned to the University of New Hampshire and analyzed within a week of collection on a three GC system equipped with two FIDs, two ECDs, and a mass

spectrometer (MS) for C<sub>2</sub>-C<sub>10</sub> NMHCs, C<sub>1</sub>-C<sub>2</sub> halocarbons and C<sub>1</sub>-C<sub>5</sub> alkyl nitrates [Sive *et al.*, 2005; Zhou *et al.*, 2005, 2008]. NMHC measurements spanning the period from 29 July through 13 August have been omitted from this analysis because a small fracture occurred in the stainless steel inlet line at the connection to the metal bellows pump, resulting in slightly elevated NMHC levels. Thus, the time period for the measurements used in this analysis spans from 2 to 28 July 2004.

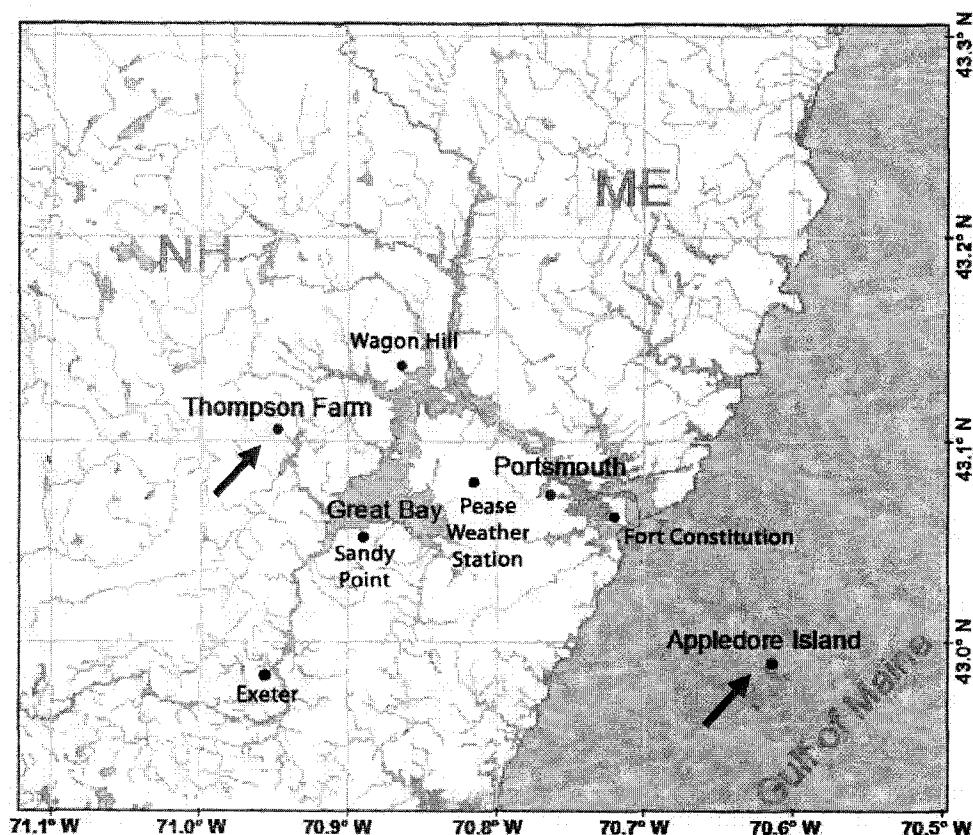


**Figure 2.1:** Measurement site locations for this study. Thompson Farm and Appledore Island are indicated by red arrows. Sites in blue were part of the 2003 regional diurnal study discussed in section 2.3.3.

At each site, additional measurements of NMHCs and OVOCs were made using a proton transfer reaction mass spectrometer (PTR-MS). Each PTR-MS was run under the same conditions with a drift tube pressure of 2 mbar, an electric field of 600 V and a 20

second dwell time for measuring 24 different VOCs; which resulted in a ~10 minute measurement cycle [Talbot *et al.*, 2005; Ambrose *et al.*, 2007]. Measurements of CH<sub>4</sub> for Appledore Island were made from an additional analysis of the canister samples at UNH using a GC-FID system, while at Thompson Farm, measurements were made every 5 minutes using a separate automated GC-FID system. Carbon monoxide (CO) mixing ratios were measured every 1 minute using infrared spectroscopy [Mao and Talbot, 2004a]. Nitrogen dioxide (NO<sub>2</sub>) was measured at Appledore Island using differential optical absorption spectroscopy (DOAS). The retroreflector was installed on the White Island lighthouse located 2.3 km away while spectra were recorded from the Appledore Island tower at approximately 40 m above sea level over a 4.6 km path length. At Thompson Farm, NO<sub>2</sub> was measured with NO using a fast response, high sensitivity photolysis system. A more detailed description of this instrument can be found in Griffin *et al.* [2007] and Ryerson *et al.* [2000].

A full list of the measured VOCs included in this analysis as well as their mean mixing ratios for the ICARTT campaign is given in Table 2.1. Mean values are presented as mean  $\pm$  standard deviation throughout unless stated otherwise. All measurements were averaged hourly for the reactivity analyses in Section 2.3.1 to allow for easier comparison between the different measurement timescales and sites. Reactivities were calculated for NMHCs, OVOCs, CH<sub>4</sub>, CO, and NO<sub>2</sub> using equation (1) and the literature rate constants for reaction with OH at 298K [Atkinson, 1994; 1997; Atkinson *et al.*, 2004]. Hourly GC and canister measurements of NMHCs were also used to calculate the ratios and net fluxes presented in Sections 2.3.2, 2.3.3, and 2.3.4.

Compound	mean ±st.dev.		Compound	mean ±st.dev.	
	TF	AI		TF	AI
<b><u>Alkanes (in pptv)</u></b>			<b><u>Aromatics (in pptv)</u></b>		
ethane (C <sub>2</sub> )	1100 ±300	1100 ±400	benzene	80 ±40	80 ±40
propane (C <sub>3</sub> )	800 ±800	800 ±700	toluene	120 ±90	100 ±100
i-butane (C <sub>4</sub> )	60 ±50	70 ±70	ethylbenzene (C <sub>8</sub> )	20 ±20	20 ±20
n-butane (C <sub>4</sub> )	110 ±80	100 ±100	m+p-xylene (C <sub>8</sub> )	70 ±60	90 ±60
i-pentane (C <sub>5</sub> )	200 ±200	200 ±200	3-ethyltoluene (C <sub>9</sub> )	20 ±20	20 ±10
n-pentane (C <sub>5</sub> )	80 ±70	70 ±70	4-ethyltoluene (C <sub>9</sub> )	11 ±7	7 ±5
cyclopentane (C <sub>5</sub> )	6 ±3	9 ±7	2-ethyltoluene (C <sub>9</sub> )	9 ±6	8 ±6
n-hexane (C <sub>6</sub> )	50 ±40	40 ±40	1,3,5-trimethylbenzene (C <sub>9</sub> )	10 ±7	7 ±5
methylcyclopentane (C <sub>6</sub> )	30 ±20	40 ±30	1,2,4-trimethylbenzene (C <sub>9</sub> )	30 ±30	20 ±20
cyclohexane (C <sub>6</sub> )	20 ±10	10 ±10	1,2,3-trimethylbenzene (C <sub>9</sub> )	9 ±7	6 ±4
n-heptane (C <sub>7</sub> )	20 ±20	20 ±20	<b><u>biogenics (in pptv)</u></b>		
methylcyclohexane (C <sub>7</sub> )	20 ±10	10 ±10	isoprene	500 ±600	100 ±100
n-octane (C <sub>8</sub> )	9 ±5	11 ±9	a-pinene	200 ±500	30 ±40
2,2,4-trimethylpentane (C <sub>8</sub> )	30 ±20	40 ±50	b-pinene	100 ±200	30 ±40
2,3,4-trimethylpentane (C <sub>8</sub> )	12 ±7	10 ±10	camphene	100 ±200	20 ±20
n-decane (C <sub>10</sub> )	12 ±7	10 ±10	limonene	40 ±60	8 ±7
<b><u>Alkenes (in pptv)</u></b>			<b><u>OVOCs (in ppbv)</u></b>		
ethene (C <sub>2</sub> )	200 ±300	200 ±200	methanol	2 ±1	2 ±1
propene (C <sub>3</sub> )	60 ±80	50 ±50	acetaldehyde	0.3 ±0.3	0.4 ±0.2
1-butene (C <sub>4</sub> )	10 ±10	10 ±9	acetone	2 ±1	1.5 ±0.7
i-butene (C <sub>4</sub> )	20 ±20	20 ±20	MEK	0.2 ±0.2	0.2 ±0.2
trans-2-butene (C <sub>4</sub> )	6 ±3	6 ±9	acetic acid	0.4 ±0.5	0.5 ±0.3
cis-2-butene (C <sub>4</sub> )	8 ±4	10 ±10	MVK/MACR	0.4 ±0.4	0.2 ±0.3
1-pentene (C <sub>5</sub> )	9 ±6	8 ±7	<b><u>Other trace gases (in ppbv)</u></b>		
trans-2-pentene (C <sub>5</sub> )	7 ±3	10 ±10	O <sub>3</sub> (ppbv)	30 ±20	40 ±20
cis-2-pentene (C <sub>5</sub> )	4 ±2	6 ±7	CO (ppbv)	170 ±50	170 ±50
2-methyl-2-butene (C <sub>5</sub> )	7 ±3	7 ±8	NO <sub>2</sub> (ppbv)	2 ±2	4 ±4
<b><u>Alkynes (in pptv)</u></b>			CH <sub>4</sub> (ppbv)	1.9 ±0.2	1.78 ±0.05
ethyne	300 ±200	300 ±200			

**Table 2.1:** All compounds included in this analysis and their mean mixing ratios ± standard deviation at Thompson Farm (TF) and Appledore Island (AI). NMHCs are separated by major compound class (alkane, alkene, alkyne, aromatics, and biogenic) and, where appropriate, carbon number (C<sub>2</sub>-C<sub>10</sub>). All mixing ratios are in pptv except for the OVOCs, O<sub>3</sub>, CO, NO<sub>2</sub> and CH<sub>4</sub>.

In addition to the ICARTT measurements, the results from a diurnal study completed in August 2003 in the New Hampshire seacoast area are presented for

comparison to the net fluxes calculated in Sections 2.3.2 and 2.3.3. This diurnal study was conducted at six locations in the Great Bay region of coastal New Hampshire (Figure 2.1) including Thompson Farm, Sandy Point Discovery Center, Stratham, (Sandy Point, 43.05 °N, 70.90 °W), Wagon Hill, Durham (Wagon Hill, 43.13 °N, 70.87 °W), Fort Constitution, Newcastle, (Fort Constitution, 43.07 °N, 70.71 °W), Downtown Boat Launch, Exeter, (Exeter, 42.98 °N, 70.95 °W), and Pease Weather Station, Portsmouth, (Pease Weather Station, 43.08 °N, 70.82 °W). At 5 of these sites (Wagon Hill, Sandy Point, Exeter, Pease Weather Station, and Fort Constitution), ambient pressure air samples were collected every hour from 1800 local time (LT) on 18 August to 1900 LT on 19 August 2003. Canisters were then returned to the University of New Hampshire for analysis on the three GC system described previously for Appledore Island measurements. Concurrent NMHC measurements were collected at Thompson Farm throughout the 25 hour period using the automated GC system described previously for this site [Sive *et al.*, 2005; Zhou *et al.*, 2005, 2008].

## **2.3 Results and Discussion**

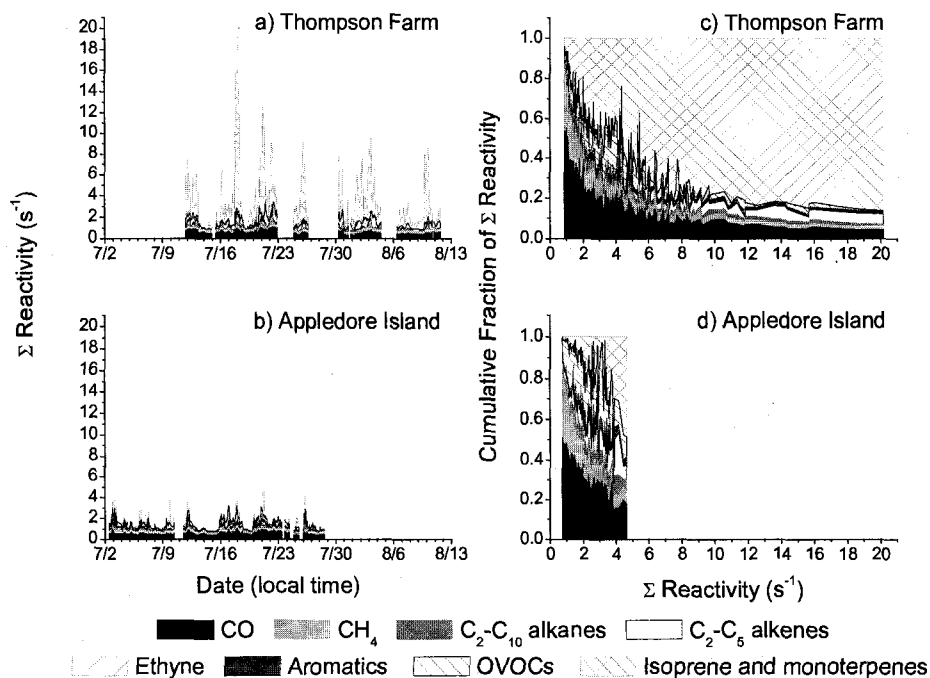
### **2.3.1 Comparison of VOC Reactivity at Thompson Farm and Appledore Island**

Table 2.2 summarizes the mean reactivities for the major classes of measured compounds contributing to OH loss at each site. The time series of cumulative reactivities and the relative contribution of each class to total VOC reactivity (with the exception of NO<sub>2</sub>) is illustrated in Figure 2.2; NO<sub>2</sub> reactivity is not included because of significant time gaps in the measurements.

	Thompson Farm		Appledore Island	
	Mean Reactivity (s <sup>-1</sup> )	Percent Total	Mean Reactivity (s <sup>-1</sup> )	Percent Total
NO <sub>2</sub>	0.62 ± 0.48	14.8	0.99 ± 0.92	38.6
CO	0.55 ± 0.15	13.3	0.55 ± 0.15	21.5
CH <sub>4</sub>	0.29 ± 0.02	6.9	0.27 ± 0.01	10.5
C <sub>2</sub> -C <sub>10</sub> Alkanes	0.10 ± 0.07	2.4	0.070 ± 0.079	2.9
C <sub>2</sub> -C <sub>5</sub> Alkenes	0.10 ± 0.15	2.4	0.10 ± 0.11	3.9
Ethyne	0.0064 ± 0.0037	0.2	0.0074 ± 0.0051	2.9
Aromatics	0.12 ± 0.10	3.0	0.051 ± 0.074	2.0
OVOCS	0.35 ± 0.32	5.8	0.29 ± 0.24	11.2
Biogenics	2.01 ± 2.57	48.5	0.24 ± 0.41	9.3
<b>Total</b>	<b>4.15 ± 2.64</b>		<b>2.57 ± 1.10</b>	

**Table 2.2:** Mean reactivities ± standard deviation and percent of the mean total reactivity for the major classes of compounds measured over the entire sampling period at Thompson Farm and Appledore Island.

The reactivities calculated for the extensive suite of VOCs measured at Thompson Farm and Appledore Island offer considerable insights into the different sources that affect each site. The most striking characteristic difference between the two locations was the larger range of VOC reactivity at Thompson Farm (1 – 20 s<sup>-1</sup>, mean ± st. dev. = 4.15 ± 2.64 s<sup>-1</sup>) compared to Appledore Island (1 – 5 s<sup>-1</sup>, mean ± st. dev. = 2.57 ± 1.10 s<sup>-1</sup>). Approximately 50% of VOC reactivity for Thompson Farm was attributable to the large concentrations of biogenic compounds (isoprene, α-pinene, β-pinene, camphene, and limonene) observed at this site. At Appledore Island, these biogenic compounds were much less prevalent (Table 2.1 and 2.2) and longer-lived compounds like NO<sub>2</sub>, CO, CH<sub>4</sub>, and the OVOCS made larger contributions to site reactivity. However, biogenic compounds did have the highest mean reactivity (0.24 ± 0.21 s<sup>-1</sup>) of all the NMHCs (alkanes, alkenes, ethyne, and aromatics) at Appledore Island, with the strongest influence in high reactivity air masses reflecting considerable transport of these short-lived gases from coastal sources (Figure 2.2d).



**Figure 2.2:** The time series of summed ( $\Sigma$ ) reactivity attributable to each class of compounds at a) Thompson Farm and b) Appledore Island and the cumulative fraction of this summed reactivity attributable to each class of compounds vs. the range of total reactivity at c) Thompson Farm and d) Appledore Island. The inorganic gas  $\text{NO}_2$  is a significant component of total measured OH reactivity at each site but was not included in these graphs because of time gaps in  $\text{NO}_2$  measurement collection.

The biogenic influence on OVOCs was evident at both sites, as the isoprene oxidation products methyl vinyl ketone (MVK) and methacrolein (MACR) were a significant component of OVOC reactivity (Figure 2.3a and b). Because the PTR-MS does not distinguish between MVK and MACR, the reactivity for these compounds was calculated by multiplying their combined concentrations by the MVK rate constant with OH ( $k_{\text{OH}}$ ), and should be interpreted as a lower limit. The greater fraction of reactivity associated with methanol and acetone in the cleanest air masses (lowest 10<sup>th</sup> percentile for total reactivity) at Thompson Farm most likely reflects direct biogenic emissions (Figure 2.3a). This result is supported by the findings in *Mao et al.* [2006a], which

suggested that vegetative emissions of methanol and acetone contributed approximately 79% and 62%, respectively, to the diurnal mixing ratio increases observed at Thompson Farm. In the same study, they also estimated that anthropogenic sources of methanol and acetone were more significant at Appledore Island comprising approximately 52% and 59% of the total source strength, respectively. This likely contributed to the drop in methanol and acetone reactivity observed in the cleanest or lowest reactivity air masses reaching Appledore Island during the ICARTT measurement campaign (Figure 2.3b).

In discussing OVOC reactivity, it should be noted that formaldehyde was not measured at either Thompson Farm or Appledore Island during the ICARTT campaign period. A rough estimate of potential formaldehyde reactivity can be gained from the range of concentrations observed in low-altitude flights over the region during INTEX-NA (1.1-4.3 ppbv or 0.24-0.97 s<sup>-1</sup>) [Heald et al. (2007) *Total observed organic carbon (TOOC): A synthesis of North American observations, Atmos. Chem. Phys., manuscript submitted*]. While formaldehyde is likely a significant contributor to OVOC reactivity at both Appledore Island and Thompson Farm, a more detailed comparison of its chemistry requires measurements specific to each site and is beyond the scope of this paper.

A comparison of the proportion of reactivity attributable to the different alkenes separated by carbon number reveals distinct differences in the pattern of pentene reactivity at the two sites (Figure 2.3c and d). While the short-lived pentenes represent a small percentage of the overall reactivity at both locations (10% ± 10% and 7% ± 8% at Thompson Farm and Appledore Island, respectively), they are a more persistent influence across a wide range of air masses at Thompson Farm. In contrast, pentene influence on alkene reactivity increased at Appledore Island with increasing total alkene reactivity,

consistent with more intermittent influences from nearby coastal sources. Observations of elevated pentene mixing ratios off the coast of New Hampshire have previously been linked to gasoline evaporation sources [Goldan *et al.*, 2005] and a more detailed analysis of pentene distributions at each site relevant to this hydrocarbon source is presented in section 2.3.4.

A closer examination of the reactivity attributable to the alkanes by carbon number also provides further evidence that both gasoline evaporation and LPG leakage influenced NMHC distributions in the region (Figure 2.3e and f). The largest fraction of alkane reactivity was actually attributable to the pentanes ( $\Sigma C_5$ -alkanes =  $30\% \pm 5\%$  and  $22\% \pm 7\%$  of total alkane reactivity at Thompson Farm and Appledore Island, respectively) reflecting the potential influence at both sites of evaporative emissions from unburned gasoline [Conner *et al.*, 1995]. Propane reactivity at both locations was also substantial ( $22\% \pm 7\%$  and  $25\% \pm 9\%$  of total alkane reactivity at Thompson Farm and Appledore Island, respectively), reflecting large-scale leakage from LPG storage tanks. The influences of these hydrocarbon sources on VOC distributions in the region are evaluated in more depth in Sections 2.3.3 and 2.3.4.

The period from 13 to 19 July 2004 presented a significant contrast in VOC reactivities at both sites for clean marine air and polluted air masses with continental origin. Marine influenced air masses prevailed throughout the region from 13 to 15 July 2004. On the evening of 15 July, the wind direction shifted from east-northeasterly to west-southwesterly flow, and persisted through 18 July. Figure 2.4 shows two representative backward trajectories for Thompson Farm simulated using the NOAA HYSPLIT transport and dispersion model [Draxler and Rolph, 2003] that correspond to

the origins of the marine (Figure 2.4a) and continentally (Figure 2.4b) influenced air masses encountered in the NH coastal region during this time period.

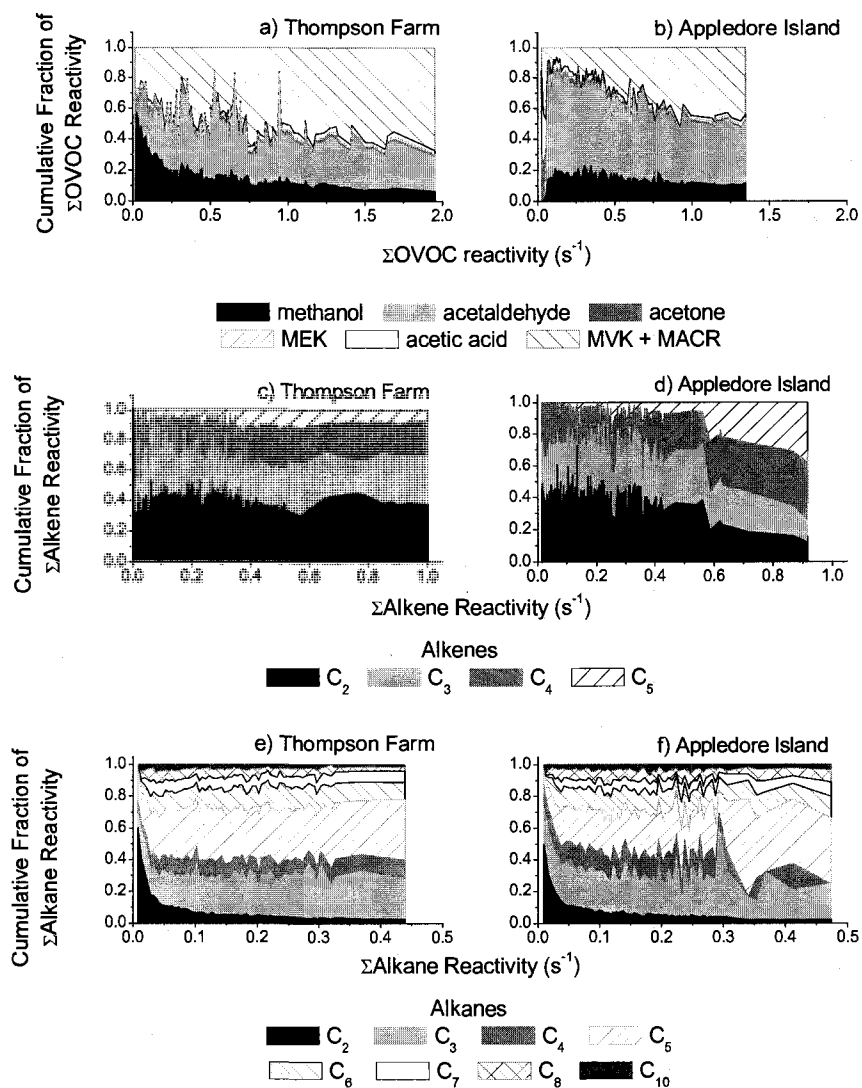


**Figure 2.3:** The cumulative fraction of summed ( $\Sigma$ ) OVOC reactivity attributable to each OVOC compound measured vs.  $\Sigma$ OVOC reactivity at a) Thompson Farm and b) Appledore Island; the cumulative fraction of  $\Sigma$ alkene reactivity attributable to alkenes separated by carbon number vs.  $\Sigma$ alkene reactivity at c) Thompson Farm and d) Appledore Island; and the cumulative fraction of  $\Sigma$ alkane reactivity attributable to alkanes separated by carbon number vs.  $\Sigma$ alkane reactivity at e) Thompson Farm and f) Appledore Island.

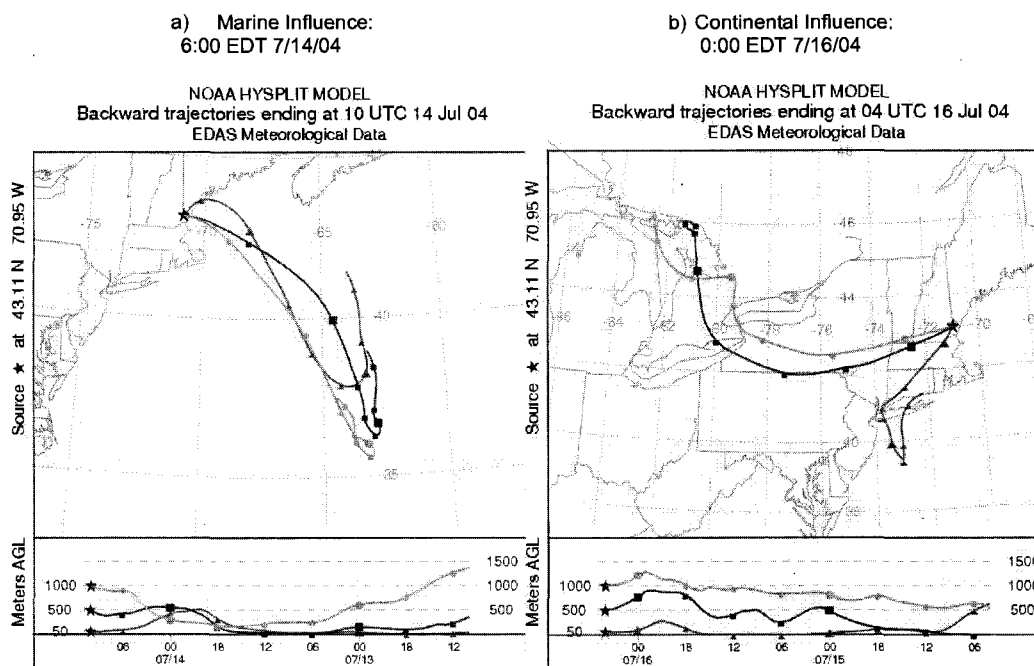


**Figure 2.4:** Characteristic NOAA HYSPLIT two-day backward trajectories indicating the shift in wind direction at Thompson Farm from a) east-northeasterly to b) west-southwesterly during the 13 to 19 July time period.

Figure 2.5 shows the contrast in reactivity between the marine and continentally influenced air masses observed at both sites from 13 to 19 July for alkanes, aromatics, biogenics, and OVOCs. For comparison, local wind speed during this time period is also shown in Figures 2.5c and d. At Thompson Farm, the marine influenced period spanning from 13 to 15 July still furnished significant alkane and aromatic reactivity, while biogenic and OVOC reactivity was generally limited (Figure 2.5a, c, e, and g). This is most likely attributable to mobile sources from two heavily traveled highways during the summer tourism season, U.S. Interstate I-95 and Route 1, and a network of smaller roads between Thompson Farm and the coast.

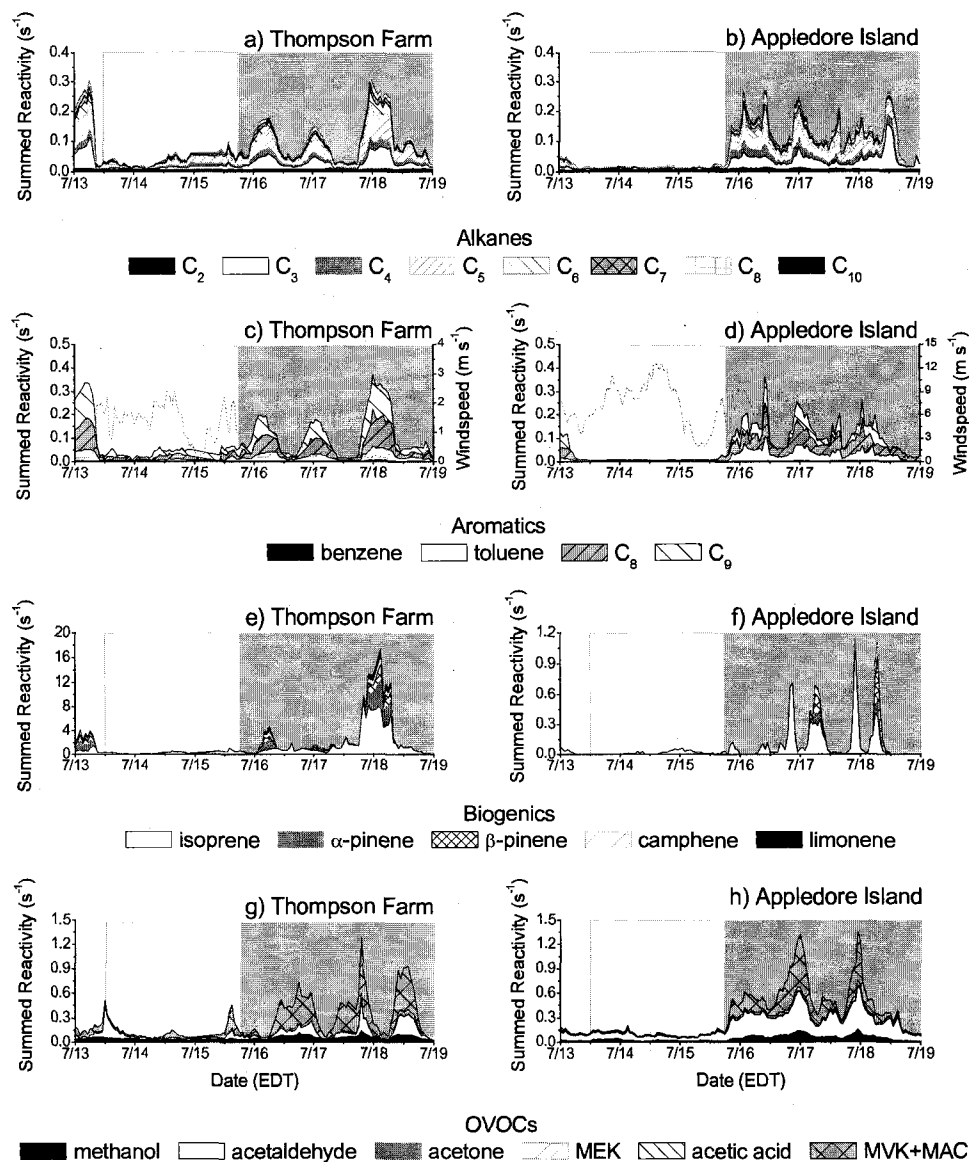


**Figure 2.5:** Marine and continental influences from 13 to 19 July on reactivities of a) and b) alkanes, c) and d) aromatics, e) and f) biogenic compounds, and g) and h) OVOCs at Thompson Farm and Appledore Island; respectively. The clear box indicates a period of marine influence with east-northeasterly air masses from 13 to 15 July. The gray box indicates a period of continental influence with west-southwesterly air masses from 15 July.

During continental outflow from 16 to 19 July, a diurnal pattern is clearly observable at Thompson Farm with nighttime reactivity maxima for alkane, aromatic and biogenic NMHCs and OVOC minima. Note that during 13 to 15 July, wind speeds generally remained above  $1 \text{ m s}^{-1}$  throughout the night whereas the nights of 16 to 19 July were calm. These stagnant conditions (wind speed  $< 0.5 \text{ m s}^{-1}$ ) occur frequently at Thompson Farm during the early morning and are characteristic of the stable nocturnal inversion layer observed at this site [Talbot *et al.*, 2005]. On these nights, poor ventilation coupled with regional emissions led to nighttime increases in alkane and aromatic mixing ratios and consequently higher VOC reactivity. Limited nighttime oxidation at Thompson Farm is further indicated by the build-up of isoprene and monoterpenes which are very reactive towards  $\text{NO}_3$  and  $\text{O}_3$ , the major oxidants at night. Minimal OVOC reactivity on these nights reflects significant deposition of these polar compounds, another characteristic feature of stable nocturnal inversion layer formation [Talbot *et al.*, 2005]. A quantitative assessment of the nocturnal VOC mixing ratio increases observed and their impact on regional emissions is addressed in Section 2.3.2.

At Appledore Island, the contrast between marine and continentally influenced air masses is particularly striking with minimal reactivity from 13 to 15 July and substantial enhancements for all VOCs from 16 to 19 July (Figures 2.5b, d, f, and h). The pattern for biogenic reactivity in continental outflow was unique compared to the other VOCs at Appledore, with limited time periods during which isoprene and the monoterpenes were actually detected. Evening peaks in isoprene (for example, 16 and 17 July, 1900-2300 LT on Figure 2.5f) generally coincided with significant increases in OVOC reactivity reflecting the outflow of daytime emissions and oxidation products. A second peak in

isoprene reactivity often occurred midmorning (for example, 17 and 18 July, 800-1100 LT on Figure 2.5f) and coincided with decreased OVOC reactivity and the presence of monoterpenes indicating the ventilation of nighttime enhancements in continental outflow.

### 2.3.2 NMHC Flux Estimates at Thompson Farm

Average hourly nighttime mixing ratio enhancements at Thompson Farm were used to estimate the net nighttime flux of several anthropogenic and biogenic hydrocarbons. This type of calculation is similar to the simple box models used for estimating nighttime O<sub>3</sub> deposition velocities [Hastie *et al.*, 1993; Talbot *et al.*, 2005], terrestrial methyl iodide emissions [Sive *et al.*, 2007], and marine halocarbon emissions [Zhou *et al.*, 2005]. In this study, we examine changes in NMHC measurements made at Thompson Farm under a nocturnal inversion layer. As described in detail by Mao and Talbot [2004a], weak wind conditions (<2 m s<sup>-1</sup>) are persistent (>70% of the time) at Thompson Farm during the night in summer. This low average nocturnal wind speed indicates transport was generally limited and there was minimal exchange between the nocturnal boundary layer and the residual layer above. Hence local sources and sinks were responsible for the net nighttime fluxes [Mao and Talbot, 2004a; Zhou *et al.*, 2005; Sive *et al.*, 2007]. Under these stagnant conditions, the net nighttime flux (NF) is the difference between local emissions (ER) and loss due to nighttime chemistry with NO<sub>3</sub> and O<sub>3</sub> (L<sub>NO3</sub> and L<sub>O3</sub>), advection (L<sub>A</sub>), and deposition (L<sub>D</sub>):

$$NF \text{ (molecules cm}^{-2} \text{ s}^{-1}\text{)} = ER - L_{NO_3} - L_{O_3} - L_A - L_D = \frac{d[C]}{dt} * ML \quad (2)$$

Net nighttime fluxes were calculated from the linear regression slopes ( $\frac{d[C]}{dt}$ ) of average hourly VOC concentrations reported in molecules  $\text{cm}^{-3}$  vs. time multiplied by the mixed layer height (*ML*). Only measurements from nights with wind speeds  $\leq 0.5 \text{ m s}^{-1}$  were included in the hourly averages to limit the influence of large scale horizontal advection on flux estimates. To minimize the effect of diurnal changes on the ML height overnight, fluxes were calculated using measurements from 0100-0400 LT only, when model estimates indicated the ML height at Thompson Farm is stable. As there were no ML measurements at Thompson Farm during ICARTT, the height of the ML was assumed to be 125 m which is the median value from the range (50 – 200 m) of nocturnal inversion layer heights measured at a variety of similar midlatitudinal rural locations. This range of ML thickness was obtained from the measurements over a flat plain in Wales [Galbally, 1968], a grass covered area of the Rhine river valley in Germany [Gusten *et al.*, 1998], and an agricultural clearing surrounded by forest in Ontario, Canada [Hastie *et al.*, 1993; Shepson *et al.*, 1992].

To assess the contribution of the major nighttime sinks to these net fluxes, estimates of loss flux rates due to reactions with  $\text{O}_3$  and  $\text{NO}_3$  ( $L_{\text{O}_3}$  and  $L_{\text{NO}_3}$ ) are also given in Table 2.3. These loss flux rates (molecules  $\text{cm}^{-2} \text{ s}^{-1}$ ) were calculated using the pseudo-first order rate equation below times the ML height:

$$L_{\text{O}_3\text{orNO}_3} = k_{\text{ox,NMHC}} * [\text{ox}]_{\text{O}_3\text{orNO}_3} * [\text{NMHC}] * \text{ML} \quad (3)$$

Table 2.4 gives the mean NMHC mixing ratios (from 0100-0400 LT when wind speeds  $\leq 0.5 \text{ m s}^{-1}$ ; values converted to molecules  $\text{cm}^{-3}$  for loss flux rate calculation) and literature rate constants,  $k_{\text{ox,NMHC}}$ . The mean concentration of  $\text{O}_3$  ([ox]) for these same time periods was  $3 (\pm 2) \times 10^{11}$  molecules  $\text{cm}^{-3}$  or  $12 \pm 8$  ppbv. Because  $\text{NO}_3$  was not

measured at Thompson Farm during the ICARTT campaign, its concentration was estimated as  $3 (\pm 4) \times 10^6$  molecules  $\text{cm}^{-3}$  or  $0.1 \pm 0.1$  pptv by assuming equilibrium between its production mechanism, reaction of  $\text{NO}_2$  and  $\text{O}_3$ , and its major loss mechanism, reaction with isoprene and monoterpenes. A full description of this type of calculation is given by *Goldan et al.* [1995]. Because NMHCs are not likely to be lost through physical processes like dry and wet deposition [*Singh and Zimmerman, 1992*],  $L_d$  was assumed to be negligible. Loss due to advection ( $L_a$ ) was also negligible under the weak wind conditions selected. As a result, gross emission rates (ER) listed in Table 2.3 were calculated as the sum of NF,  $L_{\text{O}_3}$ , and  $L_{\text{NO}_3}$ . It should be noted that errors given in Table 2.3 do not include uncertainty due to estimating the ML height.

The NMHCs that exhibited significant positive nighttime net fluxes during the ICARTT campaign are listed in Table 2.3. Considering the dominant biogenic influence at Thompson Farm, the strong positive net fluxes for the monoterpenes is not surprising. The most abundant monoterpene at Thompson Farm,  $\alpha$ -pinene, also had the highest nighttime net flux rate ( $6 (\pm 2) \times 10^9$  molecules  $\text{cm}^{-2} \text{s}^{-1}$ ), over twice that of  $\beta$ -pinene ( $1.8 (\pm 0.4) \times 10^9$  molecules  $\text{cm}^{-2} \text{s}^{-1}$ ) and over four times that of camphene or limonene ( $1.2 (\pm 0.6) \times 10^9$  and  $4 (\pm 5) \times 10^8$  molecules  $\text{cm}^{-2} \text{s}^{-1}$ ). Estimated loss rates for these reactive compounds were comparable to net fluxes with highest  $L_{\text{O}_3}$  and  $L_{\text{NO}_3}$  rates attributable to  $\alpha$ -pinene ( $6 (\pm 8) \times 10^9$  and  $5 (\pm 30) \times 10^9$  molecules  $\text{cm}^{-2} \text{s}^{-1}$ , respectively). The fact that positive nighttime net fluxes were still observed for all the monoterpenes reflects significantly higher monoterpene gross emission rates that effectively dominate nighttime chemistry at Thompson Farm. Our estimates were comparable to nighttime biogenic

Compound	Net Flux ( $\pm$ err) (molecules/cm <sup>2</sup> /sec)	r <sup>2</sup>	Loss to O <sub>3</sub> ( $\pm$ err) (molecules/cm <sup>2</sup> /sec)	Loss to NO <sub>3</sub> ( $\pm$ err) (molecules/cm <sup>2</sup> /sec)	Emission Rate ( $\pm$ err) (molecules/cm <sup>2</sup> /sec)
$\alpha$ -pinene	6 ( $\pm$ 2) x 10 <sup>9</sup>	0.85	6 ( $\pm$ 8) x 10 <sup>9</sup>	5 ( $\pm$ 30) x 10 <sup>9</sup>	2 ( $\pm$ 3) x 10 <sup>10</sup>
$\beta$ -pinene	1.8 ( $\pm$ 0.4) x 10 <sup>9</sup>	0.91	5 ( $\pm$ 5) x 10 <sup>8</sup>	9 ( $\pm$ 30) x 10 <sup>8</sup>	3 ( $\pm$ 3) x 10 <sup>9</sup>
camphene	1.2 ( $\pm$ 0.6) x 10 <sup>9</sup>	0.65	2 ( $\pm$ 2) x 10 <sup>7</sup>	2 ( $\pm$ 4) x 10 <sup>8</sup>	1.4 ( $\pm$ 0.7) x 10 <sup>9</sup>
limonene	4 ( $\pm$ 5) x 10 <sup>8</sup>	0.26	1 ( $\pm$ 2) x 10 <sup>7</sup>	1 ( $\pm$ 1) x 10 <sup>9</sup>	3 ( $\pm$ 2) x 10 <sup>9</sup>
propane	9 ( $\pm$ 2) x 10 <sup>9</sup>	0.92	1 ( $\pm$ 0.8) x 10 <sup>3</sup>	3 ( $\pm$ 20) x 10 <sup>5</sup>	9 ( $\pm$ 2) x 10 <sup>9</sup>

**Table 2.3:** Positive net nighttime flux (NF), estimated O<sub>3</sub> and NO<sub>3</sub> loss (L<sub>O<sub>3</sub></sub> and L<sub>NO<sub>3</sub></sub>), and total emission (ER) rates for NMHCs at Thompson Farm during ICARTT 2004. All rates based upon nighttime measurements from 0100-0400 LT when windspeeds were  $\leq 0.5$  m s<sup>-1</sup>. The NF error is the standard error of the regression slope and r<sup>2</sup> is the coefficient of determination indicating how well the linear regression relationship fits the average hourly data. The L<sub>O<sub>3</sub></sub> and L<sub>NO<sub>3</sub></sub> errors are propagated from the standard deviations of the oxidant and NMHC concentrations from 0100-0400 LT under stagnant conditions. The ER errors are propagated from the errors in NF, L<sub>O<sub>3</sub></sub>, and L<sub>NO<sub>3</sub></sub>.

Compound	Mean MR $\pm$ standard deviation (pptv)	k <sub>O<sub>3</sub></sub>		k <sub>NO<sub>3</sub></sub>	
		(cm <sup>3</sup> /molecules/s)	reference	(cm <sup>3</sup> /molecules/s)	reference
NO <sub>2</sub>	2000 $\pm$ 1000	3.5 x 10 <sup>-17</sup>	Atkinson [2004]		
$\alpha$ -pinene	800 $\pm$ 800	8.7 x 10 <sup>-17</sup>	Atkinson [1997]	6.2 x 10 <sup>-12</sup>	Atkinson [1997]
$\beta$ -pinene	300 $\pm$ 300	1.5 x 10 <sup>-17</sup>	Atkinson [1997]	2.5 x 10 <sup>-12</sup>	Atkinson [1997]
camphene	300 $\pm$ 200	9.0 x 10 <sup>-19</sup>	Atkinson [1997]	6.6 x 10 <sup>-13</sup>	Atkinson [1997]
limonene	80 $\pm$ 80	2.0 x 10 <sup>-16</sup>	Atkinson [1997]	1.2 x 10 <sup>-11</sup>	Atkinson [1997]
propane	1500 $\pm$ 800	6.8 x 10 <sup>-23</sup>	Fatemi [2005]	1.7 x 10 <sup>-17</sup>	Atkinson [1997]

**Table 2.4:** Mean mixing ratios for selected NMHCs from 0100-0400 LT on nights with windspeeds  $\leq 0.5$  m s<sup>-1</sup> and the rate constants and literature references used for calculating L<sub>O<sub>3</sub></sub> and L<sub>NO<sub>3</sub></sub> in Table 2.3.

emissions inventory estimates for the area ( $1 \times 10^{10}$  molecules  $\text{cm}^{-2} \text{s}^{-1}$  at 0100 LT, SMOKE v2.1 biogenic emission inventory: <http://www.smoke-model.org/data.cfm>).

Propane had the highest net flux rate at Thompson Farm ( $9 (\pm 2) \times 10^9$  molecules  $\text{cm}^{-2} \text{sec}^{-1}$ ). Because propane is not reactive towards  $\text{O}_3$  or  $\text{NO}_3$ , loss rates were minimal and the net flux rate can be considered an estimate of propane emission. This high emission rate reflects widespread LPG leakage from storage tanks throughout the seacoast region of NH which is discussed in Section 2.3.3.

### 2.3.3 The Influence of LPG Leakage Sources

Continuous measurements of NMHCs at Thompson Farm since 2002 have revealed that large enhancements of propane as well as other constituents (i.e., *i*-butane, *n*-butane, *i*-pentane, *n*-pentane and the alkenes) of LPG leakage, are observed regularly at this site (unpublished data provided by B. Sive, 2002-2007). During these events, propane was the dominant NMHC with mixing ratios that were at least 2-3 times larger than ethane which is typically the most abundant NMHC in the atmosphere. For the ICARTT campaign time period, the pronounced nighttime propane enhancement is accentuated by comparing the hourly mixing ratios of propane and ethane (Figure 2.6). On average, propane mixing ratios increased by  $\sim 1$  ppbv overnight, while some individual nights experienced enhancements  $> 3$  ppbv. In contrast, ethane levels remained relatively consistent throughout day and night over the same time period.

To determine whether the propane flux estimated in Table 2.3 reflects an isolated source near Thompson Farm or regional LPG leakage, measurements from the 2004 ICARTT campaign were compared to diurnal measurements made the previous year at six locations throughout the seacoast area of New Hampshire as part of a coastal study on

marine emissions of short-lived halocarbons [Zhou *et al.*, 2005] (Figure 2.7). On 18 to 19 August 2003, samples were collected hourly at 5 sites throughout the Great Bay region in addition to our continuous measurements at Thompson Farm (see Figure 2.1). The diurnal propane and ethyne mixing ratios are shown in Figure 2.7a and b for all six sampling sites. Nocturnal inversion layer formation was distinctly suggested by the diurnal cycles of wind speed,  $j_{\text{NO}_2}$ , and  $\text{O}_3$  observed at Thompson Farm with weak wind conditions and depleted  $\text{O}_3$  overnight followed by clear skies the next day [Talbot *et al.*, 2005] (Figures 2.7c and d). On such nights, the buildup of anthropogenic tracers is most visible due to minimal ventilation and continuous emissions. The most notable features common to all sites were that i) propane levels increased from approximately 200 pptv during the day to the 2-4 ppbv overnight while the increases in ethyne only averaged 500 pptv, and ii) propane enhancements observed at Thompson Farm were actually below the average for the seacoast region of New Hampshire.

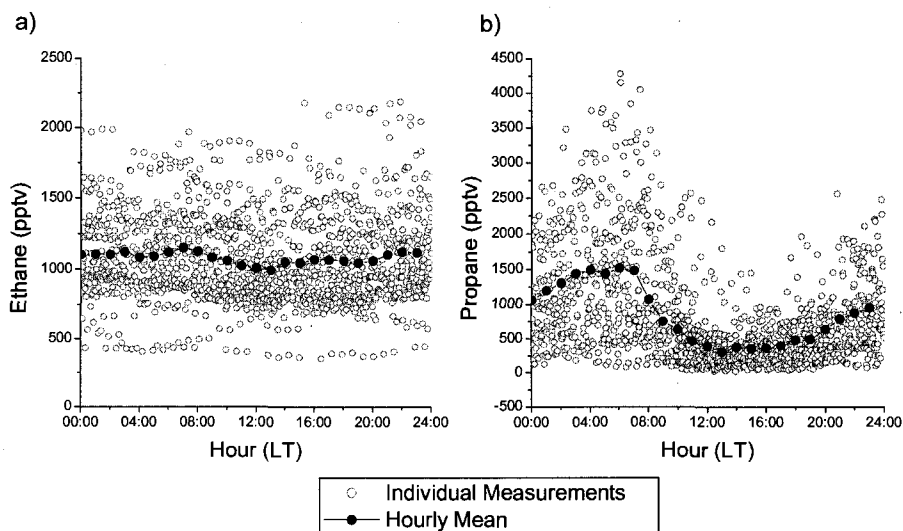


**Figure 2.6:** Hourly mixing ratios of ethane and propane at Thompson Farm during ICARTT 2004.

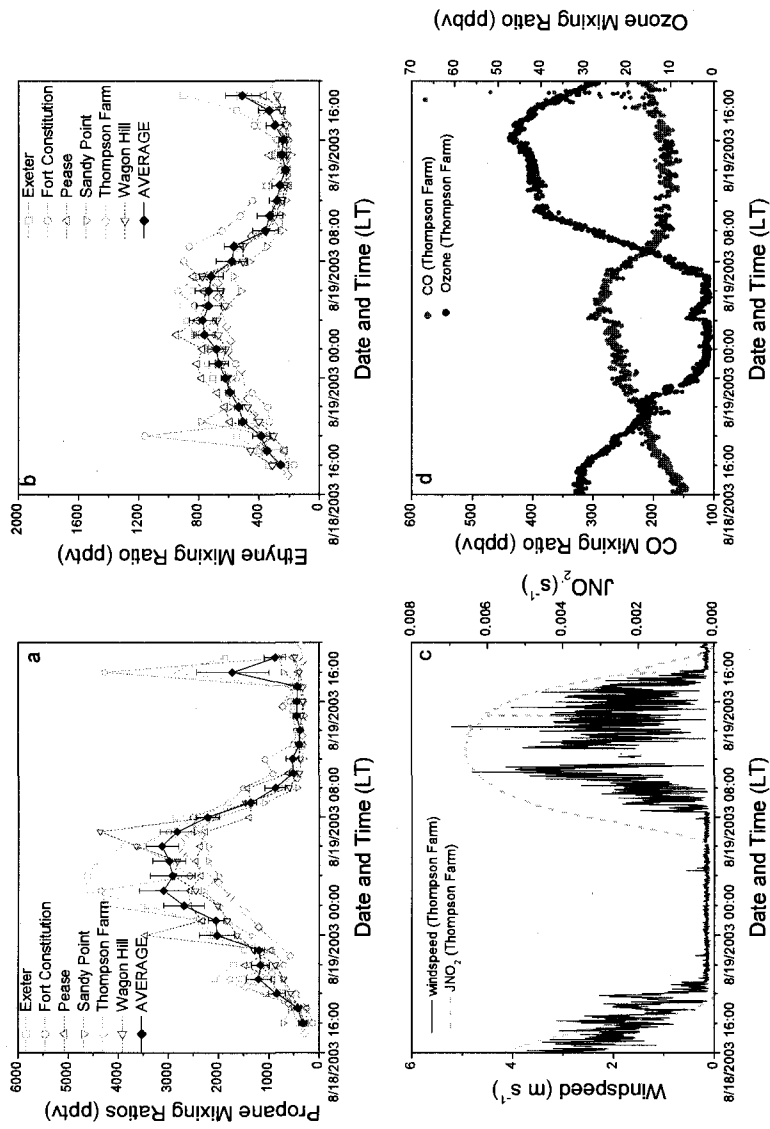


**Figure 2.7:** Results of a regional diurnal campaign from August 2003 at six sites in the New Hampshire seacoast region for a) propane and b) ethyne. Wind speed and  $J_{NO_2}$ , the  $NO_2$  photolysis rate constant, at Thompson Farm during this same time period are displayed in 2.7c to indicate day/night differences and show conditions for the formation of stable nocturnal boundary layer. The nighttime depletion of  $O_3$  and increase in CO mixing ratios, characteristics of the stable nocturnal inversion formation at Thompson Farm, are shown for the night of the study in 2.7d.

The net flux rates were estimated from 0100-0400 LT for the key constituents of LPG leakage at Thompson Farm together with all other sites sampled during the 2003 diurnal study (Table 2.5). Net propane fluxes were consistently a full order of magnitude larger than any other NMHC flux observed indicating a widespread distribution of localized sources throughout the region. The regional average and individual Thompson Farm propane net fluxes calculated for this night ( $3 (\pm 1)$  and  $2.31 (\pm 0.07) \times 10^{10}$  molecules  $\text{cm}^{-2} \text{s}^{-1}$ , respectively) were also comparable to the net flux calculated for the ICARTT campaign the following year ( $9 (\pm 2) \times 10^9$  molecules  $\text{cm}^{-2} \text{s}^{-1}$ ). In addition to propane, smaller positive net fluxes were observed at Thompson Farm for some of the minor components commonly found in LPG like the butanes, i-pentane, ethene, propene, and 1-butene [Blake and Rowland, 1995; Chen et al., 2001]. However, positive fluxes for these compounds were not a consistent feature across the region which probably reflects the variable composition of these components in LPG [Blake and Rowland, 1995] combined with the different nearby source distributions at each sampling location.

Compound	Thompson Farm		Average of all 6 locations	
	NF ( $\pm$ err) (molecules $\text{cm}^{-2} \text{s}^{-1}$ )	$r^2$	NF ( $\pm$ err) (molecules $\text{cm}^{-2} \text{s}^{-1}$ )	$r^2$
Propane	$2.31 (\pm 0.07) \times 10^{10}$	0.99	$3 (\pm 1) \times 10^{10}$	0.72
Ethene	$3.6 (\pm 0.6) \times 10^9$	0.95	$2 (\pm 2) \times 10^9$	0.31
Propene	$1.8 (\pm 0.6) \times 10^9$	0.81	$-4 (\pm 5) \times 10^8$	0.21
i-butane	$1.0 (\pm 0.1) \times 10^9$	0.97	$-2 (\pm 2) \times 10^8$	0.31
n-butane	$1.4 (\pm 0.5) \times 10^9$	0.79	$-7 (\pm 12) \times 10^8$	0.15
i-pentane	$2 (\pm 1) \times 10^9$	0.74	$-3 (\pm 4) \times 10^9$	0.28
1-butene	$3.2 (\pm 0.2) \times 10^8$	0.99	$-3 (\pm 1) \times 10^8$	0.89

**Table 2.5:** Estimates of net nighttime flux (NF) for select NMHCs during the diurnal study conducted in the New Hampshire seacoast area on 18 to 19 August 2003. Fluxes were calculated as the linear regression slope of average 0100-0400 LT hourly concentrations in molecules/ $\text{cm}^3$  times estimated planetary boundary layer height in cm vs. time. The error is the standard error of the regression slope and  $r^2$  is the coefficient of determination indicating how well the linear regression relationship fits the average hourly data.

The propane emission rates observed at Thompson Farm during the ICARTT campaign and the six sampling sites from the previous summer are significant, particularly for such rural sites located far from upwind urban and industrial source regions. Estimates of propane emission in more densely populated urban areas, such as Santiago, Chile [Chen *et al.*, 2001] and Mexico City, Mexico [Blake and Rowland, 1995], are two orders of magnitude larger than observed at Thompson Farm. For example, LPG leakage in Santiago, Chile, contributes 80 tons of propane per day to the 525 km<sup>2</sup> study area, or  $2 \times 10^{12}$  molecules/cm<sup>2</sup>/sec [Chen *et al.*, 2001]. However, LPG use occurs throughout northern New England as approximately 11% of the energy consumed for residential heating and cooking in rural New Hampshire, Maine, and Vermont is derived from LPG, more than twice the national average of 4.5% [Energy Information Administration, 2005]. Assuming the rate of emission calculated for Thompson Farm during the ICARTT campaign is applicable to all of New Hampshire, Maine, and Vermont with a combined land area of 135,000 km<sup>2</sup>, over 80 tons of propane are emitted into northern New England on a daily basis. A more detailed spatial survey is currently underway to better constrain this regional propane emission estimate. However, this initial approximation indicates that widespread LPG leakage is a major propane source to the region.

The extent of LPG leakage influence on propane mixing ratios regionally is further emphasized by a comparison of propane-to-benzene ratios at Thompson Farm and Appledore Island to gasoline evaporation (mean =  $2.0 \pm 0.4$  st.dev.) source ratios (Table 2.6 and Figure 2.8). The vehicle exhaust source ratio (mean =  $0.5 \pm 0.2$  st.dev.) is not

shown in Figures 2.8a and b as it is well below the range of values observed at either site. These source ratios were calculated from published hydrocarbon emission profiles for a variety of tunnel [Conner *et al.*, 1995; Fraser *et al.*, 1998; Kirchstetter *et al.*, 1996; McGaughey *et al.*, 2004; Rogak *et al.*, 1998; Sagebiel *et al.*, 1996] and gasoline headspace [Conner *et al.*, 1995] studies.

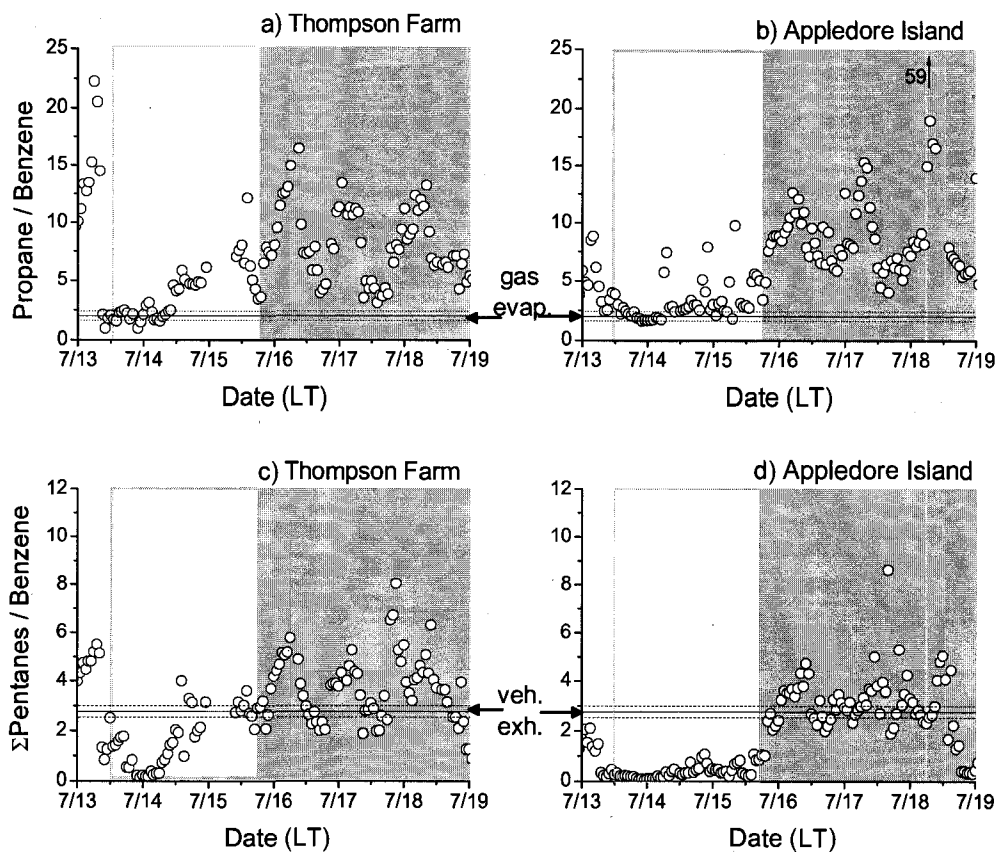


**Figure 2.8:** Time series of a) Thompson Farm and b) Appledore Island propane-to-benzene ratios and c) Thompson Farm and d) Appledore Island  $\Sigma$ pentane (n-pentane, i-pentane, and cyclopentane)-to-benzene ratios. The solid and dashed horizontal lines represent the mean and error for literature propane-to-benzene gasoline evaporation source ratios and  $\Sigma$ pentane-to-benzene vehicle exhaust source ratios as described in the text. The vertical arrow on 8b indicates measured propane-to-benzene ratios were off-scale on 18 July from 1000 – 1300 with a maximum of 59 at 1100. Clear and gray boxes denote the period of marine influence with east-northeasterly air masses from 13 to 15 July and continental influence with west-southwesterly air masses from 16 to 19 July.

At Thompson Farm, the low levels of propane-to-benzene ratios observed in the cleanest marine air encountered from 13 to 14 July were consistent with gasoline evaporation sources (Figure 2.8a). As coastal influences increased from 14 to 15 July, so did propane mixing ratios reflecting increasing inputs from LPG leakage sources. The highest propane-to-benzene mixing ratios at Thompson Farm generally occurred during low wind speed nights like those observed from 16 to 19 July. In addition to these nighttime enhancements, daytime propane-to-benzene ratios also reflected significant LPG leakage influence. Both daytime and nighttime means throughout the ICARTT campaign ( $8 \pm 5$  and  $11 \pm 6$ , respectively) were elevated well above the expected ratios from either vehicle exhaust or gasoline evaporation.

At Appledore Island, the impact of continental outflow of propane from regional LPG leakage during ICARTT was clearly seen (Figure 2.8b). While the ratio of propane-to-benzene throughout the measurement campaign (mean =  $9 \pm 6$ ) was well above both vehicle exhaust and gasoline evaporation source ratios, there was a clear demarcation between periods of marine and continental flow. The mean propane-to-benzene ratio rapidly increased from  $6 \pm 6$  in marine air masses to  $9 \pm 6$  in continental outflow with a maximum of 59 reached on 18 July 2004. Because propane is relatively long-lived compared to other NMHCs, such large inputs to air masses transported off of the continent across the Atlantic Ocean could also significantly impact tropospheric ozone production, particularly in downwind locations such as Europe.

#### 2.3.4 Influence of Gasoline Evaporation Sources

In summer 2002, comparison of measured total ( $\Sigma$ ) pentene (1-pentene, 2-methyl-2-butene, cis- and trans-2-pentene)-to-benzene ratios to source ratios was used to identify

significant fuel evaporation influences on fresh plumes coming off the Portsmouth/Kittery region of the New Hampshire coast [Goldan *et al.*, 2005]. This ratio was calculated using our measurements during ICARTT to determine if these episodes of fuel evaporation influence also occurred in the region in 2004 (Table 2.6). The vehicle exhaust and fuel evaporation source ratios given in Table 2.6 were calculated from published hydrocarbon emission profiles for a variety of tunnel [Conner *et al.*, 1995; Fraser *et al.*, 1998; Kirchstetter *et al.*, 1996; McGaughey *et al.*, 2004; Rogak *et al.*, 1998; Sagebiel *et al.*, 1996] and gasoline headspace [Conner *et al.*, 1995] studies.

At Thompson Farm and Appledore Island, the average ratio of  $\Sigma$ pentene-to-benzene throughout the campaign ( $0.16 \pm 0.12$  and  $0.18 \pm 0.21$ , respectively) was much closer to the expected ratio for vehicle exhaust ( $0.6 \pm 1.8$ ) and almost three orders of magnitude lower than those from gasoline evaporation ( $10 \pm 1$ ) (Table 2.6). However, actual pentene mixing ratios never exceeded 60 pptv at Thompson Farm or 250 pptv at Appledore Island, well below the  $>1$  ppbv levels Goldan *et al.* [2005] observed in the 2002 alkene plume off the New Hampshire coast. In areas downwind of major sources such as Thompson Farm and Appledore Island, low  $\Sigma$ pentene-to-benzene ratios do not exclude the potential influence of gasoline evaporative emissions on VOC distribution because lower ratios could simply reflect a greater degree of air mass photochemical processing with more reactive pentenes removed faster than benzene.

As pentanes are also elevated in fuel evaporation emissions [Conner *et al.*, 1995] and longer lived than pentenes [Atkinson, 1997], we also examined total measured ( $\Sigma$ ) pentane (n-pentane, i-pentane, and cyclopentane) to benzene ratios at both sites. Averaged over the entire ICARTT campaign, the  $\Sigma$ pentane-to-benzene ratios at

Thompson Farm and Appledore Island ( $3.8 \pm 1.7$  and  $2.6 \pm 1.9$ , respectively) were more consistent with a vehicle exhaust source signature ( $2.8 \pm 0.2$ ) than with fuel evaporation ( $47 \pm 3$ ) (Table 2.6). However, there was a wide degree of variability reflecting episodes of high pentane-to-benzene ratios at both locations (Figure 2.8c and d). At Thompson Farm, this variability was defined by a diurnal pattern of nighttime highs (mean =  $4.2 \pm 1.5$ ) and daytime lows (mean =  $3.6 \pm 1.8$ ) that was intermittently punctuated by short-term (2 to 6 hour) peak pentane-to-benzene events (for example, 1900-2100 LT 17 July, Figure 2.8c). There were ten of these short term peak events observed at Thompson Farm during ICARTT with maximum  $\Sigma$ pentane-to-benzene ratios ranging between 8 and 14. At Appledore Island,  $\Sigma$ pentane-to-benzene ratio variability reflected minimum values in clean marine air masses (mean =  $1.2 \pm 1.2$  st.dev.) and higher continental values (mean =  $2.8 \pm 1.9$  st.dev.) interspersed by seven different 2 to 6 hour peak pentane-to-benzene events with maxima from 7 to 17.

To further analyze the conditions under which fuel evaporation is significant at each site, the characteristic hydrocarbon ratios and HYSPLIT back trajectories for

Hydrocarbon Ratio	<u>Thompson Farm</u>		<u>Appledore Island</u>		Vehicle Exhaust	Fuel Evaporation
	All data	7/27/04 12:00 EDT	All data	7/26/04 8:00 EDT		
$\Sigma$ pentenes / benzene	$0.16 \pm 0.12$	0.12	$0.18 \pm 0.21$	1.6	$0.6 \pm 1.8$	$10 \pm 1$
$\Sigma$ pentanes / benzene	$3.8 \pm 1.7$	14	$2.6 \pm 1.9$	16	$2.8 \pm 0.2$	$47 \pm 3$
1-pentene / 1,2,4 tmb	$0.27 \pm 0.15$	0.18	$0.40 \pm 0.24$	1.8	$0.25 \pm 0.04$	$16 \pm 3$
1-pentene / 1,2,3-tmb	$1.0 \pm 0.4$	2.6	$1.5 \pm 0.9$	6.9	$1.0 \pm 0.2$	$70 \pm 10$
propane / benzene	$9.5 \pm 5.6$	19	$9.0 \pm 6.3$	13	$0.45 \pm 0.16$	$2.0 \pm 0.4$

**Table 2.6:** Representative hydrocarbon ratios at Thompson Farm and Appledore Island. Ratios are reported as mean  $\pm$  standard deviation for all data at Thompson Farm and Appledore Island. The ratios associated with the high  $\Sigma$ pentane-to-benzene ratio events corresponding to the trajectories in Figure 11 are also reported. The vehicle exhaust and fuel evaporation ratios are the mean  $\pm$  standard deviation for published tunnel and gasoline evaporation studies as described in the text.

representative high  $\Sigma$ pentane-to-benzene events were examined for two cases (Table 2.6; Figure 2.9). On 26 July,  $\Sigma$ pentane-to-benzene ratios at Appledore Island increased from a minimum of 2 at 2:00 EDT to 16 by 8:00 EDT. Short lived alkenes indicative of recent/local source influences were also significant in this air mass with  $\Sigma$ pentene-to-benzene ratios reaching the peak value observed at Appledore Island (1.6) by 0800 LT (Table 2.6). The highest  $\Sigma$ pentane-to-benzene events at both sites were often associated with air masses that had come from Maine and eastern Canada as suggested by the 24 hour backward trajectories in Figure 2.9. Population in this sector is concentrated in the southern coastal counties of Maine [U.S. Census Bureau, 2006] and fuel evaporation from mobile sources and refueling activities along the network of highways and local roads in this area is a likely pentane source.

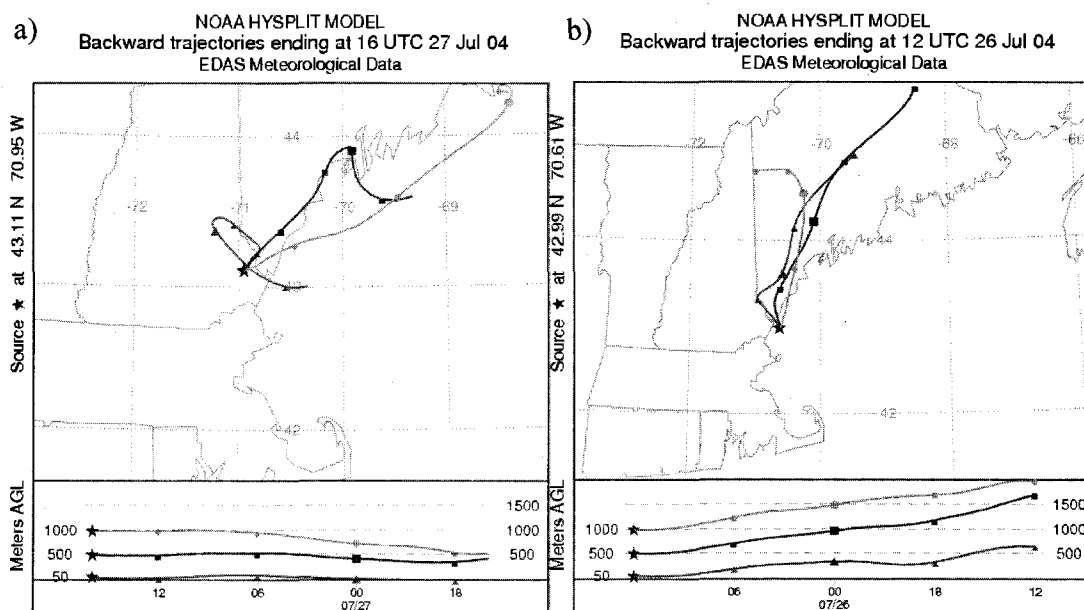


**Figure 2.9:** 24 hour HYSPLIT backward trajectories showing air mass flow during peak pentane to benzene events at a) Thompson Farm and b) Appledore Island.

Additional indicators of fuel evaporation that are less sensitive to air mass photochemical processing between source and measurement are the ratios of 1-pentene-to-1,2,4-trimethylbenzene (tmb) and to-1,2,3-tmb. The compounds 1-pentene, 1,2,4-tmb, and 1,2,3-tmb have similar OH rate constants and their source ratios for vehicle exhaust and gasoline evaporation are significantly different (Table 2.6). At Appledore Island on 26 July, the ratios of 1-pentene-to-1,2,4-tmb and 1-pentene-to-1,2,3-tmb at 0800 LT were 1.8 and 6.9, respectively, a factor of 7 higher than the representative range for vehicle exhaust ( $0.25 \pm 0.04$  and  $1.0 \pm 0.2$ , respectively). While these values were still below the range observed for gasoline evaporation ( $16 \pm 3$  and  $70 \pm 10$ , respectively), they do indicate that emissions from unburned fuel were a significant component of the VOCs observed at Appledore Island that morning. During this time period, air masses traveled over Maine and southern New Hampshire before reaching the Island (Figure 2.9b). This is consistent with the observations of *Goldan et al.* [2005] off the coast of New Hampshire of short term fuel evaporation influence on an early morning alkene plume coming from the Portsmouth/Kittery region.

In contrast, the ratios of 1-pentene-to-1,2,4-tmb and -1,2,3-tmb during the 27 July high  $\Sigma$ pentane-to-benzene event at Thompson Farm (0.18 and 2.6, respectively) were closer to vehicle exhaust source signatures reflecting a smaller influence from fuel evaporation sources (Table 2.6). The  $\Sigma$ pentene-to-benzene ratio also fell below the vehicle exhaust source signature suggesting greater photochemical processing of the air mass prior to sampling. The prevailing conditions at Thompson Farm that day were overcast with low wind speeds, as indicated by the circling back trajectory near the surface which was vertically stratified from higher elevations (Figure 2.9a). Reduced

direct sunlight and minimal vertical mixing would slow down oxidation of the less reactive pentanes relative to the pentenes, which most likely resulted in the high daytime pentane-to-benzene ratios observed.

#### **2.4 Conclusions**

Our analysis indicates that biogenic compounds were the most significant contributor to regional VOC chemistry on the New Hampshire seacoast during the ICARTT campaign. Vegetative emissions dominated local VOC reactivity, particularly at Thompson Farm where calculations of significant nighttime net monoterpene fluxes reflected large gross emission rates that effectively overwhelmed nighttime chemistry at the site. OVOCs were the second largest component of Thompson Farm reactivity and the largest VOC contributor to reactivity at Appledore Island. The secondary production of MVK+MACR from isoprene was a significant regional process and MVK+MACR were major components of OVOC reactivity at both sites. Local anthropogenic VOC sources, such as LPG leakage and gasoline evaporation, also influenced NMHC distribution at both sites, particularly for propane and the pentanes. Gasoline evaporation was an episodic source of pentanes in the seacoast area compared to vehicle exhaust sources. In contrast, propane was significantly enhanced above vehicle exhaust and gasoline evaporation source ratios throughout the measurement period at both sites. Estimates of propane emission at Thompson Farm suggest that widespread LPG leakage throughout northern New England is a major propane source impacting regional VOC distribution. An additional study is currently underway to assess more comprehensively the geographical extent of LPG leakage throughout New England and its impact on regional VOC budgets and down-wind O<sub>3</sub> production.

## CHAPTER 3

### ARE BIOGENIC EMISSIONS A SIGNIFICANT SOURCE OF SUMMERTIME ATMOSPHERIC TOLUENE IN THE RURAL NORTHEAST?

#### **3.1 Introduction**

Toluene is a ubiquitous aromatic volatile organic compound (VOC) in the troposphere [Dewulf and Van Langenhove, 1997; Singh *et al.*, 1985] that has been classified by the United States Environmental Protection Agency (U.S. EPA) as an air toxic for its detrimental effects on human central nervous system function with acute exposure [Goldhaber *et al.*, 1995]. Its oxidation in the presence of nitrogen oxides (NO<sub>x</sub>) can lead to tropospheric ozone formation, a secondary pollutant and respiratory irritant [Wang *et al.*, 1998]. Low volatility oxidation products can also partition into particulate matter becoming a significant component of fine aerosol mass [Schauer *et al.*, 2002]. This is of particular importance to air quality in rural environments as recent studies indicate that secondary organic aerosol (SOA) formation from aromatic precursors, including toluene, is substantially faster under low NO<sub>x</sub> conditions than under high NO<sub>x</sub> conditions [Ng *et al.*, 2007].

Toluene sources are primarily anthropogenic and include combustion, fuel evaporation, solvent usage, and industrial processes [Singh and Zimmerman, 1992]. It is often assumed that these sources are concentrated in urban areas and have emission rates that are consistently proportional to benzene, another widely distributed aromatic VOC and air toxic with similar anthropogenic sources. These assumptions, along with several

others regarding sinks and air mass mixing, allow the use of toluene/benzene ratios in characterizing air mass photochemical age at non-urban locations (e.g. [*deGouw et al.*, 2005; *Gelencser et al.*, 1997; *Warneke et al.*, 2007]).

However, the discovery of elevated warm season toluene mixing ratios at a rural site in northern New England brings these assumptions into question [*R.S. Russo et al.*, Long Term Measurements of Nonmethane Hydrocarbons and Halocarbons in New Hampshire (2004-2008): Seasonal Variations and Regional Sources, in preparation, 2008. Hereinafter referred to as *R.S. Russo et al.*, 2008, *in preparation*]. In the long-term data set of daily VOC measurements made at Thompson Farm in coastal New Hampshire, toluene followed a significantly different seasonal pattern than benzene and other common anthropogenic tracers which usually reached their minimum levels during summer. The presence of elevated toluene mixing ratios from late spring to early fall at this rural location, even in well-processed air masses, could reflect several influences including a seasonal cycle in urban anthropogenic emissions of toluene and/or an unidentified local warm season source.

Any seasonal cycle in urban anthropogenic toluene emissions most likely reflects changes in reformulated gasoline (RFG) hydrocarbon content to meet U.S. EPA mandated VOC volatility requirements from June 1 to September 15 of each year [*Romanow*, 2008]. To fulfill these requirements and meet fuel octane grades in summer, refineries often replace more volatile high octane compounds such as n-butane with heavier alkanes and aromatic compounds in their gasoline formulations [*Gary and Handwerk*, 2001; *Lough et al.*, 2005]. An analysis of individual hydrocarbon compound content in 2000-2001 summer and winter RFG samples from Milwaukee, Wisconsin,

indicated that toluene exhibited the largest summertime increase of all hydrocarbons increasing from 1% (weight) of fuel in winter to approximately 10% in summer [Lough *et al.*, 2005]. While tunnel studies in the Milwaukee area indicated that these changes in fuel content did not significantly alter toluene emissions or toluene-to-benzene ratios from mobile source exhaust, they did affect the percent hydrocarbon composition of fuel headspace vapors with toluene, i-pentane, and 2,2,4-trimethylpentane exhibiting the largest percent increase for summertime fuels [Lough *et al.*, 2005]. The effect these seasonal gasoline content changes could have on fuel evaporation sources suggests a distinct yearly cycle in urban toluene emissions which must be considered in evaluating seasonal toluene variability in New England.

Local plants may also be seasonal toluene sources with particular significance in extensively vegetated rural areas such as northern New England. In a series of laboratory enclosure experiments, Heiden *et al.* [1999] showed that isotopically labeled  $^{13}\text{C}$  taken up by sunflowers was emitted as  $^{13}\text{C}$  labeled toluene. In the same study, a combination of laboratory and field experiments indicated that toluene emission rates for sunflowers and pine trees increased with plant stress (e.g., pathogen attack, low nutrients, leaf wounding). Considering the significant influence regional biogenic VOC emissions have on tropospheric chemistry in coastal New England [Griffin *et al.*, 2004; Mao *et al.*, 2006a; White *et al.*, 2008], the potential contribution of vegetative toluene emissions in seasonal toluene enhancements at Thompson Farm warrants exploration.

Elevated toluene mixing ratios at rural locations have also been previously attributed to local industrial emissions. VOC measurements made as part of the Southern Oxidants Study in June 1995 revealed significant toluene enhancements at New

Hendersonville, Tennessee, which correlated strongly with winds coming from the direction of a regional toluene emitting industrial facility [McClenny *et al.*, 1998]. Such observations highlight the impact that local anthropogenic sources can have on ambient toluene variability in rural locations.

In this paper we examine all three sources in more detail for their potential relative contribution to the summer toluene enhancements observed at Thompson Farm [R.S. Russo *et al.*, 2008, *in preparation*]. In particular, we identify and quantify the contribution of seasonal changes in gasoline formulation to evaporative toluene emissions. We also present estimates of toluene emissions from alfalfa crops in New Hampshire and loblolly pine trees in North Carolina. Finally, we evaluate the impact of annual reported industrial releases of toluene in the local area around Thompson Farm.

### **3.2 Methods**

Measurements from several studies were utilized in this paper, and a brief description of each follows. All data is presented in local time (LT) which is UTC-4:00 during daylight savings time and UTC-5:00 during the rest of the year. Seasons are defined as follows: winter is December – February, spring is March – May, summer is June – August, and autumn is September – November. All means are presented as mean  $\pm$  standard error unless otherwise indicated.

#### **3.2.1 Thompson Farm Ambient VOC Measurements**

Situated 25 km from the Gulf of Maine in rural Durham, NH, USA, the University of New Hampshire AIRMAP observation site at Thompson Farm (43.11 °N, 70.95 °W, 24 m) is established on an active corn and alfalfa farm surrounded by mixed forest. Daily canister samples have been collected from 12 January 2004 to the present

from the top of the 12 m sampling tower and provide the most continuous record of interseasonal and interannual VOC variability for the site. Sample collection times ranged from 8:30 to 19:30 LT daily, with the majority of samples obtained between 12:00 and 15:00. Collected in evacuated 2 L electropolished stainless steel canisters, the air samples were analyzed at the University of New Hampshire on a three GC system equipped with two flame ionization detectors (FIDs), two electron capture detectors (ECDs), and a mass spectrometer (MS) for C<sub>2</sub>-C<sub>10</sub> NMHCs, C<sub>1</sub>-C<sub>2</sub> halocarbons and C<sub>1</sub>-C<sub>5</sub> alkyl nitrates [Sive *et al.*, 2005; Zhou *et al.*, 2008; Zhou *et al.*, 2005]. A more comprehensive analysis of the long-term VOC record from the Thompson Farm daily samples can be found in *R.S. Russo et al.* [2008, *in preparation*].

Data in the 90<sup>th</sup> percentile for ethyne (C<sub>2</sub>H<sub>2</sub>), nitrogen oxide (NO), total pentanes (i-pentane and n-pentane), and total butanes (i-butane and n-butane) for each season (winter, spring, summer, autumn) were excluded from the analyzed dataset to provide a representative picture of background mixing ratios independent of strong local vehicle exhaust and fuel evaporative influence. Data where acetonitrile levels  $\geq 150$  pptv were also excluded to eliminate strong biomass burning influences [Warneke *et al.*, 2006]. In total, both these exclusions affected approximately 25% of the dataset. While C<sub>2</sub>H<sub>2</sub>, butanes and pentanes were measured as part of the VOC analysis described above, NO was measured at the Thompson Farm observation tower using a chemiluminescent technique described by *Mao and Talbot* [2004a] and acetonitrile measurements were made using proton transfer reaction-mass spectrometry (PTR-MS) [Talbot *et al.*, 2005]. Mean monoterpene mixing ratios from summer 2004-2006 and correlations between monoterpenes and toluene in 2006 were also calculated from PTR-MS measurements.

Additionally, carbon monoxide (CO), used to calculate C<sub>2</sub>H<sub>2</sub>/CO ratios, was measured using infrared spectroscopy as described by *Mao and Talbot* [2004a].

### 3.2.2 Thompson Farm Vegetative Flux Measurements

Net toluene flux from alfalfa (*Medicago sativa*) was measured at Thompson Farm with a static chamber made of Lexan with an aluminum frame (61 cm × 61 cm × 46 cm) [*Varner et al.*, 1999]. No significant toluene emissions were observed from the empty chamber, which was tested over both a 10 year old concrete pad and a dirt road. The aluminum collar (61 cm × 61 cm) sampled was placed in an alfalfa covered plot below the AIRMAP observation tower a week before sampling. An ambient air sample was taken directly above the collar immediately prior to sampling by opening an evacuated 2 L electropolished stainless steel canister. The chamber was then placed into the collar lip and sealed with water. Three headspace samples were collected every 6 minutes in 2 L electropolished stainless steel canisters. The collar was sampled twice on 25 September 2007. For the first flux measurement (before harvest), the vegetation within the chamber was intact. The chamber was then removed and the vegetation in the collar was clipped to within 2 inches of the ground. The harvested vegetation was left lying within the collar during the second flux measurement (after harvest) which was taken approximately 2 minutes later. The same collar was sampled again without disturbing vegetation re-growth on 5 October 2007. All collar measurements on 25 September and 5 October were made between 13:30 and 15:30 LT. Net fluxes (nmol m<sup>-2</sup> d<sup>-1</sup>) were calculated as follows:

$$\text{Flux} = \frac{dC}{dt} * \frac{V_c}{A_c} \quad (4)$$

where  $\frac{dC}{dt}$  is the linear regression slope of the chamber headspace concentration (in nmol m<sup>-3</sup>) versus time (d),  $V_c$  is the chamber volume (m<sup>3</sup>), and  $A_c$  is the collar area (m<sup>2</sup>).

### 3.2.3 Duke Forest Vegetative Flux Measurements

In June 2005, VOC fluxes were measured from loblolly pine (*Pinus taeda*) and sweetgum (*Liquidambar styraciflua*) trees at the Duke Forest Free Atmospheric Enrichment (FACE) site (35° 52' N, 79° 59' W) located in Chapel Hill in the central Piedmont region of North Carolina, USA [Sive *et al.*, 2007]. Flux measurements were collected every two hours over two 48-hour sampling periods using dynamic branch enclosures made of large (36 L) clear Teflon bags supported by an external frame. A single branch from the tree sampled was carefully placed within the enclosure and exposed to a continuous flow of air from the canopy for 24 to 48 hours prior to sampling. A mass flow meter monitored the rate of air flow into the bag (3-6 L min<sup>-1</sup>) while a cold palladium catalyst was used for O<sub>3</sub> removal. Subsamples of air from the enclosure inlet and outlet were collected during each flux measurement and pressurized to 35 psig in 2 L electropolished stainless steel canisters. Canisters were then returned to UNH for analysis on the three GC system.

Vegetation fluxes (nmol m<sup>-2</sup> LA d<sup>-1</sup>) were calculated as follows:

$$\text{Flux} = \frac{[C_B - C_{PC}] * \text{flow}}{LA} \quad (5)$$

where  $C$  is the number density in nmol m<sup>-3</sup> of toluene in both the bag (B) and post-catalyst (PC) air samples, flow is the rate of air flow into the bag in m<sup>3</sup> d<sup>-1</sup>, and LA represents the leaf area (m<sup>2</sup>) of the branch enclosed. All loblolly pine fluxes presented in this paper were converted to nmol m<sup>-2</sup> ground area d<sup>-1</sup> by multiplying by the average Ring

1 leaf area index (LAI) at the Duke Forest sampling site for June 2005 (7 m<sup>2</sup> leaf area/1 m<sup>2</sup> ground area) [FACTS-1, 2006a]. While measurements were made in both ambient and elevated (+200 ppmv) CO<sub>2</sub> environments, only the ambient measurements are reported for clarity. There was no significant difference in toluene fluxes measured in the two CO<sub>2</sub> regimes.

### **3.3 Warm Season Toluene Enhancements at Thompson Farm**

The time series data for benzene and toluene, presented in Figure 3.1 with 15 day moving averages, were constructed from the daily can samples at Thompson Farm collected during 2004 - 2007 and filtered as described in the methods section. There was a distinct seasonal trend in benzene over the three year period with elevated mixing ratios in winter ( $140 \pm 2$  pptv 2004-2006) resulting from less oxidation by OH. As OH levels increased in the spring, benzene mixing ratios decreased to a mean of  $85 \pm 2$  pptv. Minimum benzene values were observed in the summer months for all three years ( $49 \pm 2$  pptv, 2004-2006 mean) and they began increasing again in autumn ( $75 \pm 2$  pptv 2004-2006, mean).

Similarly, toluene mixing ratios were elevated during winter with a seasonal mean of  $95 \pm 3$  pptv in all three years followed by a decrease to the springtime mean level of  $56 \pm 4$  pptv (Figure 3.1). However, toluene increased again beginning in April or May and remained elevated into September during all three years, with mean values of  $85 \pm 5$  and  $88 \pm 5$  pptv for summer and autumn, respectively. It should be noted that each successive year exhibited summertime toluene enhancements, with 2006 levels reaching a maximum mean of  $100 \pm 10$  pptv (Table 3.1). Subtracting the minimum toluene mixing ratios reached in April and May of each year (mean minimum for all three years =  $42 \pm 3$  pptv)

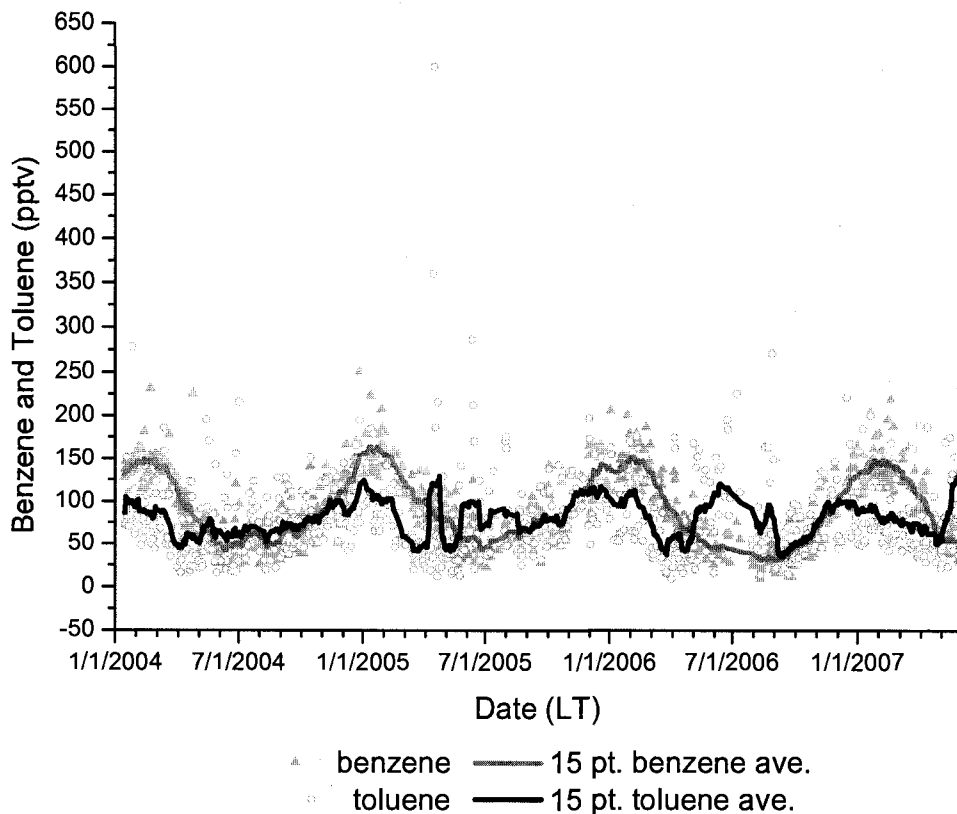


**Figure 3.1:** Benzene and toluene mixing ratios from daily can measurements made 12 January 2004 to 31 May 2007. The 15 point moving averages of the individual measurements are displayed on the graph as solid lines.

from the daily can summer means provides a rough estimate of the warm season enhancement levels ( $21 \pm 6$ ,  $43 \pm 9$ , and  $50 \pm 10$  pptv in 2004, 2005, and 2006 respectively).

These summertime toluene enhancements at Thompson Farm resulted in a toluene/benzene ratio seasonal pattern distinctly different from that of other anthropogenic VOC relationships (R.S. Russo et al., 2008, in preparation). For example, the daily can toluene/benzene ratio and  $C_2H_2/CO$  ratio is compared in Figure 3.2 over the three year study period. Combustion sources of  $C_2H_2$  and CO are largely concentrated in

Season and year	Mean ( $\pm$ standard error)		
	benzene (pptv)	toluene (pptv)	toluene/benzene (pptv/pptv)
<b>winter</b>			
2004 (n=36)	143 $\pm$ 4 <sup>a</sup>	89 $\pm$ 7 <sup>ab</sup>	0.63 $\pm$ 0.05 <sup>a</sup>
2004-5 (n=57)	144 $\pm$ 5 <sup>a</sup>	97 $\pm$ 5 <sup>ab</sup>	0.67 $\pm$ 0.03 <sup>ab</sup>
2005-6 (n=50)	141 $\pm$ 4 <sup>a</sup>	104 $\pm$ 6 <sup>b</sup>	0.73 $\pm$ 0.03 <sup>b</sup>
2006-7 (n=60)	133 $\pm$ 4 <sup>a</sup>	88 $\pm$ 5 <sup>a</sup>	0.66 $\pm$ 0.04 <sup>ab</sup>
<b>spring</b>			
2004 (n=66)	92 $\pm$ 5 <sup>a</sup>	64 $\pm$ 5 <sup>a</sup>	0.75 $\pm$ 0.06 <sup>a</sup>
2005 (n=71)	83 $\pm$ 3 <sup>a</sup>	60 $\pm$ 10 <sup>a</sup>	0.8 $\pm$ 0.1 <sup>a</sup>
2006 (n=65)	81 $\pm$ 4 <sup>a</sup>	64 $\pm$ 5 <sup>a</sup>	0.86 $\pm$ 0.08 <sup>a</sup>
2007 (n=59)	85 $\pm$ 4 <sup>a</sup>	72 $\pm$ 6 <sup>a</sup>	0.95 $\pm$ 0.08 <sup>a</sup>
<b>summer</b>			
2004 (n=56)	51 $\pm$ 3 <sup>a</sup>	63 $\pm$ 5 <sup>a</sup>	1.23 $\pm$ 0.07 <sup>a</sup>
2005 (n=41)	56 $\pm$ 3 <sup>a</sup>	85 $\pm$ 9 <sup>b</sup>	1.47 $\pm$ 0.09 <sup>b</sup>
2006 (n=35)	38 $\pm$ 3 <sup>b</sup>	100 $\pm$ 10 <sup>b</sup>	2.5 $\pm$ 0.2 <sup>c</sup>
<b>fall</b>			
2004 (n=74)	78 $\pm$ 3 <sup>a</sup>	79 $\pm$ 7 <sup>a</sup>	0.96 $\pm$ 0.06 <sup>a</sup>
2005 (n=63)	83 $\pm$ 4 <sup>a</sup>	100 $\pm$ 10 <sup>a</sup>	1.2 $\pm$ 0.1 <sup>ab</sup>
2006 (n=64)	61 $\pm$ 4 <sup>b</sup>	80 $\pm$ 8 <sup>a</sup>	1.4 $\pm$ 0.1 <sup>b</sup>

**Table 3.1:** The seasonal mean mixing ratios  $\pm$  standard errors for benzene, toluene, and the toluene/benzene ratio in the Thompson Farm daily cans from 12 January 2004 through 31 May 31 2006. The n values in parentheses are the number of samples included in the seasonal mean for that year after filtering the data set. The superscripts a, b, and c indicate statistically significant differences in the means for the column within each season (independent means t-test,  $p < 0.05$ , SPSS 15.0.1.1 for windows).

urban areas making them useful tracers of anthropogenic influence, particularly when biomass burning influences are minimal [Warneke *et al.*, 2006].  $C_2H_2$  also has a significantly faster rate of reaction with OH, its major sink, than CO making the ratio of the two compounds an indicator of air mass photochemical and mixing processes. The  $C_2H_2/CO$  ratios observed at Thompson Farm reached their minimum values in summer reflecting higher levels of OH and increased air mass photochemical processing (Figure 3.2). In contrast, the annual maximum toluene/benzene ratios at Thompson Farm occurred from June through September with the mean summer toluene-to-benzene ratio

for all three years ( $1.9 \pm 0.1$ ) significantly higher than all other months sampled ( $0.90 \pm 0.02$ ; independent means t-test:  $p < 0.001$ , SPSS v.15.0.1.1). Summer 2006 had the highest toluene/benzene ratios of all three years with a maximum (6.4 on August 28, 2006) nearly a factor of two larger than the emission ratios derived in urban plumes sampled directly in New England during NEAQS 2002 ( $3.7 \pm 0.3$ ) [deGouw *et al.*, 2005] and ICARTT 2004 (4.25) [Warneke *et al.*, 2007]. Because the daily can data set was filtered to remove the influence of fresh fuel evaporation and combustion sources on

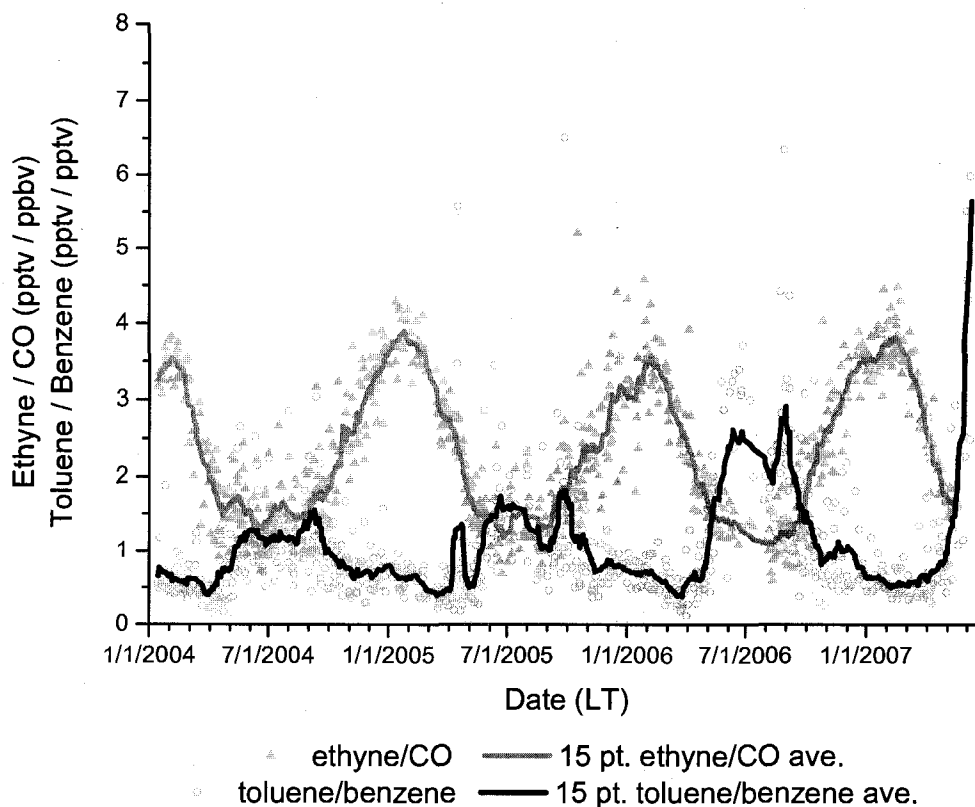


**Figure 3.2:** A comparison of  $C_2H_2/CO$  and toluene/benzene ratios as tracers of urban anthropogenic influence from the Thompson Farm daily cans from 12 January 2004 through 31 May 2007. The 15 point moving averages of the daily ratios are displayed on the graph as solid lines.

toluene mixing ratios, these anomalously high summertime toluene-to-benzene ratios must reflect an additional toluene source.

#### **3.4 Evidence for Various Toluene Source Influences at Thompson Farm**

To better characterize the influence of local and/or regional sources on toluene levels at Thompson Farm, the effect of photochemically processed urban fuel evaporation emissions on the observed toluene variability must be identified and quantified. A strong contribution from gasoline evaporation to the warm season toluene enhancements was indicated by concurrent spring and summer increases in both *i*-pentane and toluene mixing ratios (Figure 3.3). The two compounds reached their minimum levels in April or May of each year followed by similar increases as summer approached. However, a closer examination of the relationship between toluene and *i*-pentane from April to May revealed distinctly that the springtime increases in toluene were independent of those in *i*-pentane, particularly in 2005 and 2006. For example, beginning on 15 April 2005, ambient toluene at Thompson Farm was significantly elevated (up to 600 pptv) for several days while *i*-pentane levels continued to decrease. This episode was relatively short-lived, and toluene reached its springtime minimum on 10 May 2005 before rising concurrently with *i*-pentane. In contrast, springtime toluene increases in 2006 followed a different pattern with a springtime minimum on 28 April 2006 several weeks earlier than the *i*-pentane minimum on 13 May 2006. Such variability provides further support for the influence of another toluene source(s) in addition to fuel evaporation on seasonal enhancements at Thompson Farm.

The impact of these additional sources is also indicated in the scatter of the toluene/*i*-pentane correlation from June through August in 2004, 2005, and 2006 when

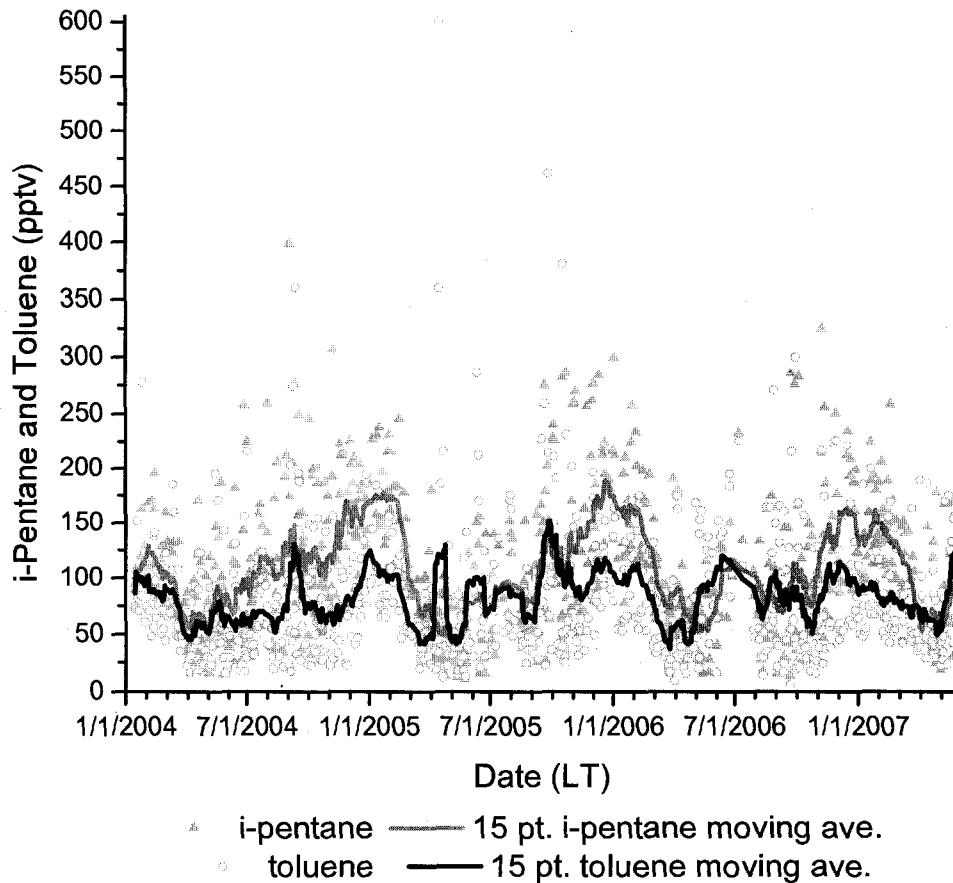


**Figure 3.3:** A comparison of i-pentane and toluene mixing ratios from the Thompson Farm daily cans from 12 January 2004 through 31 May 2007. The 15 point moving averages of the individual measurements are displayed on the graph as solid lines.

fuel evaporation emissions of toluene should have been at their greatest (Figure 3.4). The background relationships between toluene and i-pentane were defined as the linear regression equations for daily can data below the median values for i-pentane and toluene during each summer (2004-2006). The majority of the data in 2004 and 2005 corresponded closely to the background relationship indicating that fuel evaporation was a major factor influencing seasonal toluene levels during those summers. In both years, there was also significant scatter with elevated toluene over a wide range of i-pentane

levels (15-260 pptv). Elevated toluene mixing ratios were actually higher in 2005 (approximately 100-300 pptv) than in 2004 (50-200 pptv) despite a smaller range of i-pentane (15-150 pptv in summer 2005) further suggesting a strong influence from additional toluene sources besides fuel evaporation. Compared to 2004 and 2005, the background relationship of toluene and i-pentane in summer 2006 was less well-defined implying that fuel evaporation was not as dominant a source to seasonal toluene enhancements that year. A higher background slope ( $0.7 \pm 0.2$  compared to  $0.4 \pm 0.1$  and

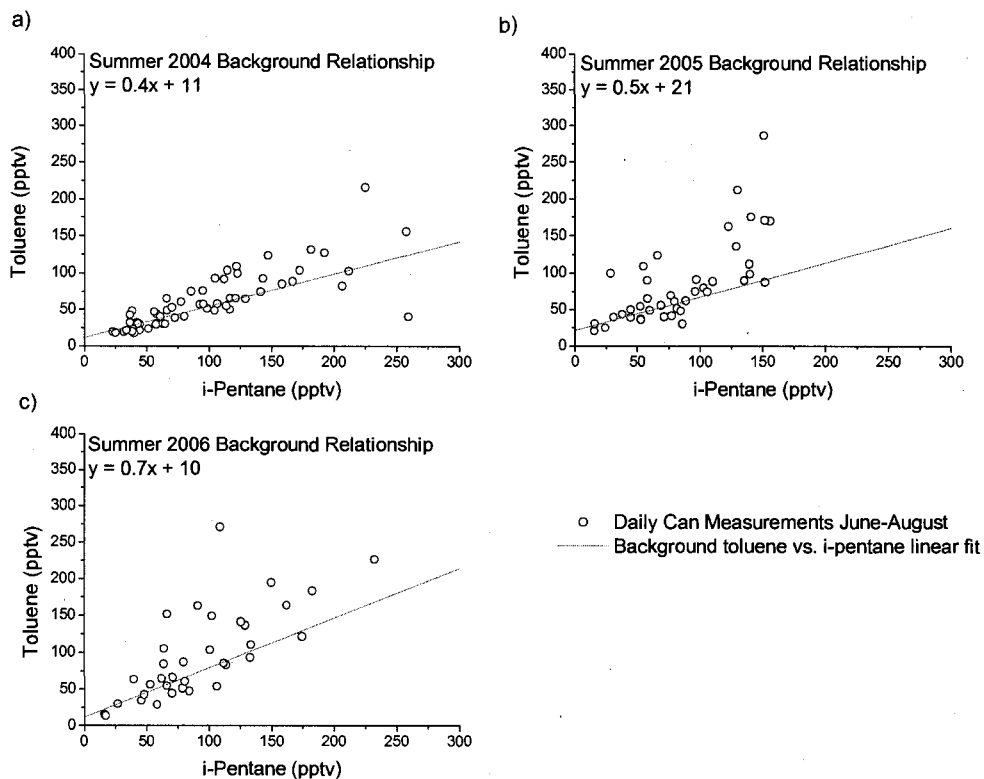


**Figure 3.4:** Toluene vs. i-pentane mixing ratios at Thompson Farm for June through August a) 2004, b) 2005, and c) 2006. The background relationships were determined from the linear regressions of measurements below the median values for i-pentane (94, 79, and 81 pptv for 2004, 2005, and 2006, respectively) and toluene (54, 70, and 85 pptv for 2004, 2005, and 2006, respectively) for each summer.

$0.5 \pm 0.2$  in 2004 and 2005, respectively) further implies input from an additional toluene source even in the cleanest air masses in 2006.

One significant change in the environment surrounding Thompson Farm in 2006 was a switch in the crops from corn to alfalfa. Static enclosure flux measurements of alfalfa conducted in September 2007 revealed significant toluene emissions, particularly when the plants were harvested (Figure 3.5 and Table 3.2). The alfalfa flux rates presented in Table 3.2 were calculated from the linear regression slopes shown in Figure 3.5 as described in Section 3.2.2. Blank chamber tests made over bare soil immediately prior to the alfalfa experiment showed that toluene increases were not chamber artifacts. Furthermore, ambient air samples taken at the enclosure site increased from approximately 80 pptv prior to harvest at 14:40 to over 400 pptv immediately after harvest at 15:10 indicating a significant release of toluene in the area. These vegetative

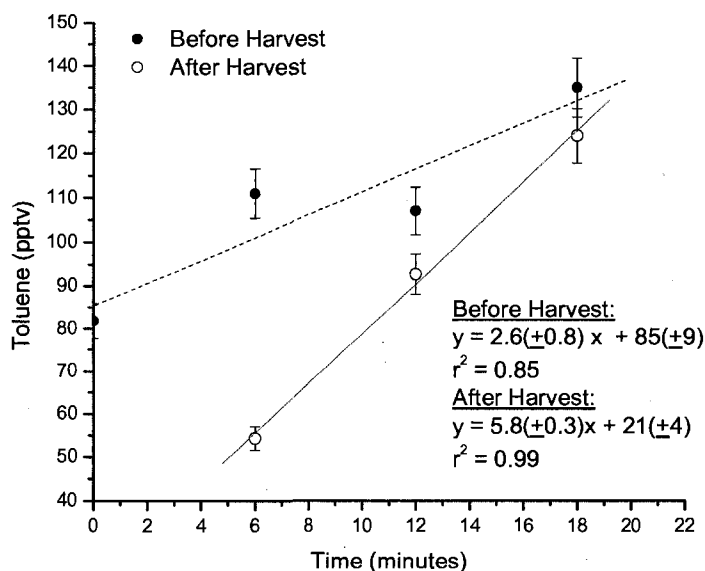


**Figure 3.5:** 25 September 2007 static chamber measurements from Thompson Farm of alfalfa toluene production before and after harvesting. Error bars represent the measurement uncertainty of the GC system.

	Toluene Flux	
	nmol m <sup>-2</sup> d <sup>-1</sup>	r <sup>2</sup>
9/25/07: Alfalfa before harvest	70 ± 60	0.62
9/25/07: Alfalfa immediately after harvest	200 ± 10	0.99
10/5/07: Alfalfa 2 weeks after harvest	80 ± 50	0.31
6/4-6/6/05: Loblolly Pine	500 ± 300	

**Table 3.2:** Vegetation toluene net flux rates from static and dynamic enclosure measurements. The loblolly pine net flux rate listed is the diurnally integrated flux rate from the 2 day sampling period. The alfalfa flux errors are the standard errors of the linear regression slopes used to calculate flux. The loblolly pine error was propagated from the individual flux measurement errors.

emissions could help explain the higher slope associated with the background toluene and i-pentane relationship that year (Figure 3.4c).

It should also be noted that the initial measurements of toluene flux rates from alfalfa presented in Table 3.2 were made at the end of September and beginning of October and emissions during the growing season could be significantly higher. For example, toluene fluxes measured from loblolly pine in North Carolina exhibited a strong temperature dependence (Figure 3.6a) that, if applicable to alfalfa, indicate a substantial increase in flux rates during warmer seasons. Assuming alfalfa emissions follow the loblolly pine temperature relationship, the average 9°C temperature difference between July and late September (2004-2007) at Thompson Farm would result in a summertime flux increase of approximately 360 nmol m<sup>-2</sup> d<sup>-1</sup> (or a total flux rate of approximately 430 nmol m<sup>-2</sup> d<sup>-1</sup> for unharvested alfalfa and 560 nmol m<sup>-2</sup> d<sup>-1</sup> after harvesting). Therefore, further study is warranted to quantify the temperature dependence of alfalfa flux and subsequently its seasonal cycle.

Our enclosure measurements of loblolly pine in North Carolina suggested comparable toluene flux magnitudes and diurnal emission patterns as those of Scots pines

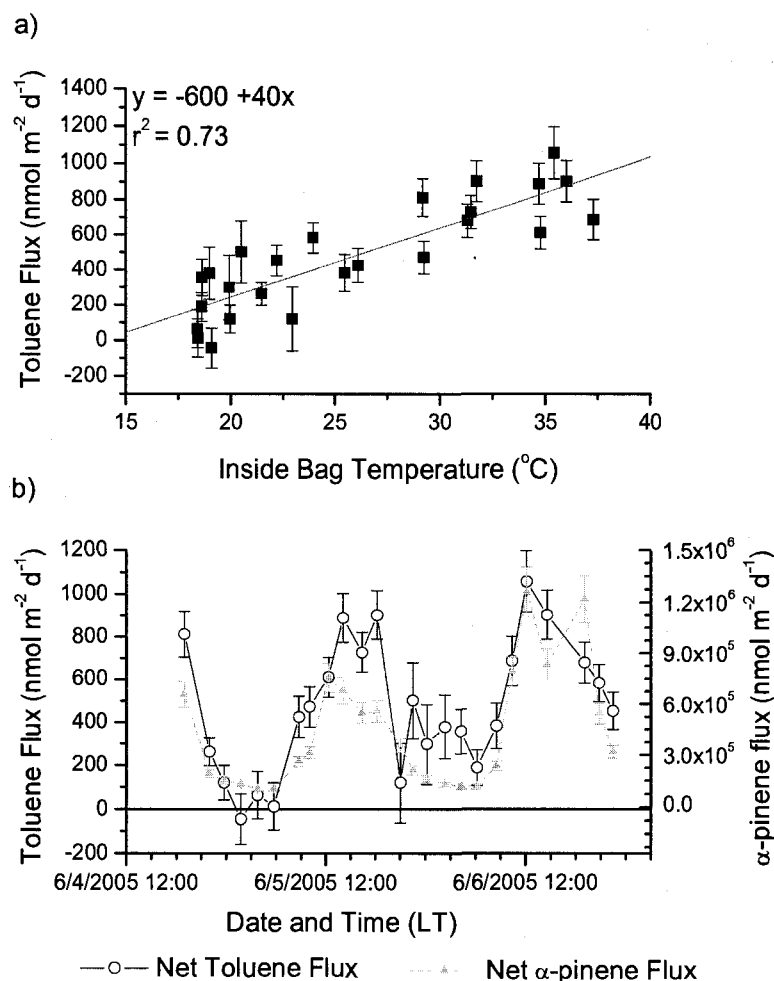


**Figure 3.6:** June 2005 dynamic branch enclosure measurements from Duke Forest in Chapel Hill, North Carolina of loblolly pine net toluene flux with a) net toluene flux vs. temperature and b) the time series of net toluene and α-pinene flux. Original fluxes were calculated as nmol m<sup>-2</sup> leaf area d<sup>-1</sup> and converted to nmol m<sup>-2</sup> ground area d<sup>-1</sup> here by multiplying by the average leaf area index (LAI) at the Duke Forest sampling site for June 2005, 7 m<sup>2</sup> leaf area/1 m<sup>2</sup> ground area. Error bars represent the individual flux error propagated from the uncertainty of measurements used in flux calculation

(*Pinus sylvestris*) sampled in Germany [Heiden *et al.*, 1999]. Loblolly pines also exhibited similar emission patterns between toluene and monoterpenes (Figure 3.6b) that were consistent with correlations observed by Heiden *et al.* [1999] and suggest that biogenic toluene emission may be widespread for evergreen trees. In contrast, negligible

toluene production was evident in branch enclosure measurements of sweet gum (*Liquidambar styraciflua*), a deciduous tree species found in North Carolina. Furthermore, springtime emissions from local coniferous trees could explain the early toluene increase in May 2006 (Figure 3.3). PTR-MS measurements of toluene and monoterpenes at Thompson Farm were more strongly correlated during the first two weeks of May ( $r^2 = 0.82$ ) than at any other time during that year (January-April 2006  $r^2 = 0.31$ , 14 May-August 2006,  $r^2 = 0.47$ , September-December  $r^2 = 0.41$ ). This is also consistent with observations by Heiden et al. [1999] that toluene emissions from Scots pine were highest in spring.

In addition to the crops and trees surrounding Thompson Farm, local industry could also influence ambient toluene mixing ratios. According to the EPA's Toxic Release Inventory, there were two industrial facilities that released approximately 11000 kg of toluene in 2005 located within a 20 km radius of Thompson Farm to the north and south [U.S. Environmental Protection Agency, 2007]. A wind direction analysis of daily can measurements at Thompson Farm from June to August, when the seasonal enhancement was at its peak, revealed no distinct relationship between toluene and wind direction. With a lifetime on the order of days, the toluene lifetime is long enough for it to be dispersed and well-mixed with ambient air obscuring a directional relationship. However, an estimate of the daily ambient mixing ratio increase attributable to these local industrial emissions can be made by calculating the daily emission rate into the 20 km radius circle surrounding Thompson Farm (assuming a planetary boundary layer height of 1 km [Mao and Talbot, 2004b; Sive et al., 2007]). This rough approximation indicates that industrial emissions increase ambient toluene at Thompson Farm by 7 pptv d<sup>-1</sup>.

While significant, this value is still much less than warm season toluene enhancements (approximately 20-50 pptv as estimated in Section 3.3). Moreover, industrial emissions cannot produce the seasonal toluene patterns observed as the facilities are in operation year round presumably with little seasonality in their source strength. All of this evidence together rules out local industry as the major source responsible for the summertime toluene enhancements.

### **3.5 Estimates of Source Contributions to Summer Toluene Enhancements**

In this section, the contributions to ambient summer toluene mixing ratios at Thompson Farm were quantified on a daily basis from the seasonal toluene sources, fuel evaporation and biogenic emissions (Table 3.3). Recognizing that there are assumptions associated with the calculations presented, these estimates provide an informative first estimate of the potential impact each toluene source could have on the seasonal enhancements observed.

#### **3.5.1 Fuel Evaporation**

Contribution to the ambient toluene level from increased fuel evaporation was estimated by multiplying the slope of the background toluene-to-i-pentane relationship (given in Figure 4a, b, and c) by the summertime i-pentane enhancements. It was assumed that the contribution from fuel evaporation to the ambient i-pentane level was minimal in winter and spring based on its dependence on temperature. Therefore, we considered the springtime minimum i-pentane mixing ratio ( $51 \pm 4$  pptv) to be a background level, and the summertime i-pentane enhancement was estimated by subtracting this background value from the June-August i-pentane mean.

The fuel evaporation contribution for June-August 2004 ( $22 \pm 7$  pptv) is consistent with the summer toluene enhancement above the springtime minimum for that

Year	Toluene from Fuel Evaporation (pptv d <sup>-1</sup> )	Toluene from Crop Plant Emissions (pptv d <sup>-1</sup> )	Toluene from Pine Tree Emissions (pptv d <sup>-1</sup> )	Summer Toluene Enhancement (pptv d <sup>-1</sup> )
2004	22 ± 7	5 ± 0.3	12 ± 7	21 ± 6
2005	16 ± 6	5 ± 0.3	12 ± 7	43 ± 9
2006	30 ± 10	5 ± 0.3	12 ± 7	50 ± 10

**Table 3.3:** Estimates of warm season toluene source contributions and June-August mean daily toluene enhancement over the springtime minimum at Thompson Farm. The errors given were propagated from the appropriate standard errors associated with the slopes and means used in calculation.

year ( $21 \pm 6$  pptv) and reflects the dominant fuel evaporation source influence indicated in the toluene versus i-pentane scatter plot for summer 2004 (Figure 4a). In contrast, the estimates of toluene fuel evaporation contributions for summer 2005 and 2006 ( $16 \pm 6$  and  $30 \pm 10$  pptv, respectively) cannot fully account for the toluene enhancements above springtime minimum in those years ( $43 \pm 9$  and  $50 \pm 10$  pptv), further reinforcing the conclusion that additional toluene sources had important influences on the seasonal enhancements in those years. The 2006 summer fuel evaporation estimate may also include additional toluene source influences as the higher slope used to calculate the estimate reflected greater scatter in the toluene versus i-pentane background relationship in that year (Figure 3.4c).

### 3.5.2 Biogenic

The potential toluene contributions from the crop plants and trees surrounding Thompson Farm were estimated by dividing the measured enclosure flux rates presented in Table 3.2 by a boundary layer height of 1 km [Mao and Talbot, 2004b; Sive et al., 2007]. It should be noted that corn, rather than alfalfa, was planted at Thompson Farm in 2004 and 2005 and the alfalfa toluene flux rates used to estimate crop toluene emissions may not be representative of this crop. Additionally, it was assumed that the diurnally

integrated flux rates measured from loblolly pine in North Carolina are comparable to toluene emissions from the New England coniferous species surrounding Thompson Farm. The resulting estimates of biogenic toluene emissions ( $5 \pm 0.3$  and  $12 \pm 7$  pptv d<sup>-1</sup> for crops and coniferous trees, respectively) are on the same order of magnitude as industrial ( $7$  pptv d<sup>-1</sup>) and fuel evaporation emission ( $16-30$  pptv d<sup>-1</sup>) estimates. Should there be a temperature dependence of toluene emission from alfalfa resembling the one presented in Figure 3.6a, local vegetation could make summer contributions to the seasonal toluene enhancements at Thompson Farm greater by a factor of 3.

However, the apparent agreement noted in section 3.5.1 between fuel evaporation estimates and summer toluene enhancements in 2004 suggest that biogenic emissions were overestimated for that summer. Significantly lower monoterpene levels in summer 2004 further indicate that regional biogenic emissions were reduced compared to the other two years (summer means from PTR-MS measurements =  $310 \pm 6$ ,  $452 \pm 2$ , and  $355 \pm 2$  pptv for 2004, 2005, and 2006, respectively. Means from all three years significantly different, independent means t-test:  $p < 0.001$ , SPSS v.15.0.1.1). Lower biogenic flux rates could reflect the cool, cloudy conditions that generally prevailed in the summer of 2004 as both the mean July-August temperature and the  $J_{\text{NO}_2}$  photolysis rate measured at Thompson Farm were significantly lower than in 2005 and 2006 (mean temperature =  $19.4 \pm 0.1$ ,  $20.8 \pm 0.1$ , and  $20.7 \pm 0.1$  °C and mean  $J_{\text{NO}_2}$  =  $0.00229 \pm 0.00005$ ,  $0.00272 \pm 0.00006$ , and  $0.00287 \pm 0.00006$  s<sup>-1</sup> for summer 2004, 2005, and 2006, respectively, independent means t-test:  $p < 0.001$ , SPSS v.15.0.1.1). In contrast, the high monoterpene levels observed during summer 2005 suggest that vegetative toluene emissions may have been underestimated for that year. If this were the case, it could

explain why the combined biogenic and fuel evaporation estimates ( $33 \pm 9$  pptv) were less than the observed summer toluene enhancement in 2005 ( $43 \pm 9$  pptv).

The combined emission estimates for summer 2006 (fuel evaporation + biogenic =  $50 \pm 10$  pptv) were actually in good agreement with the observed summer toluene enhancement that year ( $50 \pm 10$  pptv). However, the biogenic emissions estimates presented in Table 3.3 may have been underestimated for that summer as the alfalfa toluene fluxes during the height of the growing season are expected to be greater than the late September flux rates used in our calculations. It should be noted that the higher slope (Figure 3.4c) used to calculate the fuel evaporation emission estimate in 2006 indicated the influence of an additional toluene source on the background toluene and i-pentane relationship and an underestimate in biogenic emissions may have been balanced by overestimate of fuel evaporative emissions.

These initial biogenic estimates indicate the need for a more comprehensive study of the seasonal cycle and environmental controls of toluene fluxes from crops and trees to fully explain the interannual variability in vegetative toluene emissions suggested here. However, our measurements indicate the significant impact this unexpected source might have on toluene variability in rural areas.

### **3.6 Conclusions**

The summertime enhancements in toluene mixing ratios evident in long-term daily measurements at Thompson Farm are driven by a combination of fuel evaporation emissions coupled with seasonal changes in RFG toluene content and biogenic emissions. Toluene releases from local industrial processes are also likely to impact ambient mixing ratios at the site but these emissions occur year-round and are unlikely to produce

seasonal enhancements. Similar patterns of spring increases and summer correlations between i-pentane and toluene indicate that fuel evaporation emissions were the major influence on summer toluene enhancements in 2004. However, estimates of biogenic emissions from coniferous trees and crops were also significant and could not be fully dismissed, particularly in 2005 and 2006. The evidence of crop emission influences on seasonal toluene enhancements was greatest in 2006 when alfalfa was first planted in the Thompson Farm fields. Static chamber enclosure measurements revealed significantly increased toluene emissions from alfalfa after harvest. These flux measurements were made late in September and further studies are necessary to characterize the variability and controlling factors of toluene emissions from alfalfa and other vegetation more fully throughout the growing season.

## CHAPTER 4

### CARBONYL SULFIDE EXCHANGE IN A TEMPERATE LOBLOLLY PINE FOREST GROWN UNDER AMBIENT AND ELEVATED CO<sub>2</sub>

#### 4.1 Introduction

With an atmospheric lifetime of approximately 5 years and an average global mixing ratio of 500 pptv, carbonyl sulfide (COS) is both the longest-lived and most abundant sulfur-containing gas in the troposphere [*Chin and Davis, 1995; Notholt et al., 2003*]. This combination makes COS the major tropospheric sulfur gas available for transport to the stratosphere [*Chin and Davis, 1995*]. Once there, COS photolysis and oxidation contribute to the formation of the stratospheric sulfate aerosol layer. This aerosol layer influences the earth's radiation balance by reflecting incoming solar radiation [*Turco et al., 1980*] and provides a surface for heterogeneous ozone depletion reactions [*Solomon et al., 1996*].

The ocean is the major source of COS to the troposphere. This includes both indirect production from the oxidation of marine emissions of carbon disulfide (CS<sub>2</sub>) and dimethyl sulfide (DMS) [*Barnes et al., 1994; Chin and Davis, 1993*] and direct COS photochemical production from dissolved organic matter [*Weiss et al., 1995*]. Additionally, biomass burning and anthropogenic activities such as aluminum production and coal combustion are significant terrestrial sources of COS [*Chin and Davis, 1993; Kettle, 2000*]. Terrestrial ecosystems play a major role in the global COS budget as vegetative uptake is the largest global sink for the gas [*Brown and Bell, 1986; Goldan et*

*al.*, 1988; *Kettle et al.*, 2002; *Kjellstrom*, 1998] while microbial consumption in soils is the second largest [*Kesselmeier et al.*, 1999; *Kettle et al.*, 2002].

Currently, the magnitude of both of these natural sinks is poorly constrained. For example, observations of seasonal variations in COS mixing ratios at a variety of northern hemisphere surface sites were much larger than could be explained by current estimates of the COS vegetative sink [*Montzka et al.*, 2007]. Since the same enzymes that utilize CO<sub>2</sub> during photosynthesis also consume COS [*Protoschill-Krebs and Kesselmeier*, 1992], the global COS vegetation sink is commonly calculated by scaling estimates of net primary production (NPP) by the ratio of the mean mixing ratios of COS and CO<sub>2</sub> [*Goldan et al.*, 1988; *Kettle et al.*, 2002; *Kjellstrom*, 1998]. However, a variety of studies have indicated that COS uptake by plants is favored over CO<sub>2</sub> [*Geng and Mu*, 2006; *Montzka et al.*, 2007; *Sandoval-Soto et al.*, 2005; *Xu et al.*, 2002] reflecting the higher affinity of carbonic anhydrase, the initial photosynthetic enzyme for COS [*Protoschill-Krebs et al.*, 1996], the irreversible hydrolysis of COS compared to CO<sub>2</sub> [*Elliot et al.*, 1989], and respiration [*Sandoval-Soto et al.*, 2005].

Initially, soils were considered sources of COS to the atmosphere (e.g. [*Aneja et al.*, 1979]). However, this conclusion was based upon soil fluxes measured using dynamic chambers swept with S-free air. Under these conditions, an artificial gradient of COS within the chamber often forced COS soil emissions [*Castro and Galloway*, 1991]. More recent studies using enclosures flushed with ambient air have revealed that most soils actually consume COS [*deMello and Hines*, 1994; *Kuhn et al.*, 1999; *Simmons et al.*, 1999; *Steinbacher et al.*, 2004; *Yi et al.*, 2007]. However, the environmental controls over soil uptake processes were highly variable between sites and soil types. As a result,

estimates of the global soil sink strength have a wide range of uncertainty [Kettle *et al.*, 2002; Watts, 2000].

The potential effect of rising CO<sub>2</sub> levels on COS consumption in terrestrial ecosystems is also currently unclear. The warmer temperatures that should accompany higher CO<sub>2</sub> levels would likely increase plant NPP and growing seasons suggesting an enhanced vegetation sink. However, laboratory studies indicate that the rate of COS consumption drops with the decreased expression of the photosynthetic enzyme carbonic anhydrase in algae grown under elevated CO<sub>2</sub> [Protoschill-Krebs *et al.*, 1995]. For many plant species, COS uptake is also largely controlled by stomatal conductance [Geng and Mu, 2006; Sandoval-Soto *et al.*, 2005] and there is evidence that enhanced CO<sub>2</sub> conditions will result in reduced stomatal conductance and frequency for many plant species, potentially limiting the COS plant sink further [Greenwood *et al.*, 2003; Herrick *et al.*, 2004a; Kouwenberg *et al.*, 2003; Kurschner *et al.*, 1997; Wagner *et al.*, 2005]. The effect of CO<sub>2</sub> enrichment on stomatal characteristics is highly variable with a few plant species also showing slight increase in stomatal density under elevated CO<sub>2</sub> [Reid *et al.*, 2003]. In many cases, changes in stomatal conductance impact transpiration in plants exposed to elevated CO<sub>2</sub> resulting in increased soil moisture [Hungate *et al.*, 2002; Kammann *et al.*, 2005; Kettunen *et al.*, 2006; McLain *et al.*, 2002]. Such changes could have a significant impact on soil COS consumption which is a microbial process dependent on moisture content, temperature, and ambient COS concentrations [Kesselmeier *et al.*, 1999].

Measurements made at the Duke Forest (DF) Free Atmospheric Carbon Enrichment (FACE) site offer a unique opportunity to examine the magnitude and controls of vegetative and soil COS uptake in a temperate forest grown under present day

and elevated CO<sub>2</sub> conditions (<http://face.env.duke.edu/main.cfm>). Considering the limited number of field studies of COS exchange at the ecosystem level, these measurements also provide considerable insights into the natural variability of COS consumption processes and their impact on ambient COS mixing ratios. Measurements were made of ambient canopy COS levels and vegetation and soil fluxes within control (ambient CO<sub>2</sub>) and CO<sub>2</sub> enriched plots at DF in 2004 and 2005. This study presents an analysis of the diurnal cycles and major factors influencing COS consumption processes within the two plots. Estimates of net ecosystem COS flux were also made and compared to measured vegetation and soil fluxes to better understand the impacts of individual sinks on COS uptake at the site.

## **4.2 Methods**

The measurements presented here come from multiple field studies conducted at the Duke Forest FACE site in September 2004 and June and September 2005. Descriptions of the significant measurements and calculations from each study are presented below. All data is presented in local time (LT), which is UTC – 4:00. All means are presented as mean ± standard error unless otherwise indicated. Statistical analyses were conducted using SPSS v. 15.0.1.1. (SPSS, Inc.).

### **4.2.1 Site Description**

The Duke Forest FACE site (35° 52' N, 79° 59' W) is a loblolly pine (*Pinus taeda*) stand planted in Chapel Hill in the central Piedmont region of North Carolina. Pine trees dominate the forest canopy with significant subcanopy and understory contributions from deciduous sweetgum (*Liquidambar styraciflua*), elm (*Ulmus alata*), red maple (*Acer rubrum*), dogwood (*Cornus florida*) and a variety of oak-hickory species.

The soils are classified as Enon series (fine, mixed, weathered alfisols) [Oh and Richter, 2005].

The FACE experiment consists of 6 circular experimental plots, or rings, each 30m in diameter and surrounded by vertical vent pipes that extend to the top of the canopy. Three experimental rings receive additional CO<sub>2</sub> through the vent pipes to supplement atmospheric concentrations by 200 μL L<sup>-1</sup>. The remaining three control rings are exposed only to ambient CO<sub>2</sub> concentrations. Continuous (24 h d<sup>-1</sup>, 365 d yr<sup>-1</sup>) CO<sub>2</sub> fumigation began on 27 August 1996. Since 2003, fumigation has been limited to daylight hours only. In 2005, both control and treatment plots were split into two halves with one half of the ring receiving nitrogen (N) fertilization at a rate of 11.2 g N m<sup>-2</sup> yr<sup>-1</sup> [Schafer *et al.*, 2002].

All measurements described in this paper were collected within Ring 1 (R1, control) and Ring 2 (R2, +200 μL L<sup>-1</sup> CO<sub>2</sub>). All soil and vegetation flux measurements were made within the unfertilized halves of these two rings.

#### 4.2.2 Canopy Measurements, September 2004

Hourly air samples were collected in 2-liter electropolished stainless steel canisters and pressurized to 35 psig using a single head metal bellows pump (MB-302MOD, Senior Flexonics, Sharon, MA) from 15 – 28 September 2004. The canister samples were collected simultaneously in R1 and R2 from inlets at 16m above ground (tree canopy height) on the central monitoring tower within each ring. On 19 – 20 and 23 – 24 September, additional vertical gradient samples were collected simultaneously from inlets at 20m above ground in each ring. These measurements were used to calculate net ecosystem gradient fluxes as described in Section 4.2.6.1. All canisters were returned to

the University of New Hampshire (UNH) and analyzed within two weeks of collection on a three GC system equipped with two FIDs, two ECDs, and a mass spectrometer (MS) for C<sub>2</sub>-C<sub>10</sub> NMHCs, C<sub>1</sub>-C<sub>2</sub> halocarbons, C<sub>1</sub>-C<sub>5</sub> alkyl nitrates, and select oxygenated volatile organic compounds (OVOCs) and sulfur compounds including COS, CS<sub>2</sub> and DMS [Sive *et al.*, 2005, 2007; Zhou *et al.*, 2005, 2008]..

CO<sub>2</sub> was measured from 11 – 28 September simultaneously at the 16 and 20 m sampling heights in R1 and R2 using LiCor 7000 infrared gas analyzers. Mixing ratios and the difference between the two sampling heights were analyzed every 5 seconds and averaged over a one-minute interval. Wind speed and direction, air temperature and photosynthetically active radiation (PAR) were collected at one minute intervals by the FACTS-I meteorological instruments in R2. The Climatronics F460 anemometer and wind vane and LiCor quantum sensor were mounted above the tree canopy while air temperature was collected using thermocouples mounted within the midcanopy. Meteorological data were averaged hourly to facilitate comparison to VOC measurements. Precipitation data for the FACE site was collected on a daily basis from the FACTS-I all weather rain gauge.

#### 4.2.3 Vertical Profile Measurements, September 2004 and June 2005

Vertical profiles of VOC mixing ratios from ground level to above the canopy were also measured on several occasions during the September 2004 and June 2005 field campaigns. During each profile measurement, evacuated canisters were filled to ambient pressure at 5m height intervals from the surface to 20m above ground in each ring. During 2004, profiles in R1 and R2 were obtained on 26 September at 18:00 LT. During 2005, profiles were obtained in all 6 experimental rings (R1, R5, R6 = ambient CO<sub>2</sub>; R2,

R3, R4 = +200  $\mu\text{L L}^{-1} \text{CO}_2$ ) on 5 June at 15:00 LT. Additional profile measurements were made in R1 and R2 only on 6 June 2005 at 00:30 LT and 10 June 2005 at 16:00 LT. All canisters were returned to UNH and analyzed within a week of collection on the GC system described above.

#### 4.2.4 Vegetation Flux Measurements, June 2005

During the second field campaign (1 – 12 June, 2005), direct vegetation VOC fluxes were measured within R1 and R2 [Sive *et al.*, 2007]. Vegetation flux measurements were collected approximately every two hours for loblolly pine and sweetgum, the two dominant trees at the site, over two 48-hour sampling periods using dynamic branch enclosures (Figure 4.1). The enclosures were made of large clear Teflon bags supported by an external frame. A single branch from the tree sampled was placed within the enclosure and exposed to a continuous flow of air from the canopy to maintain ambient pressure. A mass flow meter (MFM) continuously monitored the rate of air flow into the bag (3-6  $\text{L min}^{-1}$ ) while a cold palladium catalyst was used for ozone ( $\text{O}_3$ ) removal. In addition to  $\text{O}_3$ , the palladium catalyst also removed a fraction of COS (0-400 pptv) and  $\text{CO}_2$  (0-170 ppmv) from the ambient canopy air pumped into the bag. A more detailed description of the effect COS depletion by the catalyst had on flux measurements is given in Section 3.2. Air from the enclosure was vented through the outlet located deep within the bag to ensure that samples were well-mixed. Branches were enclosed and exposed to  $\text{O}_3$  scrubbed canopy air for 24 hours prior to sampling. Temperature, relative humidity, and photosynthetically active radiation (PAR) within the bag were monitored continuously using thermocouples, relative humidity sensors, and photodiodes mounted on the branch sampled.

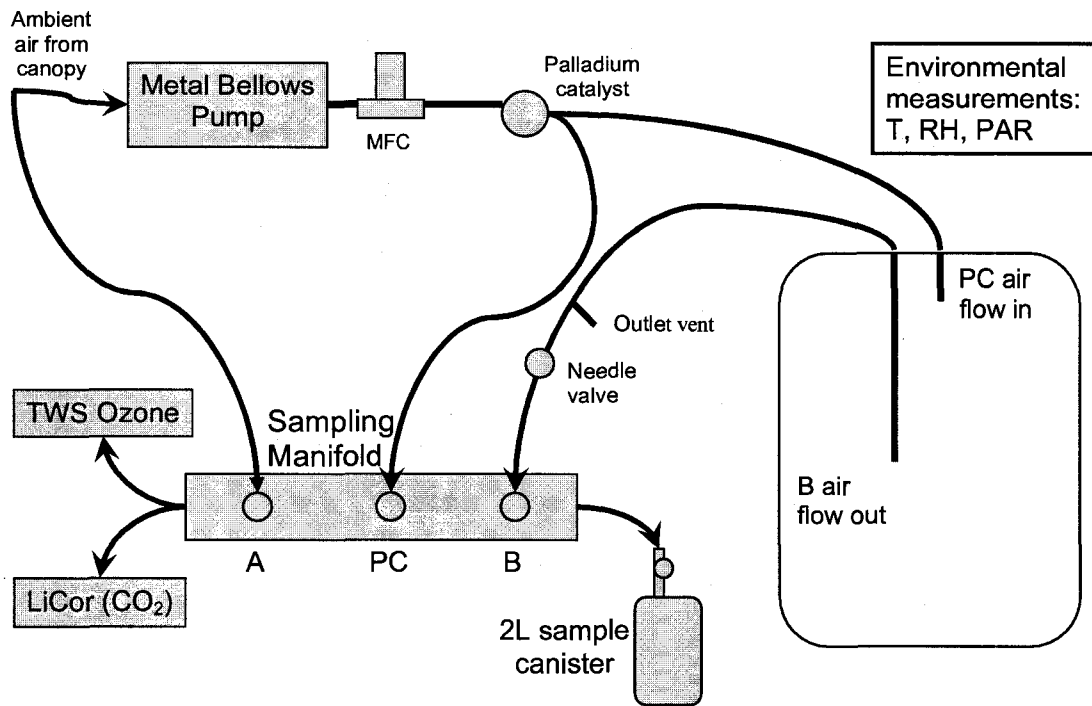


**Figure 4.1:** Schematic of the dynamic branch enclosures used to measure VOC vegetation fluxes at the Duke FACE site in June 2005.

During each flux measurement, three air samples were collected: ambient (A) air from the canopy drawn from the initial air intake, post-catalyst (PC) air sampled from the air flow entering the bag, and bag (B) air sampled from the outlet vent. The sampling flow rate was controlled using a needle valve to make sure that positive outlet vent pressure was maintained throughout. Air samples were collected for VOC analysis as described above in 2-liter electropolished stainless steel canisters and pressurized to 35 psig. A LiCor 7000 infrared gas analyzer and a miniature O<sub>3</sub> sensor [Mao *et al.*, 2006b] attached to the sampling manifold monitored CO<sub>2</sub> and O<sub>3</sub> levels in the sampled air flow. Flux measurements were made every 2 hours from 4 – 6 June 2005 for the loblolly pines

and 8 – 10 June 2005 for the sweet gum trees. After sampling, the branch enclosed was removed from the tree and returned to UNH for direct measurement of leaf dry weight and leaf area.

Vegetation fluxes ( $\text{pmol m}^{-2} \text{ LA s}^{-1}$ ) were calculated for COS and  $\text{CO}_2$  as follows:

$$\text{Flux} = [C_B - C_{PC}] * \text{flow} * \text{LA}^{-1} \quad (6)$$

where C is the concentration of COS and  $\text{CO}_2$  in  $\text{pmol m}^{-3}$  and  $\mu\text{mol m}^{-3}$ , respectively in both the bag (B) and post-catalyst (PC) air samples, flow is the rate of air flow into the bag in  $\text{m}^3 \text{ s}^{-1}$ , and LA represents the single sided leaf area ( $\text{m}^2$ ) of the branch enclosed. Flux errors were propagated from individual measurement uncertainties for COS (5%),  $\text{CO}_2$  (5%), leaf area (10%), and the standard error of the mean inlet flow rate during measurement as described by *Taylor* [1982].

#### 4.2.5 Soil Flux Measurements, June and September 2005

Soil fluxes were measured within Ring 1 and 2 on 9 June and 20 September 2005 using static enclosures as described by *Varner et al.* [1999]. Measurements were made using four 30 cm x 30 cm Teflon coated aluminum collars placed in the soil a month prior to field sampling. Two collars (labeled R1 collar A, R1 collar B, R2 collar A, and R2 collar B) were placed in both Ring 1 and Ring 2. During sampling, a Teflon coated aluminum chamber (volume approximately 30 L) was placed over each collar for approximately 30 minutes. An ambient pressure canister sample was collected from the chamber headspace every 10 -12 minutes for a total of 4 samples. On both June 9 and September 20, all soil measurements were collected between 8:00 and 19:00 local time with each collar being sampled 3 to 4 times throughout the day. Canister air samples were returned to UNH for VOC analysis as described above.

Chamber and soil temperatures at 0, 5 and 10 cm depths were measured each time a collar was sampled. Additionally, soil moisture data for 9 June and 20 September 2005 was obtained from the FACTS-1 time-domain reflectometry (TDR) instruments established in R1 and R2 [FACTS-1, 2006b]. Half-hourly soil moisture values for each ring were calculated as the average for the four instrument locations within each plot.

Soil fluxes ( $\text{pmol m}^{-2} \text{ s}^{-1}$ ) were calculated as the initial change in chamber COS concentration vs. time,  $\left(\frac{dC}{dt}\right)_{t=0}$ , in  $\text{pmol m}^{-3} \text{ s}^{-1}$  multiplied by the chamber volume,  $V_c$  ( $\text{m}^3$ ), and divided by collar area,  $A_c$  ( $\text{m}^2$ ):

$$\text{Flux} = \left(\frac{dC}{dt}\right)_{t=0} * \frac{V_c}{A_c} \quad (7)$$

In 11 of the 30 total soil flux measurements made in June and September 2005, the change in chamber concentration was linear over the time of chamber deployment. In these cases,  $\left(\frac{dC}{dt}\right)_{t=0}$  was calculated as the linear regression slope of chamber concentration vs. time. In the remaining 19 soil flux measurements, the rate of change in chamber concentration decreased with time and  $\left(\frac{dC}{dt}\right)_{t=0}$  was calculated by fitting the following exponential equation to the data [deMello and Hines, 1994]:

$$C(t) = a - b * e^{(-kt)} \quad (8)$$

where  $a$  is  $C_{\text{eq}}$ , or the concentration reached when COS within the chamber reached equilibrium with the concentration in soil micropores,  $b$  is  $C_{\text{eq}}$  minus  $C_{t=0}$ , the COS concentration at  $t=0$ , and  $k$  is a rate constant. The values of  $a$  and  $k$  were calculated iteratively for each flux measurement and used to determine  $\left(\frac{dC}{dt}\right)_{t=0}$  as follows:

$$\left(\frac{dC}{dt}\right)_{t=0} = k*(C_{eq}-C_{t=0}) = k*b \quad (9)$$

This value for  $\left(\frac{dC}{dt}\right)_{t=0}$  was then used in equation (7) to calculate net COS flux.

Soil flux errors were propagated from the standard errors for the linear regression slope or non linear coefficients,  $k$  and  $a$ , used during flux calculation as well as the individual measurement uncertainties for the chamber volume (2%), collar area (2%) and ambient COS mixing ratios (5%) as described by *Taylor* [1982].

#### 4.2.6 Estimates of Net Ecosystem COS Flux, September 2004 and June 2005

Net ecosystem COS fluxes were calculated using two methods. Gradient fluxes (GF) were calculated using the gradient measurements collected in September 2004. An independent nighttime flux (NF) assessment under stagnant nocturnal boundary layer conditions was also made using ambient canopy measurements from 15 – 16 September 2004 and 4 – 5 June 2005.

4.2.6.1 Gradient Flux Calculations. On two occasions during the 2004 sampling period, 19 – 20 and 23 – 24 September, simultaneous air samples were collected at 16m (canopy height) and 20m (above the canopy). Two types of GF calculations were applied to these measurements: 1) the modified Bowen-ratio method (e.g. [*Goldstein et al.*, 1995]); and 2) the universal flux gradient relationships described by the Monin-Obukhov similarity hypothesis (e.g. [*Rinne et al.*, 2000; *Simpson et al.*, 1998]). In both methods, the GF is calculated as the product of a turbulent exchange coefficient,  $K$  ( $m^2 s^{-1}$ ), times the concentration gradient,  $\frac{dC}{dz}$  ( $pmol m^{-4}$ ):

$$GF = -K * \frac{dC}{dz} \quad (10)$$

where  $\frac{dC}{dz}$  is approximated as the difference in the concentration of CO<sub>2</sub> in pmol m<sup>-3</sup>, C, at the two measurement heights, z<sub>1</sub> and z<sub>2</sub>, divided by the difference in height.

The difference between these two methods for flux calculation lies in the determination of K. For the modified Bowen ratio method, K is determined from an independent assessment of flux as follows:

$$K = \frac{\Phi_{CO_2}}{\left(\frac{dC_{CO_2}}{dz}\right)} \quad (11)$$

In this case,  $\Phi_{CO_2}$  was the hourly mean eddy covariance measurement of CO<sub>2</sub> flux (mmol m<sup>-2</sup> s<sup>-1</sup>) from the Ameriflux tower in R1 and  $\frac{dC_{CO_2}}{dz}$  was the gradient difference in LiCor CO<sub>2</sub> measurements (mmol m<sup>-4</sup>).

The value of K can also be calculated using the Monin-Obukhov similarity hypothesis which describes the behavior of vertical flow and turbulence within the surface layer as a function of several key parameters:

$$K = \frac{u_* k (z - d)}{\Phi_h} \quad (12)$$

where  $u_*$  is the characteristic friction velocity (m s<sup>-1</sup>), k is the von Karman constant, z is the height above ground (m), d is the zero plane displacement (assumed to be  $\frac{2}{3}z$ ), and  $\Phi_h$  is the Monin-Obukhov diabatic influence function for heat [Simpson *et al.*, 1998].

Substituting equation (12) into equation (10) and integrating over the height interval, z<sub>1</sub> to z<sub>2</sub>, yields:

$$GF = \frac{-u_*k(C_{z_1} - C_{z_2})}{\ln\left(\frac{z_2 - d}{z_1 - d}\right) - \psi_h\left(\frac{z_2 - d}{L}\right) + \psi_h\left(\frac{z_1 - d}{L}\right)} \quad (13)$$

where  $C$  is the measured concentration ( $\text{nmol m}^{-3}$ ) at the upper and lower measurement heights,  $z_2$  and  $z_1$ ,  $\psi_h$  is the integrated form of the Monin-Obukhov diabatic influence function for heat [Simpson *et al.*, 1998], and  $L$  is the Obukhov length [Rinne *et al.*, 2000]. In this study, the characteristic friction velocity,  $u_*$ , was taken from eddy covariance measurements made at the Ameriflux tower in Ring 1. The value of  $\psi_h$  was calculated using heat and momentum flux from the Ameriflux eddy covariance tower and integrated expressions of the Businger-Dyer equations described by Simpson *et al.* [1998]. The Obukhov length,  $L$ , was also calculated from the friction velocity, temperature, relative humidity, and heat flux as described by Simpson *et al.* [1998].

The Monin-Obukhov similarity hypothesis tends to break down near rough surfaces, such as a forest canopy, resulting in an underestimation of gradient fluxes [Rinne *et al.*, 2000; Simpson *et al.*, 1998]. To correct for this underestimation, fluxes calculated in this manner were multiplied by an enhancement factor,  $\gamma$ , such that:

$$\gamma = \frac{\phi_h}{\phi_h^*} = \frac{\text{Eddy covariance CO}_2 \text{ flux}}{\text{Gradient CO}_2 \text{ flux}} \quad (14)$$

In this case,  $\phi_h$  and  $\phi_h^*$  are the diabatic influence functions for heat calculated from the similarity hypothesis and from an independent flux measurement such as eddy covariance  $\text{CO}_2$  flux.

Flux errors for all GF calculations were propagated from the measurement uncertainties of canopy concentrations (5%) and the standard error of the hourly Ameriflux tower measurement averages used in calculation according to Taylor [1982].

4.2.6.2 Nighttime Flux Calculation. An alternative approach for calculating net ecosystem flux under stable nocturnal boundary layer conditions was employed by *Kuhn et al.* [1999] and has been used in a variety of studies on other trace gases (e.g. [*Sive et al.*, 2007; *Talbot et al.*, 2005; *Varner et al.*, 2008; *White et al.*, 2008; *Zhou et al.*, 2005]). Under stagnant wind conditions associated with the stable boundary layer, changes in ambient mixing ratios should reflect local sources and sinks. As a result, net nighttime fluxes, NF, can be estimated as:

$$NF \text{ (pmol m}^{-2} \text{ s}^{-1}\text{)} = \frac{dC}{dt} * ML \quad (15)$$

Where  $\frac{dC}{dt}$  is the change in concentration over time (pmol m<sup>-3</sup> s<sup>-1</sup>) and ML is the height of the mixed layer (m).

Only measurements taken when wind speeds were  $\leq 0.8 \text{ m s}^{-1}$  were used to calculate NF to limit the influence of large scale horizontal advection on our flux estimates. Unfortunately, only one night during each campaign met these conditions (15 – 16 September 2004 and 4 – 5 June 2005). As nocturnal mixing layer height was not measured during either campaign, ML height was assumed to be 125 m, which represents the median value of the nocturnal inversion layer height range (50-200 m) measured at a variety of similar midlatitudinal rural locations [*Galbally*, 1968; *Gusten et al.*, 1998; *Hastie et al.*, 1993; *Shepson et al.*, 1992]. Concentration changes were not linear over time and individual fluxes were calculated for each hour time step. Flux errors were propagated from the individual measurement uncertainties in canopy COS measurements (5%) and the estimated uncertainty in the ML height (60%) according to *Taylor* [1982].

Single sided leaf area index (LAI;  $\text{m}^2 \text{ LA m}^{-2}$  ground area) for R1 and R2 canopies used to scale September 2004 and June 2005 canopy fluxes to leaf area (Section 4.3.4.2) were taken from FACTS-1 Li-Cor LAI-2000 plant canopy analyzer monthly measurements [FACTS-1, 2006a]. LAI measurements were corrected for needle clumping and branch shading by multiplying by an enhancement factor of  $1.9 \pm 0.6$ , the mean value of the range of coniferous tree LAI enhancement factors (1.25 to 2.5) noted in Stenberg [1996].

### **4.3 Results and Discussion**

#### **4.3.1 Canopy Measurements, September 2004**

Figure 4.2 compares the simultaneous R1 and R2 measurements at 16 m canopy height for COS and ethane during the entire data collection period. Ethane mixing ratios are presented as an example of the variability between the two rings independent of any natural VOC sources or sinks. This anthropogenic trace gas exhibited a very strong 1:1 relationship indicating minimal variability associated with ring location alone. In contrast, the R1 versus R2 relationships for COS showed much greater scatter reflecting its natural sinks within temperate forests.

Figure 4.3 presents the time series of meteorological data,  $\text{CO}_2$ , and COS measurements made at 16 m above ground during the 2004 intensive. Winds generally originated from the north and east at the study site with an average wind speed throughout the campaign of  $1.9 \text{ m s}^{-1}$ . Exceptions to this pattern occurred with the passage of Hurricanes Ivan and Jeanne on 16 – 19 and 27 – 29 September, respectively, which resulted in revolving wind directions and a maximum wind speed of  $11 \text{ m s}^{-1}$  (Figure 4.3a). Winds from the southeast associated with these hurricanes also coincided with

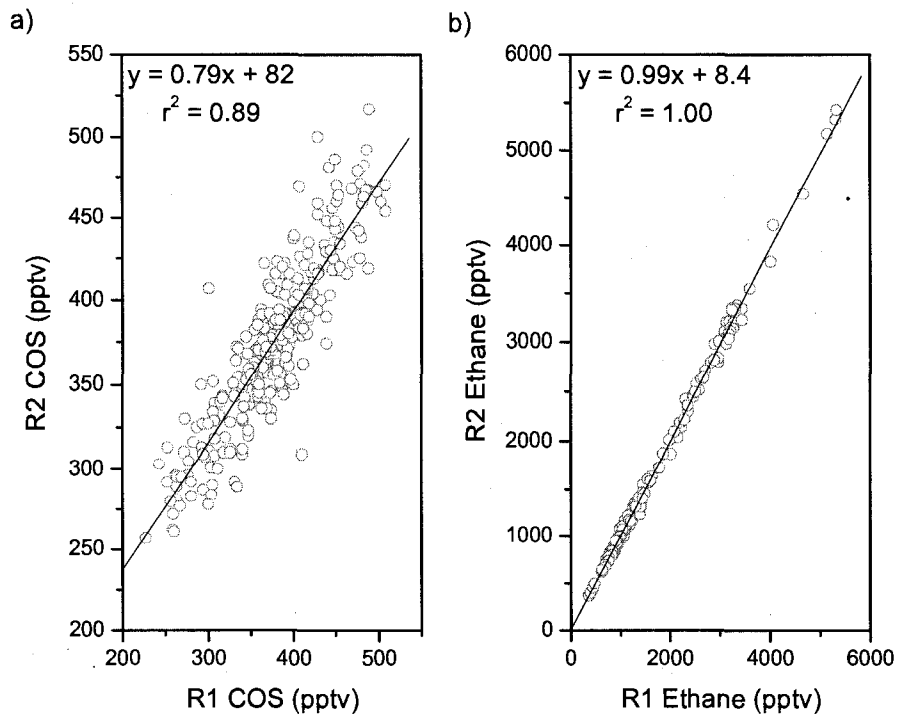


**Figure 4.2:** A comparison of R1 and R2 a) COS and b) ethane ambient mixing ratios at 16m above ground from 15 –28 September 2004.

elevated levels of COS indicative of marine influence (Figure 4.3a and c). In contrast, moderate wind speeds from the north and east, warm daytime temperatures, and sunny conditions generally prevailed at the site during 21 – 27 September (Figure 4.3a and b). During this time period, ambient  $\text{CO}_2$  mixing ratios in R1 followed a pronounced diurnal pattern with minimum levels in the late afternoon corresponding to photosynthetic uptake and maximum levels overnight.

COS mixing ratios in R1 and R2 also exhibited a diurnal pattern during this time period, although less pronounced than  $\text{CO}_2$  and with minimum mixing ratios at night (Figure 4.3c and 4.4). Similar diurnal patterns have been observed in a temperate

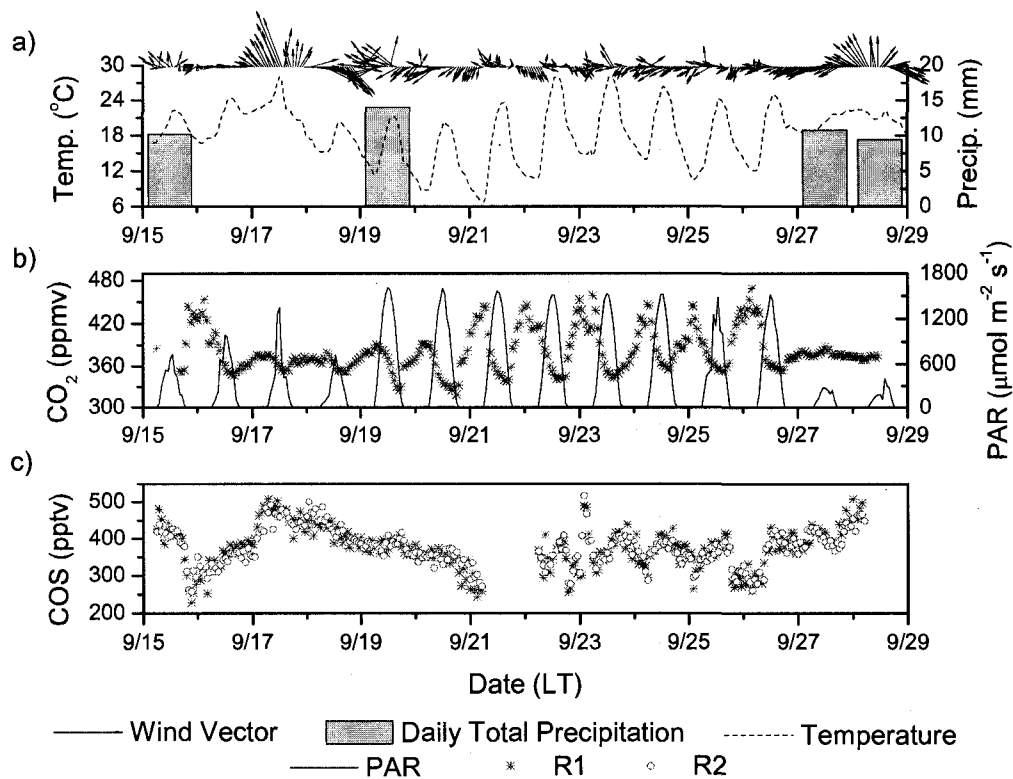


**Figure 4.3:** Select canopy measurements made at 16m above ground in September 2004 including a) air temperature, wind speed (displayed as vector) and total daily precipitation; b) ambient R1 CO<sub>2</sub> mixing ratios and photosynthetically active radiation (PAR); and c) R1 and R2 COS mixing ratios.

oak forest in California [Kuhn *et al.*, 1999], a tropical rainforest in Cameroon [Kesselmeier *et al.*, 1993], and a spruce forest in Germany [Steinbacher *et al.*, 2004] and are attributed to a combination of turbulent transport of COS during the day [Kesselmeier *et al.*, 1993] and nighttime depletion under a stable nocturnal boundary layer [Kuhn *et al.*, 1999; Steinbacher *et al.*, 2004]. Daytime mixing ratios during non-hurricane periods at DF averaged  $392 \pm 4$  pptv in R1 and  $388 \pm 4$  pptv in R2, well below the global mean mixing ratio of 500 pptv. These lower mixing ratios are consistent with observations at

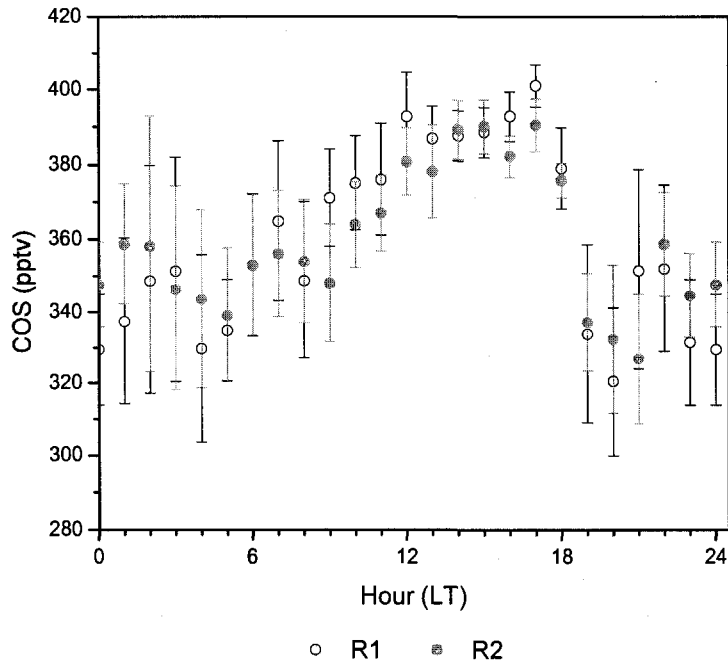


**Figure 4.4:** Hourly mean COS mixing ratios at 16 m above ground during non-hurricane periods (15-16 and 21-26 September 2004) in R1 and R2.

low altitude, northern hemisphere continental sites during summer and reflect the influences of a significant vegetation sink [Kuhn *et al.*, 1999; Montzka *et al.*, 2007; Steinbacher *et al.*, 2004].

The lowest COS mixing ratios (R1: 227 pptv, R2: 257 pptv), observed at DF on the night of 15 September, coincided with the lowest wind speeds observed during the study period and further indicate a strong nighttime deposition for this gas within the forest. From 18:00 to 01:00 LT that night, R1 COS mixing ratios were also consistently lower than R2 mixing ratios by 10-60 pptv. A closer examination of the hourly mean COS mixing ratios in each ring during non-hurricane periods (15-16 and 21-27 September) reveals that COS mixing ratios were generally lower overnight (23:00 to 04:00 LT) in R1 than in R2 (Figure 4.4). While these differences between the two rings

were small on average (0-20 pptv), they do imply that the nighttime COS sink was slightly stronger in R1 than in R2 in September 2004.

#### 4.3.2 Vertical Profile Measurements, September 2004 and June 2005

Further evidence of a forest sink for COS is found in the vertical profile obtained at 18:00 LT on 26 September 2004 (Figure 4.5a). Interestingly, R1 showed a relatively consistent reduction in COS mixing ratios on that day from 450 pptv above the canopy (20 m) to 362 pptv at ground level (0m) indicating a strong canopy and ground level sink. In contrast, R2 COS mixing ratios decreased from 413 pptv above the canopy to 370 pptv at 10 m above ground before increasing to 394 pptv again at ground level indicating a limited surface sink at that location.

Decreases in COS occurred at ground level in all profiles in June 2005, including those in R2, suggesting conditions favored a stronger surface sink at all sites during the second field study (Figures 4.5b, c, and d). The nighttime profile obtained at 00:30 LT on 6 June 2005 (Figure 4.5c) also indicates there were strong canopy sinks for both R1 and R2 with COS mixing ratios from 0 to 15 m above ground (R1 = 309-359 and R2 = 316-412 pptv) well below levels observed above the canopy (406 and 417 pptv at 20 m above ground in R1 and R2, respectively). Evidence of a canopy sink was more limited in the daytime vertical profiles taken in the six control and elevated CO<sub>2</sub> rings sampled on 5 June (Figure 4.5c) and in R1 and R2 on 10 June (Figure 4.5d). A decrease in average COS mixing ratios in the three elevated CO<sub>2</sub> rings was observed on 5 June from 490 ±20 pptv at 15 m to 435 ±9 pptv at 10 m above ground. However, profiles taken simultaneously in the three control rings indicated a slight increase in COS mixing ratios from 460 ±20 pptv to 490 ±10 pptv over the same elevation difference (Figure 4.5c).

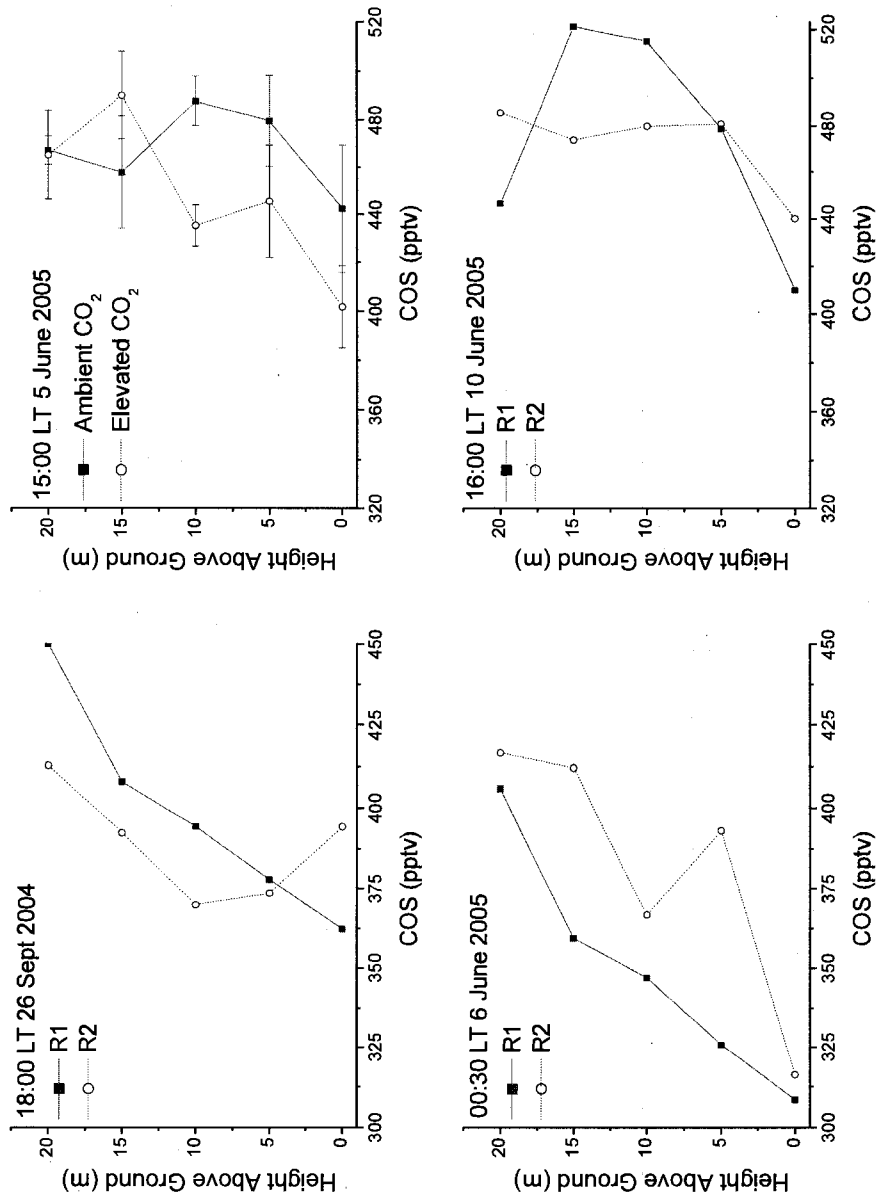


**Figure 4.5:** Ambient COS measurements from ground level (0 m) to above the forest canopy (20 m) at a) 18:00 LT on 26 September 2004, b) 15:00 LT on 5 June 2005; c) 00:30 LT 6 June 2005; and d) 16:00 LT 10 June 2005. Error bars on 5c represent standard error of the mean at each height within the three ambient (R1, R5, R6) and three elevated CO<sub>2</sub> (R2, R3, R4) rings sampled.

Furthermore, profiles taken on 10 June showed little change in COS mixing ratios throughout the canopy in R2 and an increase in R1 from  $460 \pm 20$  pptv at 20 m above ground to  $520 \pm 20$  pptv between 10 and 15 m height within the canopy (Figure 4.5d).

Previous studies of ambient COS mixing ratios in loblolly pine forests suggest that COS uptake is highly variable. Vertical profiles obtained at the University of Georgia B.F. Grant research forest, a loblolly pine stand located southeast of Atlanta, GA, suggested significant release of COS within the forest canopy [Berresheim and Vulcan, 1992]. Ambient mixing ratios in the Georgia pine stand (500-900 pptv) were also significantly higher than those observed at DF indicating COS sources dominated over sinks in that region. At DF, direct measurements of COS consumption in branch enclosure sampling of the two dominant tree species in June 2005 (Section 4.3.3) provides strong evidence that trees were not a source of COS within the canopy. Instead, the observation of canopy increases in vertical profile measurements during this same time period implies that COS transport and turbulence within the canopy may have impacted daytime vertical profile measurements in June 2005.

#### 4.3.3 Vegetation Flux Measurements, June 2005

According to the branch enclosure measurements made in June 2005, both loblolly pine and sweet gum trees were sinks for COS at DF (Figure 4.6 and 4.7). Negative fluxes, indicating uptake of COS from the atmosphere, dominated COS exchange for both species over the 48 hour sampling periods. The distinct diurnal patterns of COS fluxes observed for the two tree species reflect the multiple factors that can impact vegetative COS exchange such as ambient COS levels, environmental controls over stomatal conductance, and leaf photosynthetic capacity. The relationships between the COS

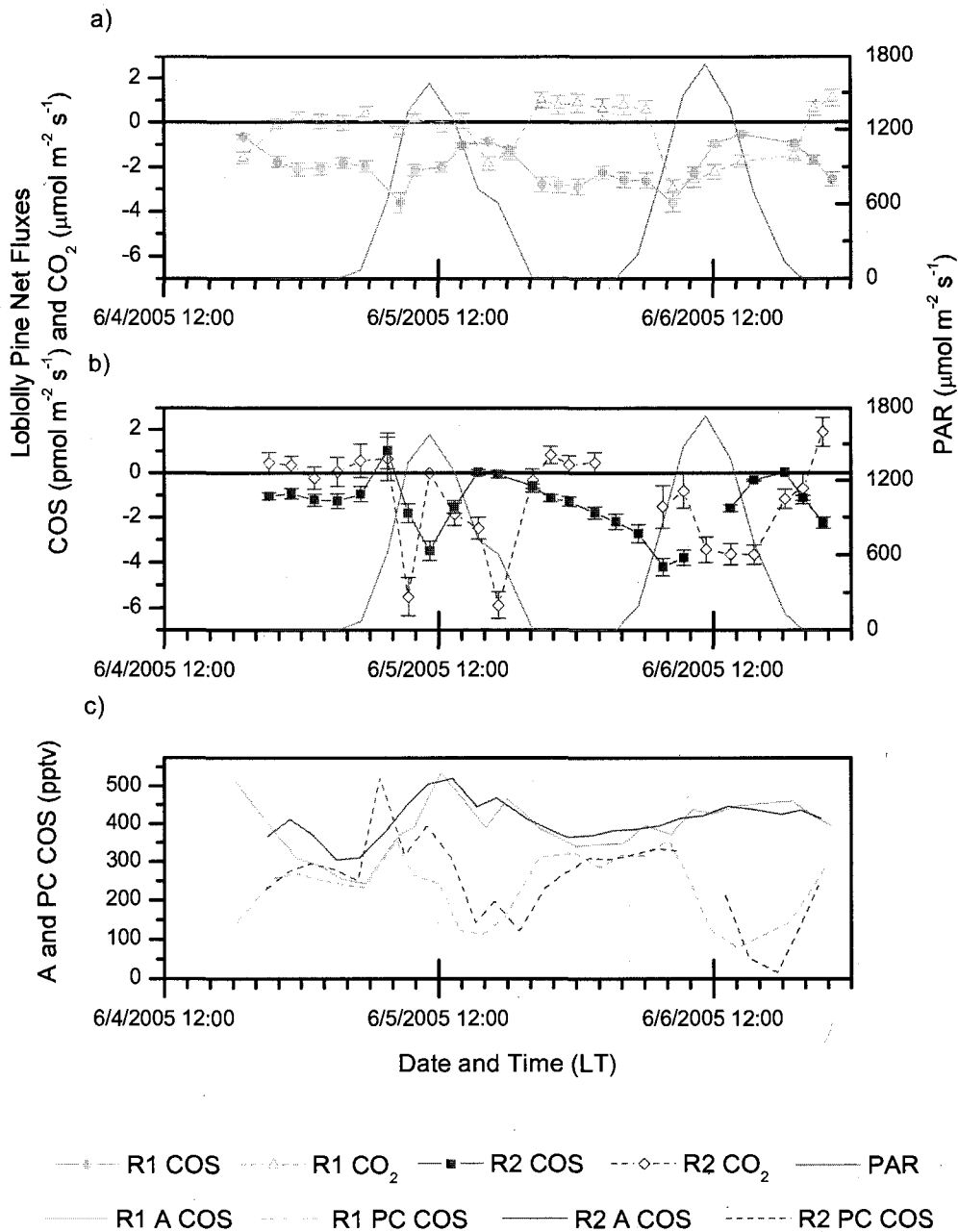


**Figure 4.6:** Time series of branch enclosure measurements of net COS and CO<sub>2</sub> flux for a) R1 loblolly pine and b) R2 loblolly pine. All fluxes are normalized to leaf area of the branch sampled (m<sup>2</sup>). Measurements of photosynthetically active radiation (PAR) for the corresponding time periods are shown in 4.6a and b to help delineate day and night periods. The corresponding measurements of ambient (A) and post-catalyst (PC) COS mixing ratios are given in 4.6c.

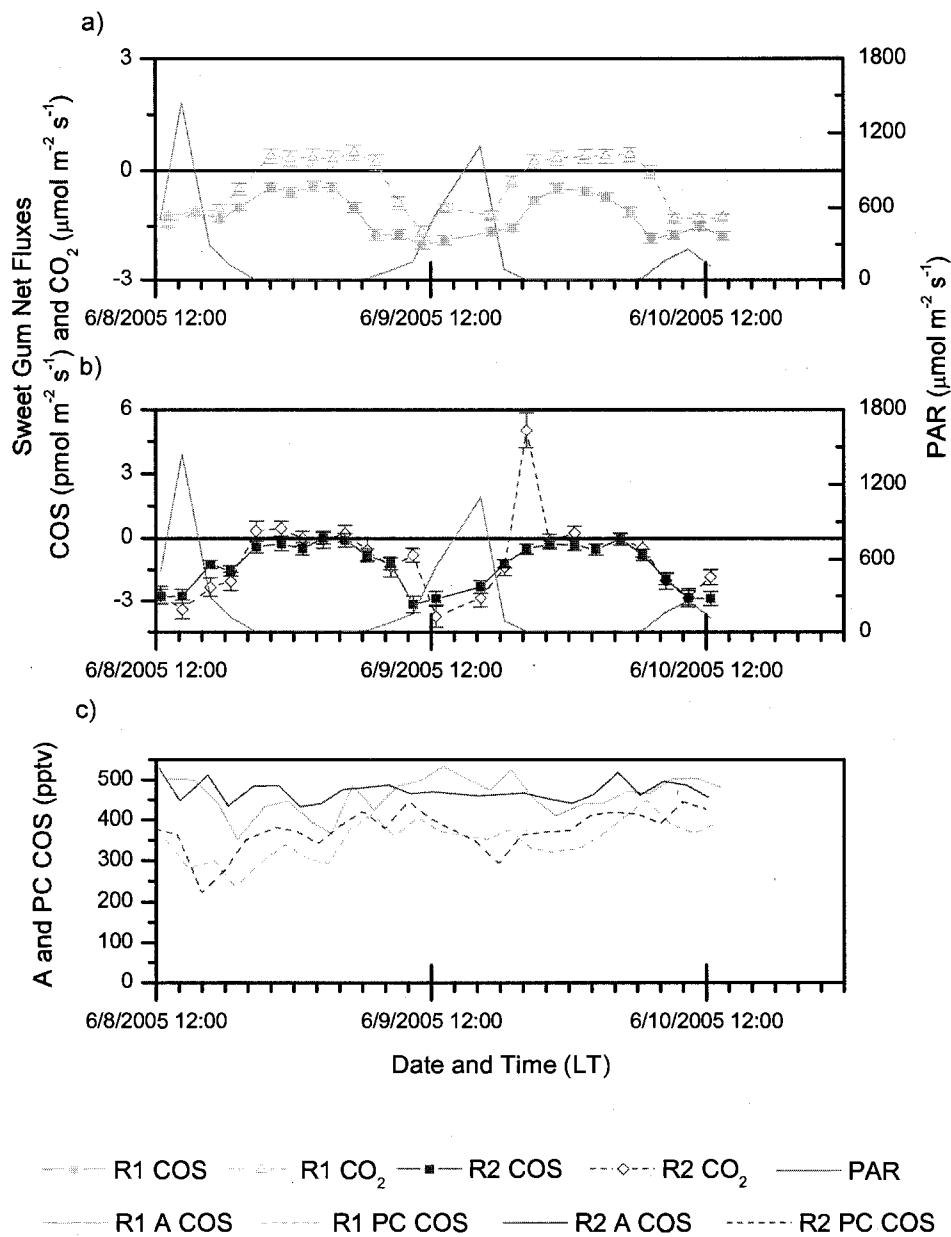


**Figure 4.7:** Time series of branch enclosure measurements of net COS and  $\text{CO}_2$  flux for a) R1 sweet gum and b) R2 sweet gum. All fluxes are normalized to leaf area of the branch sampled ( $\text{m}^2$ ). Measurements of photosynthetically active radiation (PAR) for the corresponding time periods are shown in 4.7a and b to help delineate day and night periods. The corresponding measurements of ambient (A) and post-catalyst (PC) COS mixing ratios are given in 4.7c.

vegetation fluxes measured at DF and these factors will be discussed in more depth in the following two sections.

4.3.3.1 Post-Catalyst COS Levels. For all trees sampled, net COS flux exhibited the strongest correlation with the post-catalyst (PC) COS levels flowing into the bag (Figure 4.8). Similar strong correlations have been observed for crop plants [Kesselmeier and Merk, 1993] and deciduous trees in northern China [Geng and Mu, 2006] indicating that the major factor controlling the rate of COS uptake for many plants is the amount of COS available. The linear regressions for these relationships (Figure 4.8) can be used to calculate compensation points, or the COS mixing ratios at which production and consumption processes balance each other and net flux equals zero. At DF, the daytime ( $\text{PAR} > 15 \mu\text{mol m}^{-2} \text{s}^{-1}$ ) compensation points were low (approximately 30, 20, 30, and 85 pptv for R1 and R2 loblolly pines and R1 and R2 sweet gums, respectively) compared to the ranges calculated for rapeseed and corn (90-150 pptv [Kesselmeier and Merk, 1993]) and select Chinese deciduous trees (140-870 pptv [Geng and Mu, 2006]). These low compensation points further emphasize the significance of the DF site as a net COS sink.

It should be noted that the unintentional removal of ambient COS by the palladium catalyst in the inlet airflow influenced the diurnal patterns and magnitudes of COS flux rates measured in the branch enclosures. For example, the significant afternoon depletion in PC COS mixing ratios responsible for the minimum uptake rates (least negative fluxes) observed for both R1 and R2 loblolly pines did not reflect ambient (A) COS conditions. As Figure 4.6c indicates, ambient COS levels during loblolly pine measurements actually reached maximum values during the day following a diurnal pattern similar to that observed during non-hurricane periods in September 2004. The

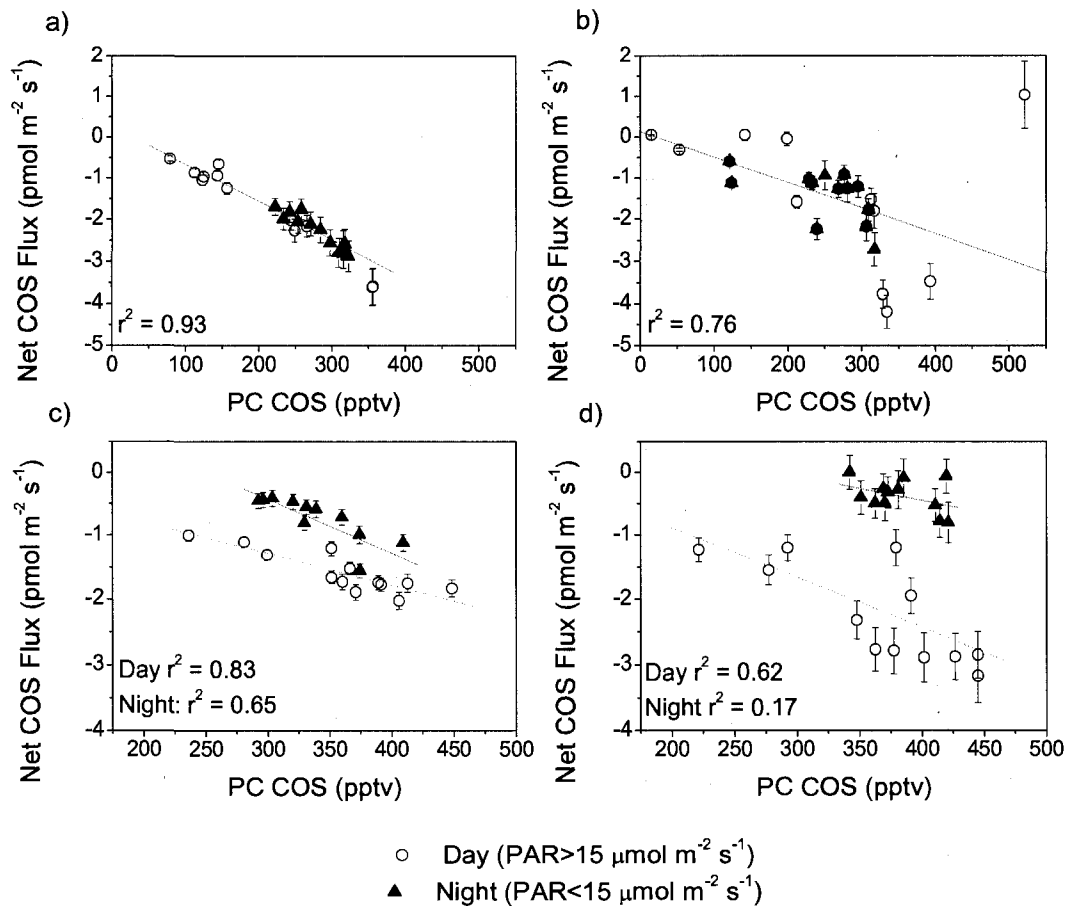


**Figure 4.8:** The relationship between net COS flux and PC COS levels entering the enclosure for a) R1 loblolly pine; b) R2 loblolly pine; c) R1 sweet gum; d) R2 sweet gum. Lines are the linear regressions for a) and b) total data displayed; and c) and d) day and night data separately. All correlations between net COS flux and PC COS were significant ( $p < 0.05$ ) except for the R2 sweet gum nighttime data.

levels of PC COS were more consistent throughout the two day sampling period for the sweet gum trees although PC COS was depleted compared to ambient COS levels (Figure 4.7c). The removal of COS from the inlet airflow suggests that the magnitude of COS uptake rates measured in both loblolly pine and sweet gum enclosures was lower than expected for the open canopy. As the strong negative correlations between PC COS

levels and net COS uptake rates indicate (Figure 4.8), higher ambient COS mixing ratios would result in higher uptake rates for all the trees sampled.

To provide a representative picture of loblolly pine and sweet gum COS uptake independent of PC COS depletion, deposition velocities,  $V_d$  ( $\text{mm s}^{-1}$ ), are provided in Table 4.1 and used in subsequent analyses. These are defined as the rate of flux divided by the corresponding PC COS levels at the time of measurement. The loblolly pine and sweet gum  $V_d$  measured at Duke Forest (daytime means =  $0.20 \pm 0.01$ ,  $0.13 \pm 0.03$ ,  $0.11 \pm 0.01$ , and  $0.15 \pm 0.01 \text{ mm s}^{-1}$  for R1 and R2 loblolly pine and R1 and R2 sweet gum, respectively) are consistent with the range of COS  $V_d$  obtained in other laboratory and field studies of deciduous and coniferous tree species ( $-0.1$  (indicating emission) to  $1.8 \text{ mm s}^{-1}$  [Geng and Mu, 2006; Kesselmeier et al., 1993; Kuhn et al., 1999; Sandoval-Soto et al., 2005; Xu et al., 2002]).

Location	Sink	Measurement Time	$V_d$ per LA ( $\text{mm s}^{-1}$ )	
			COS	$\text{CO}_2$
R1	Loblolly Pine	Day	$0.20 \pm 0.01^a$	$0.09 \pm 0.02^{ab}$
		night	$0.197 \pm 0.004^a$	$-0.032 \pm 0.007^c$
	Sweet Gum	day	$0.107 \pm 0.003^b$	$0.059 \pm 0.009^a$
		night	$0.046 \pm 0.004^c$	$-0.020 \pm 0.001^c$
R2	Loblolly Pine	day	$0.13 \pm 0.03^{abcd}$	$0.09 \pm 0.02^{ab}$
		night	$0.14 \pm 0.01^d$	$-0.01 \pm 0.02^c$
	Sweet Gum	day	$0.15 \pm 0.01^d$	$0.09 \pm 0.02^b$
		night	$0.024 \pm 0.004^e$	$-0.02 \pm 0.02^c$

**Table 4.1:** Mean COS and  $\text{CO}_2$  deposition velocities,  $V_d$ ,  $\pm$ standard error, for Ring 1 and Ring 2 vegetation.  $V_d$  were calculated from measured flux rates normalized to leaf area (LA) of the branch enclosed divided by PC COS and  $\text{CO}_2$  mixing ratios at the time of flux. Negative values reflect emission. Superscripts a,b,c,d, and e indicate significantly different means within each column ( $p < 0.05$ , independent means t-test, SPSS v. 15.0.1.1).

4.3.3.2 Stomatal Conductance and Photosynthetic Capacity. The day and night relationships between COS net flux and PC COS levels displayed in Figure 4.8 indicate distinct diurnal patterns of stomatal conductance for the loblolly pine and sweet gum trees. For example, similar relationships between day and night COS uptake rates and PC COS mixing ratios for R1 and R2 loblolly pines (Figure 4.8a and b) resulted in relatively consistent day and night  $V_d$  (Table 1; R1 =  $0.20 \pm 0.01$  and  $0.20 \pm 0.01$   $\text{mm s}^{-1}$ , R2 =  $0.12 \pm 0.04$  and  $0.14 \pm 0.01$   $\text{mm s}^{-1}$  day and night means, respectively). Substantial overnight COS flux is surprising since vegetative uptake of this gas occurs through plant stomata which presumably close at night. Increasing evidence indicates that a wide variety of plants, including several pine species, exhibit significant nighttime stomatal conductance [Caird *et al.*, 2007]. The COS uptake patterns observed in this study indicate that loblolly pine may fall into this category as well.

The absence of a strong relationship between PAR and COS  $V_d$  for the loblolly pine trees is particularly significant when considering the nighttime depletion observed in the ambient canopy measurements from September 2004. Previous observations of nighttime depletion in ambient forest COS mixing ratios have been attributed primarily to soil sinks as vegetative uptake was largely limited to daylight hours [Kuhn *et al.*, 1999; Steinbacher *et al.*, 2004]. However, comparable day and night  $V_d$  for the dominant tree species in the FACE rings at DF suggests vegetative uptake was a major nocturnal sink at this site, a possibility that will be explored in more depth in Section 4.3.5.2.

It is also interesting to note that COS uptake by loblolly pine trees did not have a significant correlation with  $\text{CO}_2$   $V_d$  (Figure 4.9). Several previous studies of vegetative COS consumption have indicated a strong relationship between photosynthetic  $\text{CO}_2$

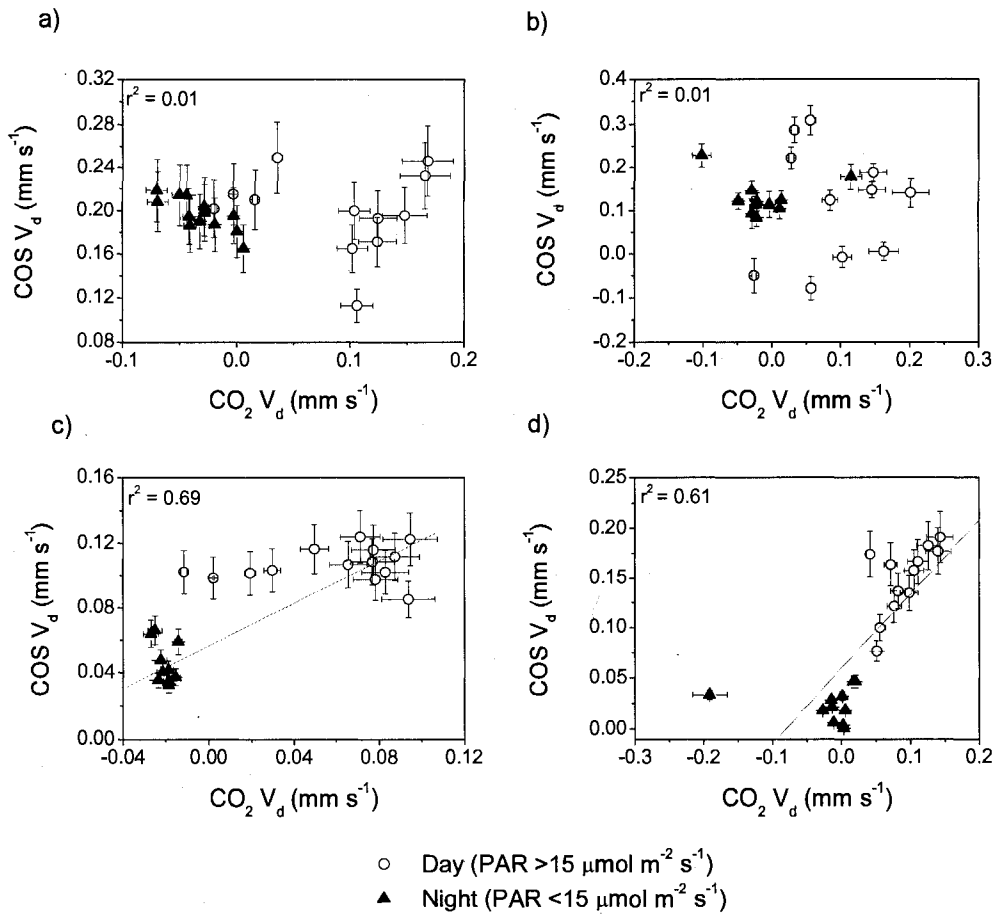


**Figure 4.9:** The relationship between COS and  $\text{CO}_2 V_d$  for a) R1 loblolly pine; b) R2 loblolly pine; c) R1 sweet gum; d) R2 sweet gum. Negative values indicate emission to the atmosphere. Lines shown in c) and d) are the linear regressions for total data displayed. Correlations between COS and  $\text{CO}_2 V_d$  were only significant ( $p < 0.05$ ) for the sweet gum trees.

assimilation and COS exchange [Geng and Mu, 2006; Kesselmeier and Merk, 1993; Kuhn et al., 1999; Xu et al., 2002]. However, Geng and Mu [2006] noted that strong correlations between  $\text{CO}_2$  and COS uptake in two Chinese deciduous trees were only observed during diurnal measurements made over one day. No significant linear correlations were observed when a larger data set of measurements was considered, which the authors attributed to the large variation in ambient COS mixing ratios [Geng and Mu,

2006]. *Montzka et al.* [2007] also noted the important influence of respiration and CO<sub>2</sub> loss during photosynthesis on vegetative CO<sub>2</sub> exchange, processes which are not mirrored in vegetative COS exchange. It is possible that any daytime relationship between COS uptake and CO<sub>2</sub> assimilation for the loblolly pines was obscured by the significant influence of the wide range of PC COS mixing ratios on net COS flux in combination with loblolly pine respiration and CO<sub>2</sub> loss. However, the large nighttime COS V<sub>d</sub> measured in this study indicates significant COS consumption occurred independently of CO<sub>2</sub> assimilation in the loblolly pines.

Interestingly, the mean nighttime R2 loblolly pine V<sub>d</sub> was significantly lower than the day and night means for the R1 loblolly pine (Table 4.1). Long-term photosynthetic acclimation to elevated CO<sub>2</sub> in loblolly pines at DF has been linked to reduced activity of the carboxylation enzyme Rubisco, involved in the light-independent reactions of the Calvin cycle, in one-year old needles [*Rogers and Ellsworth, 2002*]. As Rubisco can enhance COS uptake by consuming the CO<sub>2</sub> or HCO<sub>3</sub><sup>-</sup> produced by COS hydrolysis [*Protoschill-Krebs and Kesselmeier, 1992*], any reduction in its activity is likely to affect COS uptake rates as well. As a result, reduced V<sub>d</sub> for the R2 loblolly pine could reflect photosynthetic acclimation to long-term elevated CO<sub>2</sub> exposure [*Rogers and Ellsworth, 2002*]. However, the similar magnitude of daytime CO<sub>2</sub> V<sub>d</sub> between the R1 and R2 loblolly pines (Table 4.1; 0.09 ± 0.02 and 0.10 ± 0.02 mm s<sup>-1</sup>) suggests there was actually little difference in the photosynthetic capacity of the two branches sampled.

Instead, differences in the nighttime means of COS V<sub>d</sub> between the two rings most likely reflects decreased stomatal conductance for the R2 loblolly pine branch. It is unlikely this reduced stomatal conductance resulted from elevated CO<sub>2</sub> exposure as CO<sub>2</sub>

enrichment has had no significant effect on either stomatal conductance or density in loblolly pine [Ellsworth, 1999]. Differences in environmental conditions of the enclosures surrounding the two branches are the more likely cause of lower stomatal conductance for the R2 loblolly pine. In support of this, variations in nighttime R2 loblolly pine  $V_d$  were negatively correlated with enclosure temperature ( $r^2 = 0.49$ ,  $p=0.008$ ) indicating a certain degree of environmental influence on COS uptake. Furthermore, nighttime temperatures in the R2 loblolly pine enclosure were significantly warmer than those observed in the R1 enclosure (R1 =  $20.2 \pm 0.5$  and R2 =  $32 \pm 1$  °C night means) which would induce a decrease in stomatal conductance.

In contrast to the loblolly pines, the clear separation between day and nighttime flux relationships with PC COS for the deciduous sweet gum trees does reflect substantial stomatal closure at night (Figure 4.8c and d). The significantly different day and night mean sweet gum  $V_d$  values (Table 4.1; R1 =  $0.11 \pm 0.01$  and  $0.05 \pm 0.01$ , R2 =  $0.15 \pm 0.01$  and  $0.02 \pm 0.01$  mm s<sup>-1</sup> day and night means, respectively) are consistent with field measurements of live oak (*Quercus agrifolia*), a deciduous macrophyte in a California oak forest [Kuhn et al., 1999], and a variety of deciduous trees in northern China [Geng and Mu, 2006], all of which showed strong relationships between net COS uptake and light. As a result, the R1 and R2 sweet gum  $V_d$  values (combined day and night) were significantly correlated to changes in PAR (R1  $r^2 = 0.23$ ,  $p = 0.02$ ; R2  $r^2 = 0.48$ ,  $p < 0.001$ ), enclosure temperature (R1  $r^2 = 0.54$ ,  $p < 0.001$ ; R2  $r^2 = 0.74$ ,  $p < 0.001$ ), and CO<sub>2</sub>  $V_d$  (R1  $r^2 = 0.65$ ,  $p < 0.001$ ; R2  $r^2 = 0.61$ ,  $p < 0.001$ ), reflecting similar diurnal cycles.

For the R1 sweet gum, net nighttime flux and PC COS mixing ratios did exhibit a significant correlation (Figure 4.8c), suggesting that its stomates were still partially open

overnight. In support of this, variations in night  $V_d$  for the R1 sweet gum were also strongly correlated to enclosure temperature ( $r^2=0.77$ ,  $p<0.001$ ), similar to the R2 loblolly pine night  $V_d$ . However, this was not the case for the R2 sweet gum. Nighttime net COS fluxes for the R2 sweet gum were consistently near zero and nighttime  $V_d$  values had no significant relationship to PC COS levels (Figure 4.8d) suggesting that the R2 sweet gum stomates were generally closed overnight. Sweet gum trees exposed to elevated  $CO_2$ , like those in R2, have shown significant reductions in stomatal conductance [Herrick *et al.*, 2004b]. If this  $CO_2$  enrichment effect was responsible for the minimal nighttime  $V_d$  observed in R2, a similar reduction in the R2 sweet gum day  $V_d$  should also occur. Instead, mean daytime sweet gum  $V_d$  were significantly higher in R2 compared to R1 (Table 4.1;  $R1 = 0.11 \pm 0.01 \text{ mm s}^{-1}$ ,  $R2 = 0.15 \pm 0.01 \text{ mm s}^{-1}$ ). Significantly higher daytime  $CO_2$   $V_d$  in R2 (Table 4.1;  $R1 = 0.06 \pm 0.01 \text{ mm s}^{-1}$ ,  $R2 = 0.09 \pm 0.02 \text{ mm s}^{-1}$ ) actually suggests that the sweet gum branch sampled in R2 had a higher photosynthetic capacity than that in R1. These differences in COS and  $CO_2$   $V_d$  most likely reflect variations in the canopy position of the two sweet gum branches sampled as the branch in R1 was more sheltered (less open sunlight) than the R2 branch. Observations of sweet gum sun and shade leaves at DF indicates that the photosynthetic capacity of sun leaves at the top of the canopy was 80% more than that of shade leaves in the understory [Herrick and Thomas, 2001]. Similarly, sun leaf stomatal conductance was more than twice that of shade leaves [Herrick *et al.*, 2004b]. Similar effects of canopy position on COS consumption rates have also been noted for a tropical rainforest tree species in Cameroon where COS deposition at the top of the canopy was nearly 4 times that measured for the same species growing at ground level [Kesselmeier *et al.*, 1993].

It should be noted that the limited sample size in this study may have prevented direct observations of the effect of CO<sub>2</sub> enrichment on COS uptake. As noted previously, long term CO<sub>2</sub> enrichment does have significant effects on both photosynthetic capacity and stomatal conductance in loblolly pines and sweet gums [Herrick *et al.*, 2004b; Rogers and Ellsworth, 2002]. Because stomatal conductance and photosynthetic capacity variability resulting from environmental and spatial heterogeneity were major factors impacting COS uptake rates in this study, it is probable that CO<sub>2</sub> effects on these characteristics will also have an impact on vegetative COS uptake within the two rings. This potential influence on the net ecosystem flux estimates for the two rings will be considered more in Section 4.3.5.2.

#### 4.3.4 Soil Flux Measurements, June and September 2005

Soil was also a net sink for COS at DF (Table 4.2, Figure 4.10). The range of net fluxes observed in the soil static chamber measurements (R1: -3 to -0.53 pmol m<sup>-2</sup> s<sup>-1</sup>; R2: -2.7 to 0 pmol m<sup>-2</sup> s<sup>-1</sup>) were comparable to other field measurement from a spruce forest in Germany (-1.38 to -0.23 pmol m<sup>-2</sup> s<sup>-1</sup> [Steinbacher *et al.*, 2004]), a California oak forest (-13.3 to -8.8 pmol m<sup>-2</sup> s<sup>-1</sup> [Kuhn *et al.*, 1999]), and three types of Chinese subtropical forest (-11.82 to -1.22 pmol m<sup>-2</sup> s<sup>-1</sup> [Yi *et al.*, 2007]). There were no significant differences between R1 and R2 mean net fluxes indicating that CO<sub>2</sub> enrichment had little effect on soil COS consumption.

Instead, the one significant difference observed in the soil fluxes at DF was between R2 collar A and B on 9 June 2005 (Figure 4.10a). The mean R2 collar B flux for that sampling day was  $-0.4 \pm 0.2$  pmol m<sup>-2</sup> s<sup>-1</sup> compared to  $-2.0 \pm 0.2$  pmol m<sup>-2</sup> s<sup>-1</sup> for R2 collar A. This was not a consistent difference as the mean R2 collar fluxes were more

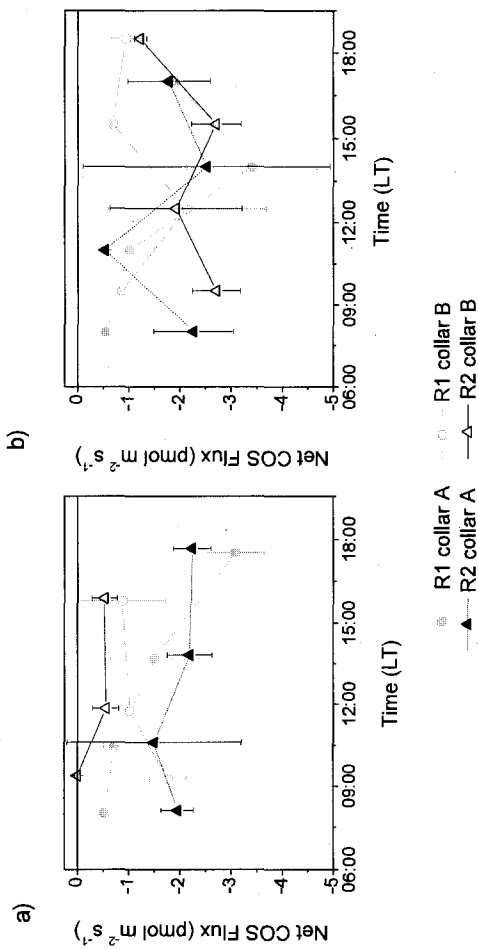


**Figure 4.10:** Chamber measurements of soil COS flux on a) 9 June 2005 and b) 20 September 2005. All fluxes are normalized to ground area ( $\text{m}^2$ ).

Month	Ring	Net COS flux ( $\text{pmol m}^{-2} \text{s}^{-1}$ )	Ambient COS (pptv)	$\text{COS } V_d$ per GA ( $\text{s}^{-1}$ )	Air Temp ( $^{\circ}\text{C}$ )	Surface Temp ( $^{\circ}\text{C}$ )	5 cm Depth Temp ( $^{\circ}\text{C}$ )	10 cm Depth Temp ( $^{\circ}\text{C}$ )	Volumetric Soil Moisture ( $\text{m}^3 \text{m}^{-3}$ )
June	1	$-1.4 \pm 0.3^a$	$520 \pm 30^a$	$0.06 \pm 0.01^a$	$24.3 \pm 0.6^a$	$22.8 \pm 0.4^a$	$20.1 \pm 0.2^a$	$19.7 \pm 0.2^a$	$0.296 \pm 0.007^a$
	2	$-1.3 \pm 0.3^a$	$500 \pm 30^a$	$0.06 \pm 0.02^a$	$24.6 \pm 0.6^a$	$22.5 \pm 0.5^a$	$20.5 \pm 0.2^a$	$19.8 \pm 0.2^a$	$0.384 \pm 0.009^b$
Sept.	1	$-1.4 \pm 0.3^a$	$340 \pm 10^b$	$0.10 \pm 0.02^{ab}$	$27.7 \pm 0.7^b$	$26.5 \pm 0.8^b$	$22.7 \pm 0.2^b$	$22.3 \pm 0.1^b$	$0.205 \pm 0.001^c$
	2	$-2.0 \pm 0.3^a$	$352 \pm 6^b$	$0.14 \pm 0.02^b$	$27.3 \pm 0.8^b$	$27.2 \pm 0.8^b$	$22.6 \pm 0.1^b$	$22.3 \pm 0.2^b$	$0.233 \pm 0.001^d$

**Table 4.2:** Means  $\pm$  standard error for the soil static chamber measurements made in June and September 2005. Mean fluxes and deposition velocities,  $V_d$ , are normalized to ground area (GA). Superscripts a, b, c, and d indicate significantly different means within each column ( $p < 0.05$ , independent means t-test, SPSS v. 15.0.1.1).

comparable on 20 September 2005 (Collar A =  $-1.8 \pm 0.4$  pmol m<sup>-2</sup> s<sup>-1</sup>, Collar B =  $-2. \pm 0.4$  pmol m<sup>-2</sup> s<sup>-1</sup>). Laboratory studies indicate that soil temperature, water content, and ambient levels of COS all can affect COS consumption in soils [Kesselmeier *et al.*, 1999]. While there were no significant differences in soil temperature or ambient COS levels between the two collars on 9 June, the variability in measured fluxes could reflect a spatial difference in soil moisture content or microbial community activity in Ring 2 that was not captured by our measurements. For example, soil incubations indicate that COS uptake rates can decrease rapidly with increasing soil moisture content [Kesselmeier *et al.*, 1999] and TDR measurements of volumetric soil moisture in Ring 2 were high on 9 June 2005 (Table 4.2) reflecting intermittent rain that day. However, spatial variability from differences in topography and/or vegetation was not captured in the ring averages; localized lower soil moisture conditions might have favored COS consumption at R2 collar A and the two R1 collars compared to R2 collar B.

The relationships observed between COS uptake and soil water content and ambient COS levels in laboratory studies were not clearly apparent from our measurements at DF. For example, there was no significant correlation between soil moisture and COS uptake rates when soil flux measurements from both June and September were considered (Figure 4.11a). Similarly, changes in ambient COS mixing ratios were not correlated to COS uptake rates (Figure 4.11b). The only correlation observed for the DF soil fluxes was with the soil surface temperature (Figure 4.11c,  $R^2 = 0.16$ ,  $p = 0.03$ ). Using deposition velocities,  $V_d$ , instead of flux rates improved the soil surface temperature correlation slightly (Figure 4.11d) and indicates that ambient COS levels did have a minor effect on COS consumption rates. The proportion of  $V_d$

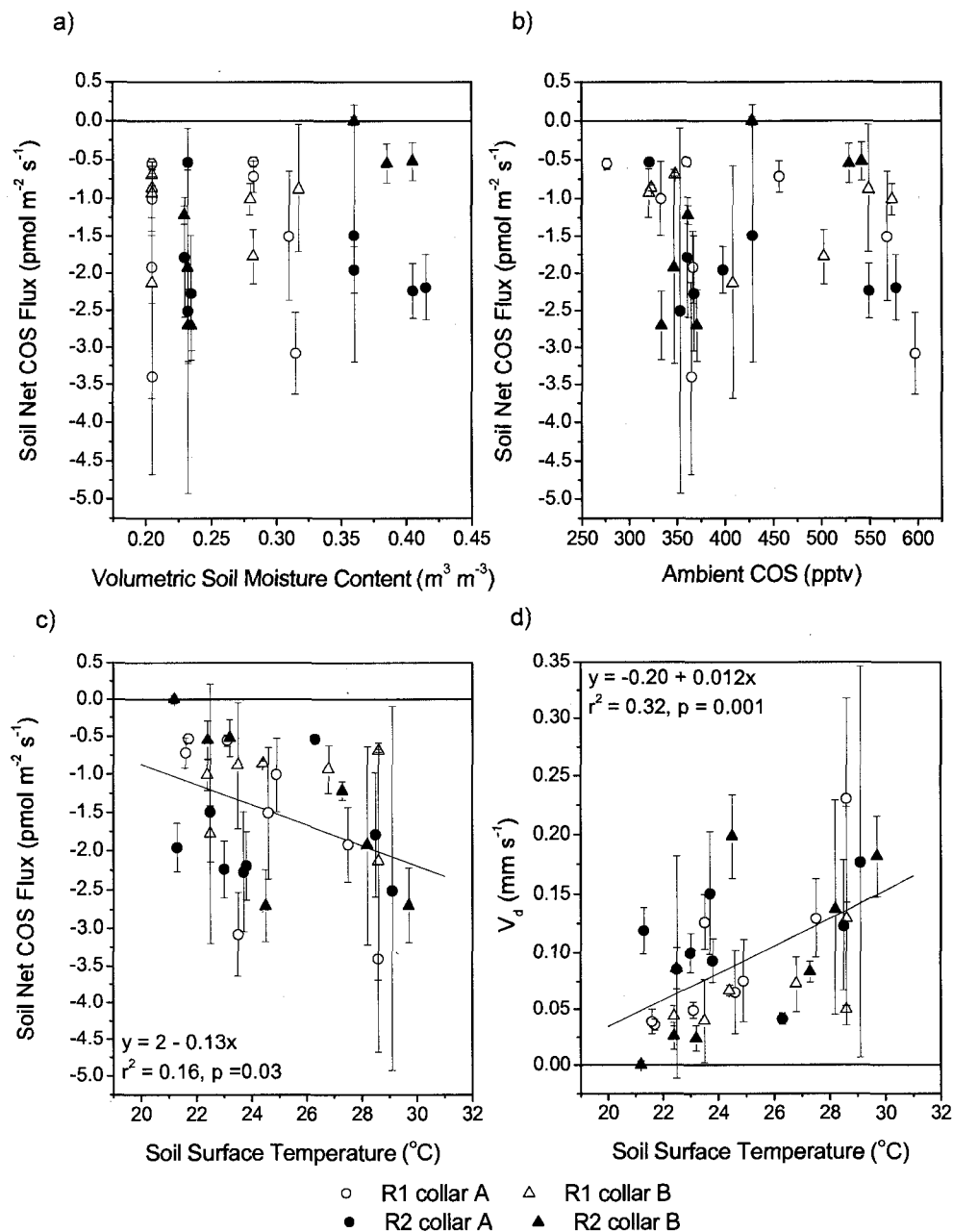


**Figure 4.11:** Soil net COS fluxes versus a) volumetric soil moisture; b) ambient COS mixing ratios; and c) soil surface temperature. Figure 4.11d displays the relationship between soil COS deposition velocity,  $V_d$ , versus surface temperature.

variability attributable to the temperature relationship, indicated by the coefficient of determination ( $r^2$ ), was small and suggests that there were other major unidentified factors affecting COS flux at DF. However, the temperature relationship observed at DF was in contrast to laboratory studies, which showed maximum COS uptake between 16 and 20 °C with decreasing rates of consumption between 20 and 30 °C [Kesselmeier *et al.*, 1999]. At DF, all soil temperatures were between 19 and 30 °C and deposition velocities increased with increasing temperature (Figure 4.11d).

Other field studies of forest soils have also shown variable responses to these factors. For example, optimum net fluxes were observed between 8 and 9 °C over a 5 to 15 °C soil temperature range in a German spruce forest while significant uptake was observed at soil moisture contents well above laboratory optimal conditions [Steinbacher *et al.*, 2004]. In three subtropical forest types in China, net COS soil uptake was not correlated with soil moisture or temperature except when considered together in multiple regression second order polynomial fits [Yi *et al.*, 2007]. The strongest individual correlations observed in these Chinese forests were actually with soil respiration and ambient levels of COS. Such highly variable relationships with COS net flux reflect both the complexity of competing interactions in natural environments as well as the potential effect of different soil types and microbial communities on COS gas exchange.

#### 4.3.5 Estimates of Net Ecosystem Flux, September 2004 and June 2005

Table 4.3 summarizes the mean values and ranges for the net ecosystem COS flux estimates calculated using gradient flux (GF) and nightly net flux (NF) methods. The estimates indicate a wide range of both COS emission and uptake at DF. In particular, the range of COS net fluxes calculated with the gradient methods (R1: -1000 to 1200 pmol

Date	Method	Net Ecosystem COS Flux ( $\text{pmol m}^{-2} \text{s}^{-1}$ )			
		Ring 1		Ring 2	
		mean	range	mean	range
19-20 Sept. 2004	Bowen Ratio GF	20 $\pm$ 80	-1000 to 1200	20 $\pm$ 70	-1100 to 1000
19-20 Sept. 2004	Similarity Hypothesis GF	20 $\pm$ 80	-1000 to 1200	20 $\pm$ 70	-1100 to 1000
23-24 Sept. 2004	Bowen Ratio GF	-40 $\pm$ 20	-300 to 40	20 $\pm$ 20	-200 to 200
23-24 Sept. 2004	Similarity Hypothesis GF	-40 $\pm$ 20	-300 to 30	20 $\pm$ 20	-200 to 200
15-16 Sept. 2004	NF	-30 $\pm$ 20	-70 to 30	-20 $\pm$ 10	-70 to -10
5-6 June 2005	NF	-30 $\pm$ 20	-50 to -8	-10 $\pm$ 10	-50 to 30

**Table 4.3:** A comparison of the means  $\pm$ standard error and ranges of net ecosystem COS flux estimates made for September 2004 and June 2005 using gradient (GF) and net nightly (NF) flux methods.

$\text{m}^{-2} \text{s}^{-1}$ ; R2: -1100 to 1000  $\text{pmol m}^{-2} \text{s}^{-1}$ ) encompassed values three orders of magnitude larger than measured plant and soil fluxes at DF. Such a wide range suggests that the gradient measurements were influenced by more than just COS exchange processes within the forest, a possibility which will be discussed in more depth in Section 4.3.5.1. In contrast, the range of NF estimates (-70 to 30  $\text{pmol m}^{-2} \text{s}^{-1}$ ) were comparable in magnitude to the mean ecosystem COS fluxes of -2.4 and -93  $\text{pmol m}^{-2} \text{s}^{-1}$  observed for a temperate oak [Kuhn *et al.*, 1999] and spruce [Xu *et al.*, 2002] forest, respectively. Section 4.3.5.2 presents a comparison of the individual vegetation and soil sink strengths measured within the two rings to the ecosystem NF estimates.

4.3.5.1 Gradient Flux Estimates. Figure 4.12 presents the time series of net ecosystem GF estimates calculated from the gradient air samples collected at 16m (canopy height) and 20m (above the canopy) on 19 – 20 and 23 – 24 September 2004. Because the fluxes calculated according to the Monin-Obukhov similarity hypothesis equations were very similar to those calculated using the modified Bowen ratio method, only the Bowen ratio GF are shown in Figure 4.12 for clarity. In addition to COS fluxes, ethane flux estimates are shown as representative of a trace gas with no known sources or

sinks in the forest. The large ethane fluxes calculated indicate that the gradient measurements at DF did not provide an accurate assessment of actual fluxes within the two rings (Figures 4.12a and b). Even within the lower range of GF estimates (-100 to 100 pmol m<sup>-2</sup> s<sup>-1</sup>; Figures 4.12c and d), net ethane fluxes were generally of the same magnitude or greater than COS flux estimates suggesting that the gradient measurements were predominantly influenced by processes other than vegetation and soil exchange.

In order for gradient measurements to reflect near source or sink influence, the length scale of turbulent transport eddies has to be smaller than the scalar concentration gradient [*Simpson et al.*, 1998]. Above forests, turbulence length scales can be on the same order as the canopy height and the best conditions for gradient measurements are usually found above the roughness sublayer, two to three canopy heights above the ground [*Arya*, 2001]. Since most gradient measurements are limited for practical reasons to the roughness sublayer, GF calculations are usually corrected by scaling against an independent assessment of flux [*Rinne et al.*, 2000]. In modified Bowen ratio calculations, this is incorporated into the turbulent exchange coefficient while fluxes calculated directly from similarity theory relationships are corrected by multiplying by an enhancement factor,  $\gamma$ . Observed values for  $\gamma$  range from 1 to 3 over a variety of forests [*Simpson et al.*, 1998]. However, the values of  $\gamma$  calculated at DF using equation (14) were generally less than 1 and often negative (means =  $-0.4 \pm 0.4$  for 19 – 20 September 2004 and  $0.5 \pm 0.2$  for 23 – 24 September 2004) reflecting gradients of CO<sub>2</sub> over DF that were often larger and opposite in direction than expected from eddy covariance measurements of CO<sub>2</sub> flux.

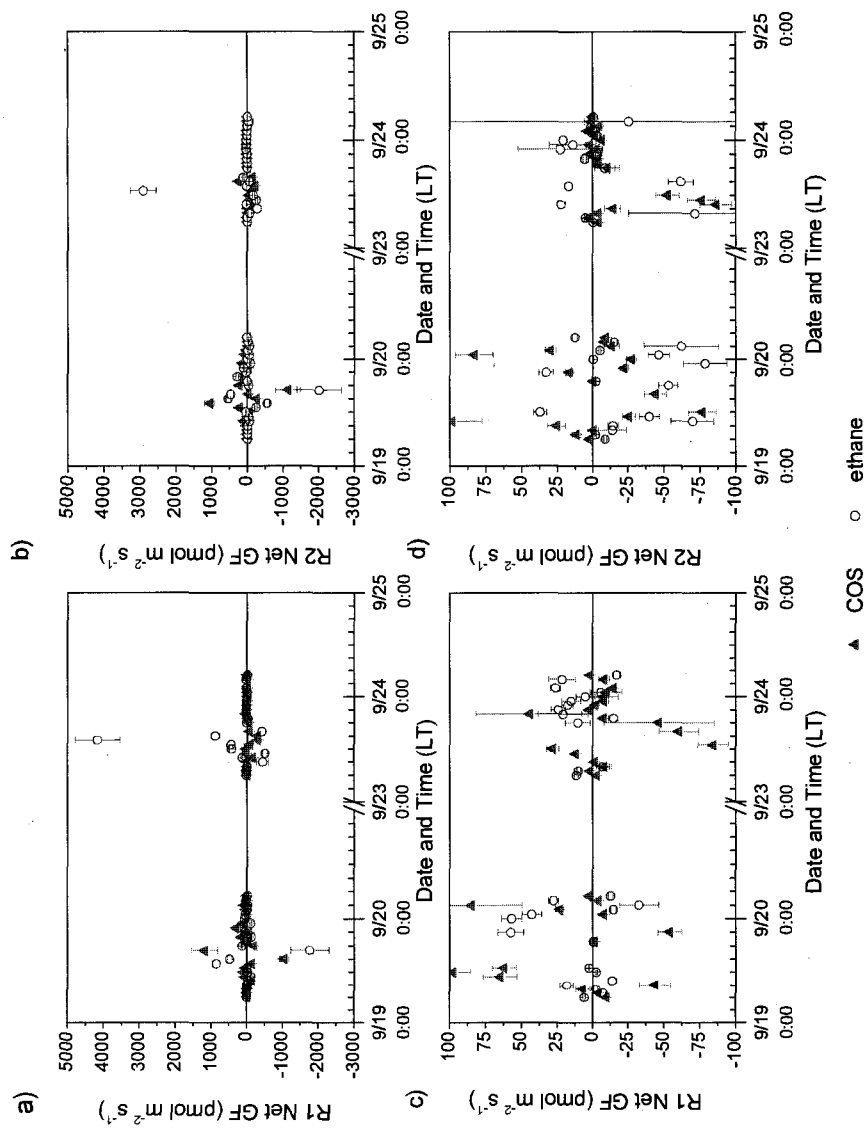


**Figure 4.12:** A comparison of COS and ethane gradient fluxes (GF) calculated using modified Bowen-ratios method for R1 and R2 from a) 18 – 19 September 2004; and b) 23 – 24 September 2004. Figures 10c and d present the same time series focused on GF within the range of  $-100 \text{ pmol m}^{-2} \text{s}^{-1}$  and  $100 \text{ pmol m}^{-2} \text{s}^{-1}$  to facilitate comparison of lower ethane and COS flux magnitude

Breakdown in similarity theory (which underlies both the modified Bowen-ratio and similarity theory flux calculations) has previously been attributed to the dominating influence of large wind gusts or turbulent transport on concentration gradients [Simpson *et al.*, 1998]. The evidence indicates that turbulent transport was indeed significant on both gradient sampling periods. On 19 – 20 September 2004, the DF site experienced the tail end of Hurricane Ivan. Relatively high wind speeds during that time (mean =  $2.5 \pm 0.8 \text{ m s}^{-1}$ ) suggest that transport impacted gradient concentrations more than local sources; this could explain the unexpected reversal in sign for the CO<sub>2</sub> gradient above the canopy compared to eddy covariance measurements. Wind speeds were lower on 23 – 24 September 2004 (mean =  $1.6 \pm 0.3 \text{ m s}^{-1}$ ). However, anthropogenic compound mixing ratios were significantly elevated during this time period reflecting a strong regional anthropogenic influence. For example, mean 16m ethane mixing ratios in both rings during these two days was  $3400 \pm 200 \text{ pptv}$ . Anthropogenic concentration differences between the 16m and 20m measurement heights were also large with ethane differences ranging from -300 to 200 pptv. Such substantial differences suggest that turbulence in the forest roughness sublayer had a major impact on gradient measurements, even under calm conditions. As a result, the GF estimates of net ecosystem COS flux at DF cannot be considered reliable representations of forest sources and sinks.

4.3.5.2 Nighttime Flux Estimates. The NF results represent the best estimate of nighttime exchange processes at DF. It should be noted that the limited number of low wind speed nights and the lack of ML height measurements contributed to the large uncertainty for these calculations. However as a first approximation, the NF estimates

allow a valuable comparison between the individual vegetation and soil sinks measured and the net COS ecosystem flux at DF.

Estimates of individual vegetation and soil flux rates on 15 to 16 September 2004 and 4 to 5 June 2005 are also presented in Table 4.4 for comparison. The vegetation flux rates were calculated as follows:

$$\text{Veg. Flux} = V_{d,\text{veg}} * \text{LAI} * A_{\text{COS}} \quad (16)$$

where  $V_{d,\text{veg}}$  is the mean nighttime deposition velocity for LP and SG trees measured in each ring in June 2005, LAI is the mean leaf area index ( $\text{m}^2 \text{ LA m}^{-2} \text{ GA}$ ) corrected for needle clumping during September 2004 or June 2005, and  $A_{\text{COS}}$  is the mean ambient COS levels in  $\text{pmol m}^{-3}$  during the net ecosystem flux night. Similarly, soil flux rates were calculated as:

$$\text{Soil Flux} = V_{d,\text{soil}} * A_{\text{COS}} \quad (17)$$

The mean September 2005 soil deposition velocities,  $V_{d,\text{soil}}$ , in each ring were used for the night of 15 to 16 September 2004 while the mean June 2005  $V_{d,\text{soil}}$  were used for the night of 4 to 5 June 2005. For comparison, estimates of daytime net flux rates in June 2005 in each ring are also presented based on the mean daytime  $V_d$  and  $A_{\text{COS}}$  measured during the June 2005 enclosure experiments.

The mean ecosystem NF estimates generally agreed well with the combined vegetation and soil fluxes (Table 4.4). It should be noted that the vegetation and soil fluxes for 15 September 2004 ( $19 \pm 6$  and  $13 \pm 4 \text{ pmol m}^{-2} \text{ s}^{-1}$  for R1 and R2, respectively) were calculated using deposition velocities measured at other times during the year and the slightly higher mean NF estimates for that night ( $30 \pm 20 \text{ pmol m}^{-2} \text{ s}^{-1}$  for both R1 and R2) could reflect the effect of seasonal differences in temperature and/or soil moisture on

stomatal conductance and COS uptake rates. In contrast, the June 2005 NF estimates ( $20 \pm 10$  and  $10 \pm 10$   $\text{pmol m}^{-2} \text{s}^{-1}$  in R1 and R2, respectively) and vegetation and soil fluxes ( $22 \pm 8$  and  $17 \pm 6$   $\text{pmol m}^{-2} \text{s}^{-1}$  in R1 and R2, respectively) were all calculated from measurements made within the same week. The agreement between the COS flux calculations indicates that the NF estimates and enclosure measurements did reasonably represent ecosystem exchange processes.

It is worth noting that NF estimates of R2 ecosystem COS uptake in June 2005 ( $10 \pm 10$   $\text{pmol m}^{-2} \text{s}^{-1}$ ) were approximately half the NF estimates in R1 ( $20 \pm 10$   $\text{pmol m}^{-2} \text{s}^{-1}$ ). Because of the large uncertainties associated with the NF calculations listed in Table 4.4, these differences cannot be considered significant. However, the observations of reduced stomatal conductance in sweet gum trees and photosynthetic downregulation in loblolly pines associated with long term  $\text{CO}_2$  enrichment at DF [Herrick *et al.*, 2004b; Rogers and Ellsworth, 2002] suggests that lower ecosystem COS uptake rates in R2 most likely reflect the effects of  $\text{CO}_2$  enrichment. A reduction in the vegetative COS uptake capacity due to  $\text{CO}_2$  enrichment effects would also explain why significantly higher overnight canopy COS levels in R2 on 4 – 5 June 2005 ( $\text{R1} = 290 \pm 20$  pptv,  $\text{R2} = 350 \pm 20$  pptv) did not result in greater R2 net ecosystem COS uptake rates. However, similar NF estimates in R1 and R2 in September 2004 suggest that the magnitude of this effect was not consistent throughout the year and may depend upon the variability of other environmental controls over stomatal conductance and photosynthetic capacity such as temperature, soil moisture, or dominant leaf age.

Ring	Date	Time	Ambient COS (pptv)	Temp. (°C)	LAI (m <sup>2</sup> LA m <sup>2</sup> GA)	Flux Type	V <sub>d</sub> per LA (mm s <sup>-1</sup> )	V <sub>d</sub> per GA (mm s <sup>-1</sup> )	Flux (pmol m <sup>-2</sup> s <sup>-1</sup> )
1	9/15 – 9/16/2004	Night	280 ±10	17.9 ±0.5	11 ±4	NF Veg. Ave. Soil Total Veg+Soil	0.2 ±0.2 0.13 ±0.02	2 ±1 0.10 ±0.02	-30 ±20 -17 ±6 -1.2 ±0.3 -19 ±6
2	9/15 – 9/16/2004	Night	300 ±10	17.9 ±0.5	11 ±4	NF Veg. Ave. Soil Total Veg+Soil	0.2 ±0.2 0.09 ±0.01	2 ±1 0.14 ±0.02	-30 ±20 -11 ±4 -1.7 ±0.2 -13 ±4
1	6/4 – 6/5/2005	Night	290 ±20	20.3 ±0.7	13 ±4	NF Veg. Ave. Soil Total Veg+Soil	0.2 ±0.1 0.13 ±0.02	2 ±1 0.06 ±0.01	-20 ±10 -21 ±8 -0.8 ±0.2 -22 ±8
2	6/4 – 6/5/2005	Night	350 ±20	20.3 ±0.7	12 ±4	NF Veg. Ave. Soil Total Veg+Soil	0.05 ±0.08 0.09 ±0.01	0.7 ±0.9 0.06 ±0.02	-10 ±10 -16 ±6 -0.9 ±0.3 -17 ±6
1	6/4 – 6/10/2005	Day	460 ±10	24.1 ±0.3	13 ±4	Veg. Ave. Soil Total Veg+Soil	0.15 ±0.01	0.06 ±0.01	-40 ±10 -1.2 ±0.2 -40 ±10
2	6/4 – 6/10/2005	Day	459 ±8	24.1 ±0.3	12 ±4	Veg. Ave. Soil Total Veg+Soil	0.13 ±0.02	0.06 ±0.02	-30 ±10 -1.2 ±0.3 -30 ±10

**Table 4.4:** Comparison of net ecosystem nighttime flux (NF), vegetation, and soil flux estimates for September 2004 and June 2005. LAI values are the mean monthly measurement for the ring corrected for needle clumping. All deposition velocity, V<sub>d</sub>, and flux errors were propagated from the standard errors of the measurements used in calculation.

Compared to other forest studies, the estimates of nighttime net ecosystem COS uptake at DF were large. Similar NF estimates of net ecosystem flux in a California oak forest ( $-2.4 \text{ pmol m}^{-2} \text{ s}^{-1}$  [Kuhn *et al.*, 1999]) were an order of magnitude smaller than those calculated for DF, while nighttime COS fluxes measured using relaxed eddy accumulation (REA) methods in a German spruce forest were generally positive indicating emission [Xu *et al.*, 2002]. Soil was the only observed COS nighttime sink in both of those studies. In contrast, the significant overnight deposition rates observed for loblolly pines at DF strongly influenced nighttime COS fluxes as COS consumption by vegetation comprised 37 to 100% of observed NF net ecosystem flux estimates (Table 4.4).

These results have important implications for global estimates of the vegetative COS sink strength. Sandoval-Soto *et al.* [2005] and Montzka *et al.* [2007] have pointed out that estimates of the global COS vegetative sink made by scaling net primary productivity ( $\text{NPP} = \text{CO}_2 \text{ consumption} - \text{respiration}$ ) by the ratio of the mean atmospheric mixing ratios for COS and  $\text{CO}_2$  [Goldan *et al.*, 1988; Kettle *et al.*, 2002; Kjellstrom, 1998] should be reconsidered to account for the larger vegetative  $V_d$  of COS compared to  $\text{CO}_2$ . Observations of significant nighttime stomatal conductance in loblolly pine and a wide variety of other plant species [Caird *et al.*, 2007] suggests that COS vegetative uptake that occurs independently of  $\text{CO}_2$  photosynthetic assimilation could also be substantial and must be considered in global vegetative sink strength estimates as well. Nighttime vegetative COS consumption rates at DF were over 50% of daytime values (day:  $-40 \pm 10$  and  $-30 \pm 10$  and night:  $-21 \pm 8$  and  $16 \pm 6 \text{ pmol m}^{-2} \text{ s}^{-1}$  in R1 and R2,

respectively). This means that as much as 33% of the COS vegetative consumption at DF occurred independently of CO<sub>2</sub> assimilation.

#### **4.4 Conclusions**

Vegetation, soil, and canopy COS measurements in 2004 and 2005 all indicate that the Duke Forest FACE site was generally a net sink for COS. Vegetative uptake patterns for the loblolly pine and sweet gum trees sampled were significantly different in R1 and R2, but these differences most likely reflected environmental and canopy spatial effects on the stomatal conductance and photosynthetic capacity of the branches measured rather than CO<sub>2</sub> enrichment effects. However, observations of lower nighttime net ecosystem COS uptake in R2 compared to R1 in June 2005 does suggest that the total canopy vegetative COS uptake capacity was reduced with elevated CO<sub>2</sub> exposure. This effect was not observed in September 2004 and may have depended on the variability of other environmental controls over vegetation stomatal conductance and photosynthetic capacity. Soil consumption, which was a minor component of net ecosystem COS uptake in both ambient and enhanced CO<sub>2</sub> rings, was not significantly different between R1 and R2.

Nighttime minimums in canopy COS mixing ratios reflected significant nighttime COS consumption by loblolly pines in both ambient and enhanced CO<sub>2</sub> rings. Nighttime vegetation uptake rates were approximately 50% of daytime vegetation rates. These observations of substantial vegetative COS consumption that occurred independently of CO<sub>2</sub> assimilation suggest that current estimates of the global vegetative COS sink, which assume that COS and CO<sub>2</sub> assimilation occur simultaneously, may need to be re-evaluated.

## REFERENCES

- Ambrose, J. L., H. Mao, H. R. Mayne, J. Stutz, R. Talbot, and B. C. Sive (2007), Nighttime nitrate radical chemistry at Appledore Island, Maine during the 2004 International Consortium for Atmospheric Research on Transport and Transformation, *J. Geophys. Res.*, *112*, D21302, doi:10.1029/2007JD008756.
- Aneja, V. P., J. H. Overton, L. T. Cupitt, J. L. Durham, and W. E. Wilson (1979), Carbon disulphide and carbonyl sulphide from biogenic sources and their contributions to the global sulphur cycle, *Nature*, *282*, 493-496.
- Arya, S. P. (2001), *Introduction to Micrometeorology*, Academic Press, San Diego, California.
- Atkinson, R. (1994), Gas-Phase Tropospheric Chemistry of Organic-Compounds, *J. Phys. Chem. Ref. Data Monogr.*, *2*, 1-216.
- Atkinson, R. (1997), Gas-phase tropospheric chemistry of volatile organic compounds .1. Alkanes and alkenes, *J. Phys. Chem. Ref. Data*, *26*, 215-290.
- Atkinson, R., D. L. Baulch, R. A. Cox, J. N. Crowley, R. F. Hampson, R. G. Hynes, M. E. Jenkin, M. J. Rossi, and J. Troe (2004), Evaluated kinetic and photochemical data for atmospheric chemistry: Volume 1 - gas phase reactions of O<sub>x</sub>, HO<sub>x</sub>, NO<sub>x</sub> and SO<sub>x</sub> species, *Atmos. Chem. Phys.*, *4*, 1461-1738.
- Barnes, I., K. H. Becker, and I. Patroescu (1994), The tropospheric oxidation of dimethyl sulfide: A new source of carbonyl sulfide, *Geophys. Res. Lett.*, *21*, 2389-2392.
- Berresheim, H., and V. D. Vulcan (1992), Vertical distributions of COS, CS<sub>2</sub>, DMS and other sulfur compounds in a loblolly pine forest, *Atmos. Environ.*, *26A*, 2031-2036.
- Blake, D. R., and F. S. Rowland (1995), Urban leakage of liquefied petroleum gas and its impact on Mexico City air quality, *Science*, *269*, 953-956.
- Bowman, F. M., C. Pilinis, and J. H. Seinfeld (1995), Ozone and aerosol productivity of reactive organics, *Atmos. Environ.*, *29*, 579-589.
- Brasseur, G. P., J. J. Orlando, and G. S. Tyndall (Eds.) (1999), *Atmospheric Chemistry and Global Change*, Oxford University Press, New York.
- Brown, K. A., and J. N. B. Bell (1986), Vegetation - the missing sink in the global cycle of carbonyl sulphide (COS), *Atmos. Environ.*, *20*, 537-540.

- Brown, S. S., et al. (2004), Nighttime removal of NO<sub>x</sub> in the summer marine boundary layer, *Geophys. Res. Lett.*, *31*, doi:1029/2004GL019412.
- Caird, M. A., J. H. Richards, and L. A. Donovan (2007), Nighttime stomatal conductance and transpiration in C<sub>3</sub> and C<sub>4</sub> plants, *Plant Physiol.*, *143*, 4-10.
- Carter, W. P. L. (1994), Development of ozone reactivity scales for volatile organic compounds, *J. Air Waste Manag. Assoc.*, *44*, 881-899.
- Castro, M. S., and J. N. Galloway (1991), A comparison of sulfur-free and ambient air enclosure techniques for measuring the exchange of reduced sulfur gases between soils and the atmosphere, *J. Geophys. Res.*, *96*, 15427-15437.
- Charlson, R. J., J. Langner, and H. Rodhe (1990), Sulfate Aerosol and Climate, *Nature*, *348*, 22-22.
- Chen, T. Y., I. J. Simpson, D. R. Blake, and F. S. Rowland (2001), Impact of the leakage of liquefied petroleum gas (LPG) on Santiago air quality, *Geophys. Res. Lett.*, *28*, 2193-2196.
- Chin, M., and D. D. Davis (1993), Global sources and sinks of OCS and CS<sub>2</sub> and their distribution, *Global Biogeochem. Cycles*, *7*, 321-337.
- Chin, M., and D. D. Davis (1995), A reanalysis of carbonyl sulfide as a source of stratospheric background sulfur aerosol, *J. Geophys. Res.*, *100*, 8993-9005.
- Conner, T. L., W. A. Lonneman, and R. L. Seila (1995), Transportation-related volatile hydrocarbon source profiles measured in Atlanta, *J. Air Waste Manag. Assoc.*, *45*, 383-394.
- Daum, P. H., L. I. Kleinman, L. Newman, W. T. Luke, J. Weinstein-Lloyd, C. M. Berkowitz, and K. M. Busness (1996), Chemical and physical properties of plumes of anthropogenic pollutants transported over the North Atlantic during the North Atlantic Regional Experiment, *J. Geophys. Res.*, *101*, 29029-29042.
- deGouw, J. A., et al. (2005), Budget of organic carbon in a polluted atmosphere: results from the New England Air Quality Study in 2002, *J. Geophys. Res.*, *110*, doi:10.1029/2004JD005623.
- deMello, W. Z., and M. E. Hines (1994), Application of static and dynamic enclosures for determining dimethyl sulfide and carbonyl sulfide exchange in Sphagnum peatlands: Implications for the magnitude and direction of flux, *J. Geophys. Res.*, *99*, 14601-14607.
- Dewulf, J., and H. Van Langenhove (1997), Analytical techniques for the determination and measurement data of 7 chlorinated C1- and C2- hydrocarbons and 6 monocyclic

aromatic hydrocarbons in remote air masses: an overview, *Atmos. Environ.*, 31, 3291-3307.

Draxler, R. R., and G. D. Rolph (2003), HYSPLIT (HYbrid Single-Particle Lagrangian Integrated Trajectory) Model access via NOAA ARL READY Website (<http://www.arl.noaa.gov/ready/hysplit4.html>)., edited, NOAA Air Resources Laboratory, Silver Spring, MD.

Elliot, S., E. Lu, and F. S. Rowland (1989), Rates and mechanisms for the hydrolysis of carbonyl sulfide in natural waters, *Environ. Sci. Technol.*, 23, 458-461.

Ellsworth, D. S. (1999), CO<sub>2</sub> enrichment in a maturing pine forest: are CO<sub>2</sub> exchange and water status in the canopy affected?, *Plant Cell Environ.*, 22, 461-472.

Energy Information Administration, U. S. D. O. E. (2005), Table F6: Liquefied Petroleum Gases Consumption, Price, and Expenditure Estimates by Sector, 2005, in [http://www.eia.doe.gov/emeu/states/sep\\_fuel/html/fuel\\_lg.html](http://www.eia.doe.gov/emeu/states/sep_fuel/html/fuel_lg.html), edited, U.S. Department of Energy, Washington D.C.

FACTS-1 (2006a), FACTS-1 LAI-2000 Leaf Area Index measurements, edited, Duke University Forest-Atmosphere Carbon Transfer and Storage (FACTS-1) Facility, <http://face.env.duke.edu/products.cfm>

FACTS-1 (2006b), FACTS-1 Soil moisture measurements, edited, Duke University Forest-Atmosphere Carbon Transfer and Storage (FACTS-1) Facility, <http://face.env.duke.edu/products.cfm>.

Fatemi, M.H. (2005), Prediction of ozone tropospheric degradation rate constant for organic compounds by using artificial neural networks, *Anal. Chim. Acta*, 556, 355-363.

Fehsenfeld, F. C., et al. (2006), International Consortium for Atmospheric Research on Transport and Transformation (ICARTT): North America to Europe - overview of the 2004 summer field study, *J. Geophys. Res.*, 111, D23S01, doi:10.1029/2006JD007829.

Finlayson-Pitts, B. J. (1993), Chlorine atoms as a potential tropospheric oxidant in the marine boundary layer, *Res. Chem. Intermed.*, 19, 235-249.

Fischer, E. V., R. W. Talbot, J. E. Dibb, J. L. Moody, and G. L. Murray (2004), Summertime ozone at Mount Washington: Meteorological controls at the highest peak in the northeast, *J. Geophys. Res.*, 109, D24303, doi:10.1029/2004JD004841.

Fraser, M. P., G. R. Cass, and B. R. T. Simoneit (1998), Gas-phase and particle-phase organic compounds emitted from motor vehicle traffic in a Los Angeles roadway tunnel, *Environ. Sci. Tech.*, 32, 2051-2060.

- Galbally, I. (1968), Some measurements of ozone variation and destruction in the atmospheric surface layer, *Nature*, 218, 456-457.
- Gary, J. H., and G. E. Handwerk (2001), *Petroleum Refining: Technology and Economics*, 8-13 pp., Marcel Dekker, Inc., New York.
- Gelencser, A., K. Siszler, and J. Hlavay (1997), Toluene-benzene concentration ratio as a tool for characterizing the distance from vehicular emission sources, *Environ. Sci. Technol.*, 31, 2869-2872.
- Geng, C., and Y. Mu (2006), Carbonyl sulfide and dimethyl sulfide exchange between trees and the atmosphere, *Atmos. Environ.*, 40, 1373-1383.
- Geyer, A., and U. Platt (2002), Temperature dependence of the NO<sub>3</sub> loss frequency: A new indicator for the contribution of NO<sub>3</sub> to the oxidation of monoterpenes and NO<sub>x</sub> removal in the atmosphere, *J. Geophys. Res.*, 107, 4431, doi:10.1029/2001JD001215.
- Goldan, P. D., R. Fall, W. C. Kuster, and F. C. Fehsenfeld (1988), Uptake of COS by growing vegetation: A major tropospheric sink, *J. Geophys. Res.*, 93, 14186-14192.
- Goldan, P. D., M. Trainer, W. C. Kuster, D. D. Parrish, J. Carpenter, J. M. Roberts, J. E. Yee, and F. C. Fehsenfeld (1995), Measurements of hydrocarbons, oxygenated hydrocarbons, carbon monoxide, and nitrogen oxides in an urban basin in Colorado: Implications for Emission Inventories, *J. Geophys. Res.*, 100, 22771-22783.
- Goldhaber, S., S. Wolf, and M. Laney (1995), Health Effects Notebook for Hazardous Air Pollutants, edited, U.S. Environmental Protection Agency, <http://www.epa.gov/ttn/atw/hlthef/hapindex.html>.
- Goldstein, A. H., B. C. Daube, J. W. Munger, and S. C. Wofsy (1995), Automated in-situ monitoring of atmospheric non-methane hydrocarbon concentrations and gradients, *J. Atmos. Chem.*, 21, 43-59.
- Goldstein, A. H., M. McKay, M. R. Kurpius, G. W. Schade, A. Lee, R. Holzinger, and R. A. Rasmussen (2004), Forest thinning experiment confirms ozone deposition to forest canopy is dominated by reaction with biogenic VOCs, *Geophys. Res. Lett.*, 31, doi:10.1029/2004GL021259.
- Greenwood, D. R., M. J. Scarr, and D. C. Christophel (2003), Leaf stomatal frequency in the Australian tropical rainforest tree *Neolitsea dealbata* (Lauraceae) as a proxy measure of atmospheric pCO<sub>2</sub>, *Palaeogeog. Palaeoclim. Palaeoecol.*, 196, 375-393.
- Griffin, R.J., C. A. Johnson, R. W. Talbot, H. Mao, R. S. Russo, Y. Zhou, and B. C. Sive (2004), Quantification of ozone formation metrics at Thompson Farm during the New England Air Quality Study (NEAQS) 2002, *J. Geophys. Res.*, 109, doi:10.1029/2004JD005344.

Griffin, R., P. J. Beckman, R. Talbot, B. Sive, and R. K. Varner (2007), Deviations from ozone photostationary state during the International Consortium for Atmospheric Research on Transport and Transformation 2004: Use of measurements and photochemical modeling to assess potential causes, *J. Geophys. Res.*, *112*, doi:10.1029/2006JD007604.

Guenther, A., et al. (1995), A global model of natural volatile organic compound emissions, *J. Geophys. Res.*, *100*, 8873-8892.

Gusten, H., G. Heinrich, and D. Sprung (1998), Nocturnal depletion of ozone in the Upper Rhine Valley, *Atmos. Environ.*, *32*, 1195-1202.

Hastie, D. R., P. B. Shepson, S. Sharma, and H. I. Schiff (1993), The influence of the nocturnal boundary layer on secondary trace species in the atmosphere at Dorset, Ontario, *Atmos. Environ.*, *27*, 533-541.

Heiden, A. C., K. Kobel, M. Komenda, R. Koppmann, M. Shao, and J. Wildt (1999), Toluene emissions from plants, *Geophys. Res. Lett.*, *26*, 1283-1286.

Herrick, J. D., and R. B. Thomas (2001), No photosynthetic down-regulation in sweetgum trees (*Liquidambar styraciflua* L.) after three years of CO<sub>2</sub> enrichment at the Duke Forest FACE experiment, *Plant Cell Environ.*, *24*, 53-64.

Herrick, J. D., H. Maherali, and R. B. Thomas (2004a), Reduced stomatal conductance in sweetgum (*Liquidambar styraciflua*) sustained over long-term CO<sub>2</sub> enrichment, *New Phytol.*, *162*, 387-396.

Herrick, J. D., H. Maherali, and R. B. Thomas (2004b), Reduced stomatal conductance in sweetgum (*Liquidambar styraciflua*) sustained over long-term CO<sub>2</sub> enrichment, *New Phytol.*, *162*, 387-396.

Hungate, B. A., M. Reichstein, P. Dijkstra, D. Johnson, G. Hymus, J. D. Tenhunen, C. R. Hinkle, and B. G. Drake (2002), Evapotranspiration and soil water content in a scrub-oak woodland under carbon dioxide enrichment, *Global Change Biol.*, *8*, 289-298.

Kammann, C., L. Grunhage, U. Gruters, S. Janze, and H. J. Jager (2005), Response of aboveground grassland biomass and soil moisture to moderate long-term CO<sub>2</sub> enrichment, *Basic Appl. Ecol.*, *6*, 351-365.

Kesselmeier, J., and L. Merk (1993), Exchange of carbonyl sulfide (COS) between agricultural plants and the atmosphere: Studies on the deposition of COS to peas, corn and rapeseed, *Biogeochem.*, *23*, 47-59.

- Kesselmeier, J., F. X. Meixner, U. Hofmann, A.-L. Ajavon, S. Leimbach, and M. O. Andreae (1993), Reduced sulfur compound exchange between the atmosphere and tropical tree species in southern Cameroon, *Biogeochem.*, 23, 23-45.
- Kesselmeier, J., N. Teusch, and U. Kuhn (1999), Controlling variables for the uptake of atmospheric carbonyl sulfide by soil, *J. Geophys. Res.*, 104, 11577-11584.
- Kettle, A. J. (2000), Comparison of dynamic models to predict the concentration of a photochemical tracer in the upper ocean as a function of depth and time, *Mar. Freshwater Res.*, 51, 289-304.
- Kettle, A. J., U. Kuhn, M. v. Hobe, J. Kesselmeier, and M. O. Andreae (2002), Global budget of atmospheric carbonyl sulfide: Temporal and spatial variations of the dominant sources and sinks, *J. Geophys. Res.*, 107, 4658, doi:10.1029/2002JD002187.
- Kettunen, R., S. Saarnio, P. J. Martikainen, and J. Silvola (2006), Increase of N<sub>2</sub>O fluxes in agricultural peat and sandy soil under elevated CO<sub>2</sub> concentration: concomitant changes in soil moisture, groundwater table and biomass production of *Phleum pratense*, *Nutr. Cycl. Agroecosys.*, 74, 175-189.
- Kirchstetter, T. W., B. C. Singer, R. A. Harley, G. R. Kendall, and W. Chan (1996), Impact of oxygenated gasoline use on California light-duty vehicle emissions, *Environ. Sci. Tech.*, 30, 661-670.
- Kjellstrom, E. (1998), A three-dimensional global model study of carbonyl sulfide in the troposphere and the lower stratosphere, *J. Atmos. Chem.*, 29, 151-177.
- Kouwenberg, L. L. R., J. C. McElwain, W. M. Kurschner, F. Wagner, D. J. Beerling, F. E. Mayle, and H. Visscher (2003), Stomatal frequency adjustment of four conifer species to historical changes in atmospheric CO<sub>2</sub>, *Am. J. Bot.*, 90, 610-619.
- Kuhn, U., C. Ammann, A. Wolf, F. X. Meixner, M. O. Andreae, and J. Kesselmeier (1999), Carbonyl sulfide exchange on an ecosystem scale: soil represents a dominant sink for atmospheric COS, *Atmos. Environ.*, 33, 995-1008.
- Kurschner, W. M., F. Wagner, E. H. Visscher, and H. Visscher (1997), Predicting the response of leaf stomatal frequency to a future CO<sub>2</sub>-enriched atmosphere: constraints from historical observations, *Geologische Rundschau*, 86, 512-517.
- Kurylo, M. J., et al. (1999), Short-lived ozone-related compounds, in *Scientific Assessment of Ozone Depletion: 1998, Global Ozone Research and Monitoring Project - Report no. 44*, edited by C. A. Ennis, pp. 2.1-2.56, World Meteorological Organization, Geneva, Switzerland.

Lough, G. C., J. J. Schauer, W. A. Lonneman, and M. K. Allen (2005), Summer and winter nonmethane hydrocarbon emissions from on-road motor vehicles in the midwestern United States, *J. Air Waste Manag. Assoc.*, *55*, 629-646.

Lewis, A. C., et al. (2007), Chemical composition observed over the mid-Atlantic and the detection of pollution signatures far from source regions, *J. Geophys. Res.*, *112*, doi:10.1029/2006JD007584.

Mao, H., and R. Talbot (2004a), O<sub>3</sub> and CO in New England: Temporal variations and relationships, *J. Geophys. Res.*, *109*, D21304, doi: 10. 1029/2004JD004913.

Mao, H., and R. Talbot (2004b), Role of meteorological processes in two New England ozone episodes during summer 2001, *J. Geophys. Res.*, *109*, doi:10.1029/2004JD004850.

Mao, H., R. Talbot, C. Nielsen, and B. Sive (2006a), Controls on methanol and acetone in marine and continental atmospheres, *Geophys. Res. Lett.*, *33*, doi:10.1029/2005GL024810.

Mao, H., R. Talbot, D. Troop, R. Johnson, S. Businger, and A. E. Thompson (2006b), Smart balloon observations over the North Atlantic: O<sub>3</sub> data analysis and modelling, *J. Geophys. Res.*, *111*, D23S56, doi:10.1029/2005JD006507.

McClenny, W. A., E. H. Daughtrey, J. R. Adams, K. D. Oliver, and K. G. Kronmiller (1998), Volatile organic compound concentration patterns at the New Hendersonville monitoring site in the 1995 Southern Oxidants Study in the Nashville, Tennessee, area, *J. Geophys. Res.*, *103*, 22509-22518.

McGaughey, G. R., et al. (2004), Analysis of motor vehicle emissions in a Houston tunnel during the Texas Air Quality Study 2000, *Atmos. Environ.*, *38*, 3363-3372.

McLain, J. E. T., T. B. Kepler, and D. M. Ahmann (2002), Belowground factors mediating changes in methane consumption in a forest soil under elevated CO<sub>2</sub>, *Global Biogeochem. Cycles*, *16*, 1050, doi:10.1029/2001GB001439.

Millet, D. B., et al. (2006), Chemical characteristics of North American surface layer outflow: Insights from Chebogue Point, Nova Scotia, *J. Geophys. Res.*, *111*, D23S53, doi:10.1029/2006JD007287.

Montzka, S. A., P. Calvert, B. D. Hall, J. W. Elkins, T. J. Conway, P. P. Tans, and C. Sweeney (2007), On the global distribution, seasonality, and budget of atmospheric carbonyl sulfide (COS) and some similarities to CO<sub>2</sub>, *J. Geophys. Res.*, *112*, D09302, doi:10.1029/2006JD007665.

Ng, N. L., J. H. Kroll, A. W. H. Chan, P. S. Chhabra, R. C. Flagan, and J. H. Seinfeld (2007), Secondary organic aerosol formation from m-xylene, toluene, and benzene, *Atmos. Chem. Phys.*, *7*, 3909-3922.

- Notholt, J., et al. (2003), Enhanced upper tropical tropospheric COS: Impact on the stratospheric aerosol layer, *Nature*, 300, 307-310.
- Oh, N. H., and D. D. Richter (2005), Elemental translocation and loss from three highly weathered soil-bedrock profiles in the southeastern United States, *Geoderma*, 126, 5-25.
- Protoschill-Krebs, G., and J. Kesselmeier (1992), Enzymatic pathways for the consumption of carbonyl sulphide (COS) by higher plants, *Botanica Acta*, 105, 206-212.
- Protoschill-Krebs, G., C. Wilhelm, and J. Kesselmeier (1995), Consumption of carbonyl sulphide by *Chlamydomonas reinhardtii* with different activities of carbonic anhydrase (CA) induced by different CO<sub>2</sub> growing regimes, *Botanica Acta*, 108, 445-448.
- Protoschill-Krebs, G., C. Wilhelm, and J. Kesselmeier (1996), Consumption of carbonyl sulfide (COS) by higher plant carbonic anhydrase (CA), *Atmos. Environ.*, 30, 3151-3156.
- Ray, J. D., R. L. Heavner, and M. Flores (1996), Surface level measurements of ozone and precursors at coastal and offshore locations in the Gulf of Maine, *J. Geophys. Res.*, 101, 29005-29011.
- Reid, C. D., H. Maherali, H. B. Johnson, S. D. Smith, S. D. Wullschleger, and R. B. Jackson (2003), On the relationship between stomatal characters and atmospheric CO<sub>2</sub>, *Geophys. Res. Lett.*, 30, doi:10.1029/2003GL017775.
- Rinne, J., J.-P. Tuovinen, T. Laurila, H. Hakola, M. Aurela, and H. Hypon (2000), Measurements of hydrocarbon fluxes by a gradient method above a northern boreal forest, *Agricult. Forest Meteorol.*, 102, 25-37.
- Robertson, G. P., E. A. Paul, and R. R. Harwood (2000), Greenhouse gases in intensive agriculture: contributions of individual gases to the radiative forcing of the atmosphere, *Science*, 289, 1922-1925.
- Romanow, S. (2008), Fuel Trends Report: Gasoline 1995-2005, Compliance and Innovative Strategies Division, Office of Transportation and Air Quality, U.S. Environmental Protection Agency.
- Rogak, S. N., U. Pott, T. Dann, and D. Wang (1998), Gaseous emissions from vehicles in a traffic tunnel in Vancouver, British Columbia, *J. Air Waste Manag. Assoc.*, 48.
- Rogers, A., and D. S. Ellsworth (2002), Photosynthetic acclimation of *Pinus taeda* (loblolly pine) to long-term growth in elevated pCO<sub>2</sub> (FACE), *Plant Cell Environ.*, 25, 851-858.
- Ryerson, T. B., E. J. Williams, and F. C. Fehsenfeld (2000), An efficient photolysis system for fast-response NO<sub>2</sub> measurements, *J. Geophys. Res.*, 105, 26,447-426,461.

Sagebiel, J. C., B. Zielinska, W. R. Pierson, and A. W. Gertler (1996), Real-world emissions and calculated reactivities of organic species from motor vehicles, *Atmos. Environ.*, *30*, 2287-2296.

Sandoval-Soto, L., M. Stanimirov, M. v. Hobe, V. Schmitt, J. Valdes, A. Wild, and J. Kesselmeier (2005), Global uptake of carbonyl sulfide (COS) by terrestrial vegetation: Estimates corrected by deposition velocities normalized to the uptake of carbon dioxide (CO<sub>2</sub>), *Biogeosciences Discuss.*, *2*, 183-201.

Schafer, K. V. R., R. Oren, C.-T. Lai, and G. G. Katul (2002), Hydrologic balance in an intact temperate forest ecosystem under ambient and elevated atmospheric CO<sub>2</sub> concentration, *Global Change Biol.*, *8*, 895-211.

Schauer, J. J., M. P. Fraser, G. R. Cass, and B. R. T. Simoneit (2002), Source reconciliation of atmospheric gas phase and particle phase pollutants during a severe photochemical smog episode, *Environ. Sci. Tech.*, *36*, 3806-3814.

Shepson, P. B., J. W. Bottenheim, D. R. Hastie, and A. Venkatram (1992), Determination of the relative ozone and pan deposition velocities at night, *Geophys. Res. Lett.*, *19*, 1121-1124.

Simmons, J. S., L. Lemedtsson, H. Hultberg, and M. E. Hines (1999), Consumption of atmospheric carbonyl sulfide by coniferous boreal forest soils, *J. Geophys. Res.*, *104*, 11569-11576.

Simpson, I. J., G. W. Thurtell, H. H. Neumann, G. DenHartog, and G. C. Edwards (1998), The validity of similarity theory in the roughness sublayer above forests, *Boundary Layer Meteorol.*, *87*, 69-99.

Singh, H. B., and P. B. Zimmerman (1992), Atmospheric distribution and sources of nonmethane hydrocarbons, in *Gaseous Pollutants: Characterization and Cycling*, edited by J. O. Nriagu, p. 182, John Wiley & Sons, Inc., New York.

Singh, H. B., L. J. Salas, B. K. Cantrell, and R. M. Redmond (1985), Distribution of aromatic hydrocarbons in the ambient air, *Atmos. Environ.*, *19*, 1911-1919.

Sive, B. C., Y. Zhou, D. Troop, Y. Wang, W. C. Little, O. W. Wingenter, R. S. Russo, R. K. Varner, and R. Talbot (2005), Development of a cryogen-free concentration system for measurements of volatile organic compounds, *Anal. Chem.*, *77*, 6989-6998.

Sive, B. C., R. K. Varner, H. Mao, D. R. Blake, O. W. Wingenter, and R. Talbot (2007), A large terrestrial source of methyl iodide, *Geophys. Res. Lett.*, *34*, L17808, doi:10.1029/2007GL030528.

- Solomon, S., R. W. Portmann, R. R. Garcia, L. W. Thomason, L. R. Poole, and M. P. McCormick (1996), The role of aerosol variations in anthropogenic ozone depletion at northern midlatitudes, *J. Geophys. Res.*, *101*, 6713-6727.
- Steinbacher, M., H. G. Bingemar, and U. Schmidt (2004), Measurements of the exchange of carbonyl sulfide (OCS) and carbon disulfide (CS<sub>2</sub>) between soil and atmosphere in a spruce forest in central Germany, *Atmos. Environ.*, *38*, 6043-6052.
- Stenberg, P. (1996), Correcting LAI-2000 estimates for the clumping of needles in shoots of conifers, *Agric. Forest Meteorol.*, *79*, 1-8.
- Stohl, A., and T. Trickl (1999), A textbook example of long-range transport: Simultaneous observation of ozone maxima of stratospheric and North American origin in the free troposphere over Europe, *J. Geophys. Res.*, *104*, 30445-30462.
- Talbot, R., H. Mao, and B. Sive (2005), Diurnal characteristics of surface level O<sub>3</sub> and other important trace gases in New England, *J. Geophys. Res.*, *110*, doi:10.1029/2004JD005449.
- Taylor, J. R. (1982), *An introduction to error analysis: the study of uncertainties in physical measurements*, University Science Books, Sausalito, CA.
- Thompson, A. M. (1992), The oxidizing capacity of the earth's atmosphere: Probable past and future changes, *Science*, *256*, 1157-1163.
- Turco, R. P., R. C. Whitten, O. B. Toon, J. B. Pollack, and P. Hamill (1980), OCS, stratospheric aerosols and climate, *Nature*, *283*, 283-286.
- U.S. Census Bureau (2006), 2006 Population Estimates: Persons per square mile (TM-M2), edited, <<http://factfinder.census.gov>>.
- U.S. Environmental Protection Agency (2007), Toxic Release Inventory (TRI) Explorer Online Database, <http://www.epa.gov/triexplorer/>, edited.
- Varner, R. K., P. M. Crill, and R. W. Talbot (1999), Wetlands: a potentially significant source of atmospheric methyl bromide and methyl chloride, *Geophys. Res. Lett.*, *26*, 2433-2436.
- Varner, R. K., Y. Zhou, R. S. Russo, O. W. Wingenter, E. Atlas, C. Stroud, H. Mao, R. Talbot, and B. C. Sive (2008), Controls on atmospheric chloroiodomethane (CH<sub>2</sub>CI) in marine environments, *J. Geophys. Res.*, *113*, doi:10.1029/2007JD008889.
- Wagner, F., D. L. Dilcher, and H. Visscher (2005), Stomatal frequency responses in hardwood-swamp vegetation from Florida during a 60-year continuous CO<sub>2</sub> increase, *Am. J. Bot.*, *92*, 690-695.

Wang, Y., D. J. Jacob, and J. A. Logan (1998), Global simulation of tropospheric O<sub>3</sub>-NO<sub>x</sub>-hydrocarbon chemistry: 3. Origin of tropospheric ozone and effects of nonmethane hydrocarbons, *J. Geophys. Res.*, *103*, 10757-10767.

Watts, S. F. (2000), The mass budgets of carbonyl sulfide, dimethyl sulfide, carbon disulfide, and hydrogen sulfide, *Atmos. Environ.*, *34*, 761-779.

Warneke, C., et al. (2006), Biomass burning and anthropogenic sources of CO over New England in the summer 2004, *J. Geophys. Res.*, *111*, D23S15, doi:10.1029/2005JD006878.

Warneke, C., et al. (2007), Determination of urban volatile organic compound emission ratios and comparison with an emissions database, *J. Geophys. Res.*, *112*, doi:10.1029/2006JD007930.

Watts, S. F. (2000), The mass budgets of carbonyl sulfide, dimethyl sulfide, carbon disulfide, and hydrogen sulfide, *Atmos. Environ.*, *34*, 761-779.

Weiss, P. S., S. S. Andrews, J. E. Johnson, and O. C. Zafiriou (1995), Photoproduction of Carbonyl Sulfide in South-Pacific Ocean Waters as a Function of Irradiation Wavelength, *Geophys. Res. Lett.*, *22*, 215-218.

White, M. L., et al. (2008), Volatile organic compounds in northern New England marine and continental environments during the ICARTT 2004 Campaign, *J. Geophys. Res.*, *113*, D08S90, doi:10.1029/2007JD009161.

Wingenter, O. W., D. R. Blake, N. J. Blake, B. C. Sive, and F. S. Rowland (1999), Tropospheric hydroxyl and atomic chlorine concentrations, and mixing timescales determined from hydrocarbon and halocarbon measurements made over the Southern Ocean, *J. Geophys. Res.*, *104*, 21819-21828.

Xu, X., H. G. Bingemer, and U. Schmidt (2002), The flux of carbonyl sulfide and carbon disulfide between the atmosphere and a spruce forest, *Atmos. Chem. Phys.*, *2*, 171-181.

Yi, Z., X. Wang, G. Sheng, D. Zhang, G. Zhou, and J. Fu (2007), Soil uptake of carbonyl sulfide in subtropical forests with different successional stages in south China, *J. Geophys. Res.*, *112*, D08302, doi:10.1029/2006JD008408.

Zhou, Y., R. K. Varner, R. S. Russo, O. W. Wingenter, K. B. Haase, R. Talbot, and B. C. Sive (2005), Coastal water source of short-lived halocarbons in New England, *J. Geophys. Res.*, *110*, D21302, doi:10.1029/2004JD005603.

Zhou, Y., et al. (2008), Bromoform and dibromomethane measurements in the seacoast region of New Hampshire, 2002-2004, *J. Geophys. Res.*, *113*, doi:10.1029/2007JD009103.